

The COMPA manual

J. Mierzejewski^a, A.A. Pasternak^b, M. Komorowska^a, J. Srebrny^a, E. Grodner^c, M. Kowalczyk^{a,c}

^a*Heavy Ion Laboratory, University of Warsaw, Poland*

^b*A.F. Ioffe Physical-Technical Institute, St.-Petersburg, Russia*

^c*Institute of Experimental Physics, Faculty of Physics, University of Warsaw, Poland*

Abstract

COMPA is a piece of software based on the statistical theory. It works in *event by event* mode, providing complete information on the reaction products: the *entry state* spin and energy distribution, the reaction point coordinates, the directions and velocities of the recoil and the emitted light particles. Models of the stopping of the reaction products in the passive elements of the setup, such as the target and backing, are also used. This enables COMPA to use a Monte-Carlo based analysis of the experimental data and quickly evaluate the experimental setup. Basic comparisons of predictions with the experimental results can be easily obtained. The code is a handy tool at the planning stage of the lifetime measurements using the Doppler Shift Attenuation Method (DSAM) and the Recoil Distance Method (RDM). This manual is focused on the preparation of the input and on the description of the physical phenomena the code is supposed to model. In order to showcase the usefulness of COMPA we present some comparisons of simulations with experimental results.

Contents

1	Introduction	5
2	Structure of COMPA code	5
2.1	Directory structure	5
2.2	Installation and executing	5
2.2.1	Software requirements	5
2.2.2	MANUAL mode	5
2.2.3	AUTO mode - Graphic User Interface (GUI)	5
2.3	Input files	14
2.3.1	Main input - compa.inp	14
2.3.2	Yrast line information - yrastinput.inp	14
2.3.3	Fission barrier - bf.inp	15
2.3.4	Mass excess table - massdefects.inp .	15
2.3.5	Stopping powers for beam and light particles - s12.inp	15
2.4	Aggregate output file - compa.txt	15
2.5	Plots	15
2.6	Source files, list of modules and block scheme	15
2.6.1	read.cpp	15
2.6.2	momenta.cpp	16
2.6.3	evapor.cpp	16
2.6.4	fission.cpp	16
2.6.5	kinematics.cpp	16
2.6.6	utils.cpp	16
2.6.7	Block scheme	16
3	Physics	19
3.1	Creation of the compound nucleus	19
3.1.1	Summary - input parameters	19
3.2	Competition between particle evaporation, gamma emission and fission	19
3.2.1	Evaporation	19
3.2.2	“Hot spot” particle emission	20
3.2.3	Gamma emission	21
3.2.4	Fission	22
3.2.5	Amplification of the probabilities	23
3.2.6	Entry state distribution	23
3.2.7	Summary - input parameters	23
3.3	Experimental setup and products stopping in the material.	23
3.3.1	Beam stopping	24
3.3.2	Proton and α particle stopping.	25
3.3.3	Neutron, proton and α particle gating and detection.	25
3.3.4	Recoils	25
3.3.5	Summary - input parameters	27
4	Comparison with experiment.	29
4.1	Complete fusion and fission	29
4.1.1	Fusion in the $^{16}\text{O}+^{148,150,152,154}\text{Sm}$ reaction	29
4.1.2	Fusion in the $^{16,18}\text{O}+^{92}\text{Mo}$ reaction	29
4.1.3	Fission in the $^{40}\text{Ar}+^{109}\text{Ag}$ system .	30

5 Acknowledgments 32

Appendix A	The transmission coefficients for fusion	33
Appendix A.1	Heavy projectiles ($A>5$).	33
Appendix A.2	Close to the Coulomb barrier	35
Appendix A.3	Light projectiles	35
Appendix A.4	Transmission coefficient for fusion cut-off	35
Appendix A.5	Summary - input parameters	35
Appendix B	Yrast lines	36
Appendix B.1	Moments of inertia	38
Appendix B.2	Pairing shift	39
Appendix B.3	Summary - input parameters	39
Appendix C	Transmission coefficients for evaporated particles.	40
Appendix C.1	Reduction of α particle yield.	40
Appendix C.2	Evaporated particle coefficients cut-off.	41
Appendix C.3	Summary - input parameters	42
Appendix D	E1 GDR strength functions.	42
Appendix E	Fission barrier calculations.	42
Appendix E.1	Summary - input parameters	44
Appendix F	Level densities	44
Appendix F.1	Temperature correction	45
Appendix F.2	Summary - input parameters	45
Appendix G	Remaining output files	47
Appendix G.1	tlese.txt	47
Appendix G.2	xsections	47
Appendix G.3	recoils	47
Appendix G.4	nuclei	47
Appendix G.5	particles	48
Appendix G.6	gammas	49
Appendix G.7	level density	49
Appendix G.8	stopping	49
Appendix G.9	Agata Simulation Code	50
Appendix G.10	others	50

1. Introduction

In order to calculate all the necessary quantities by means of the Statistical Model [1] numerous input parameters are required. The description of the creation of the compound nucleus requires calculation of the transmission coefficients for fusion. When a highly excited compound nucleus is formed, it is necessary to decide whether the nucleus will split or emit a γ ray or light particle (α particle, neutron or proton). This requires such parameters as nuclear level densities, temperature, fission barrier, γ strength functions and transmission coefficients for the evaporated particles.

COMPACT provides complete information on the reaction products: the *entry state* spin and energy distribution, the reaction point coordinates, the directions and velocities of the recoil and the emitted light particles. Models of stopping of the reaction products in the passive elements of the setup, such as the target and backing, are also used. In the case of recoils, when velocities are relatively low ($\approx 2\%c$), a model [2] based on the parametrisation of Linhard, Scharff and Schiøtt [3] of stopping powers is applied. In the case of beam and light charged particles, stopping powers from the SRIM2006 [4] code are used.

The code works in *event-by-event* mode. This enables COMPACT to use a Monte-Carlo based analysis of the experimental data and quickly evaluate the experimental setup. Basic comparisons of predictions with the experimental results can be easily obtained.

COMPACT is part of the software package devoted to lifetime measurements using the Doppler Shift Attenuation Method (DSAM) and the Recoil Distance Method (RDM) written by Alexander Pasternak. The package also includes code that performs simulations of γ emission (GAMMA) and lineshape analysis (SHAPE). The GAMMA [5, 6, 7] code calculates the time correlated emission of γ rays in the quasicontinuum and continuum area, with the recoil stopping model included. The SHAPE [5, 8, 9] code handles the lineshape analysis of measured γ spectra.

The package was originally written in Fortran. Recently COMPACT was ported into C++. This manual is focused on the preparation of the input and on the description of the physical phenomena the code is supposed to model. In order to showcase the usefulness of COMPACT we present some comparisons of simulations with experimental results.

2. Structure of COMPACT code

2.1. Directory structure

The full COMPACT system has the following directory structure:

- inputs/ - input files (see Section 2.3).
- outputs/ - output files (see Section 2.4).

- program/ - program source files (see Section 2.6).
- GUI/ - files for the Graphic User Interface (see Section 2.2.3).
- plots/ - postscript files with plotted data (see Section 2.5).
- start.sh - bash script for program executing in AUTO mode (see Section 2.2.3).

2.2. Installation and executing

In order to execute COMPACT several open source programs must be installed. There are two ways of running COMPACT: the **MANUAL** mode and the **AUTO** mode with Graphic User Interface.

2.2.1. Software requirements

The following open source software must be installed:

- Standard c++ compiler.
- GNU Scientific Libraries (GSL). The program uses random generator and spline functions from GSL.
- GNUPLOT Version 4.4 patchlevel 2 or newer. For postscript figure drawing.
- Python. For Graphic User Interface purposes in AUTO mode.
- Guide GTK+ and library Libglade. For Graphic User Interface purposes in AUTO mode.

Please note that the version presented is for Linux only.

2.2.2. MANUAL mode

To run COMPACT in MANUAL mode do the following:

1. Edit all necessary input files (see Section 2.3).
2. Enter the program/ folder by typing "cd program/"
3. Compile COMPACT by typing "make".
4. Run it by typing "./COMPACT".

All you need to install for this part is the c++ compiler and the GSL libraries. All output files will be prepared (see Section 2.4).

2.2.3. AUTO mode - Graphic User Interface (GUI)

The COMPACT input requires over 80 input parameters grouped in the text file "inputs/compa.inp" (see Section 2.3.1). Preparation of such a complex input is difficult and often unnecessary, as even over 60 parameters can take default values. A Graphic User Interface (GUI) was thus prepared, which provides control over a maximum of 56 input parameters. Parameters are defined in an easy and intuitive way. The basic and less exact calculations can be performed after defining only 7 parameters. Thanks to the GUI, COMPACT calculations become easy.

To use COMPACT in AUTO mode, run the script start.sh which does the following:

- runs the GUI which will help you create the input (inputs/compa.inp, see Section 2.3.1).
- compiles and runs the code.

- prepares input for gnuplot and prints some figures in postscript format (in the folder “outputs/plots”, (see section 2.5)).

Inputs can be stored using the “save” icon and read using the “load” icon. The interface is illustrated on the following pages.

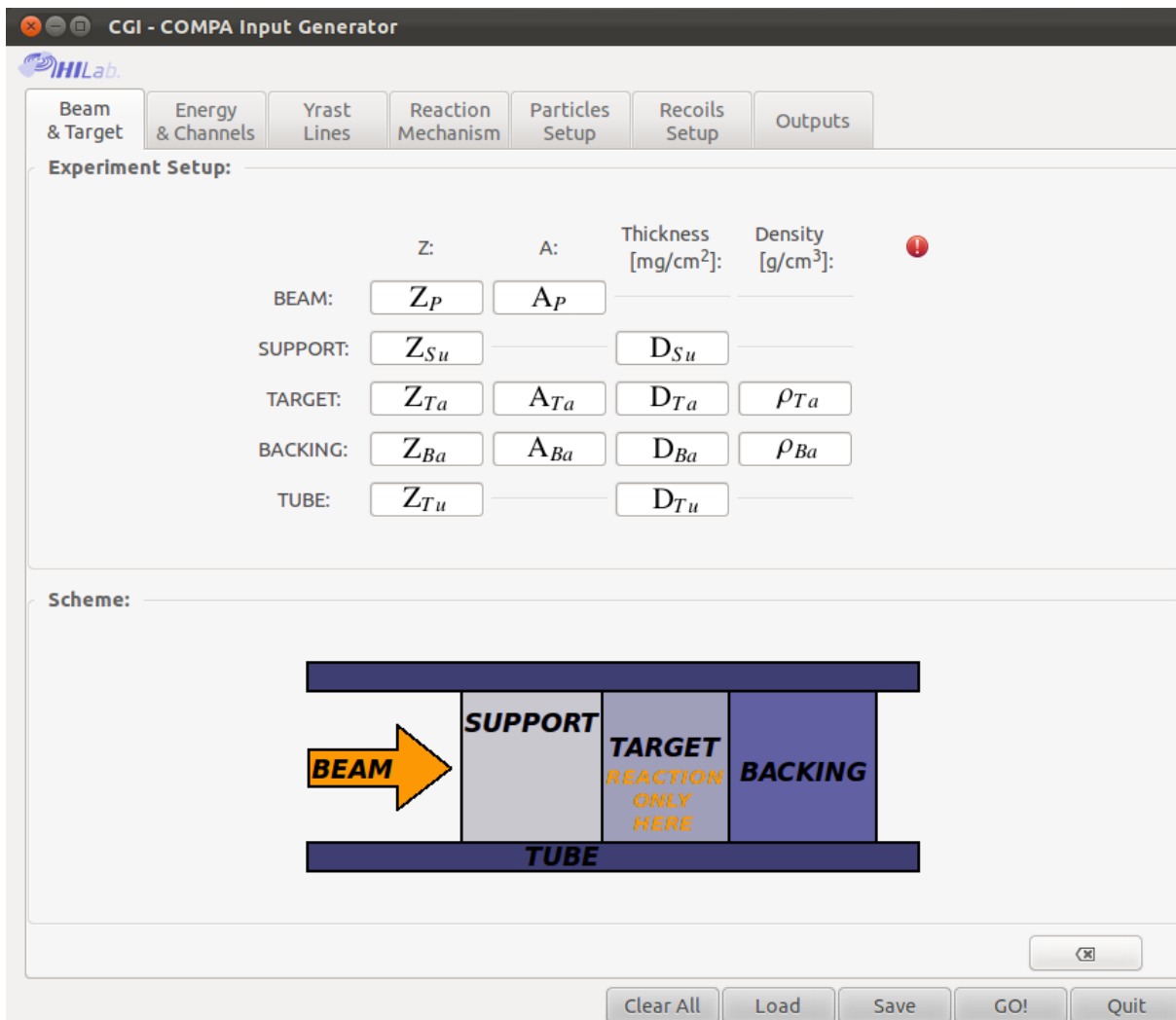


Figure 1: *

The first menu of the GUI. The Corresponding input parameters from the “compa.inp” file are marked. This is where the user defines the configuration of the experimental setup.

The beam (Z_P, A_P) hits the target ($Z_{Ta}, A_{Ta}, D_{Ta}, \rho_{Ta}$). Targets are usually self supporting, however, they are often placed on a supporting layer made of a different material. A supporting layer that is facing backwards with respect to the incident beam is called a “backing” ($Z_{Ba}, A_{Ba}, D_{Ba}, \rho_{Ba}$), while one facing forward is called a “support” (Z_{Su}, D_{Su}).

Si detectors are often used particle detection. Since they are vulnerable to heavy ions of relatively large kinetic energy, the target has to be mounted in an absorber tube (Z_{Tu}, D_{Tu}) that stops the scattered beam but lets the protons and the α particles pass through.

The reaction can only take place inside the target. The Beam can be slowed down in the support, target and backing. The evaporated particles can be slowed down in the support, target, backing and tube. The recoils can be slowed down in the target and the support. Since the LSS theory is used for recoil stopping, the mass numbers and densities of the target and the backing nuclei are also required. The SRIM2006 stopping powers are used. For stopping the beam and evaporated particles, the SRIM2006 stopping powers are used and the mass numbers of the absorbers are not required.

Author’s advice: In order to perform the calculations, at least the beam and target must be defined. It might be practical to run calculations with a self-supporting target first and then subsequently add new elements.

NOTE: BASIC CALCULATIONS CAN BE PERFORMED AFTER FILLING IN THE FIRST THREE MENUS OF THE GUI.

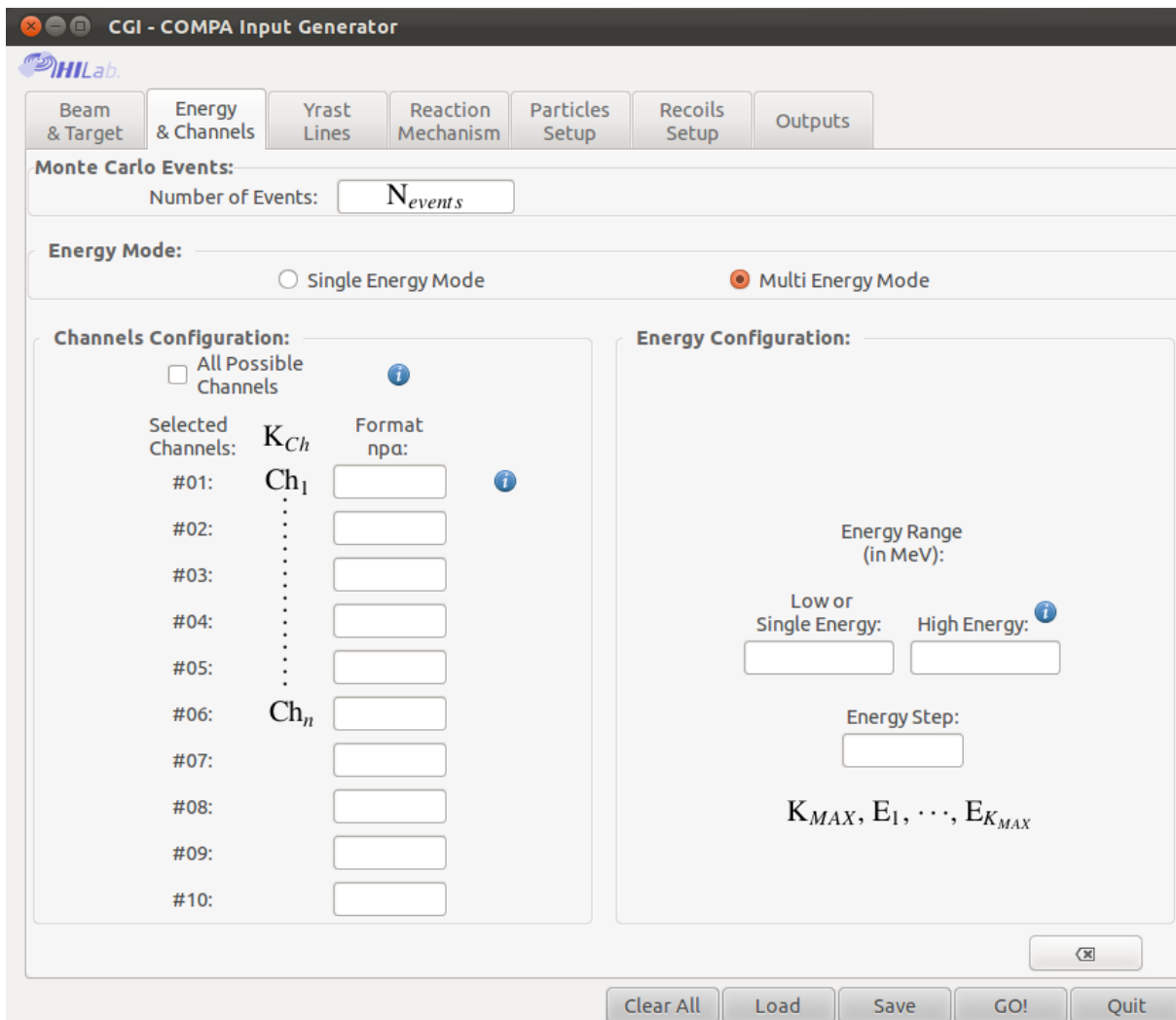


Figure 2: *

The second menu of the GUI. Corresponding input parameters from the “compa.inp” file are marked. In this menu the user defines the number of Monte Carlo events (N_{events}) for defined beam energies ($K_{MAX}, E_1, \dots, E_{K_{MAX}}$). Calculations can be performed for all possible channels (see checkbox) or certain channels of interest can be defined ($K_{Ch}, Ch_1, \dots, Ch_n$). Ch_n is a channel code in xyz format, where x is the number of neutrons, y - protons and z - α particles (see Section 2.3.1).

Two so-called “energy modes” are introduced. A “multi energy mode” for calculating the excitation functions. The user can define the ranges of energies. $N_{events} = 5 \cdot 10^4$ is a good starting value. For weakly populated channels, the number of events should be higher. The excitation functions are available in the “output/xsections/” folder (see Section Appendix G.2) and plotted in the “plots/xsection.ps” (see Section 2.5). In a “single energy mode” only one beam energy can be defined. This option is recommended when detailed information is needed and higher statistics are required. $N_{events} = 5 \cdot 10^5$ is a good starting value. The most complete description is available in the “outputs/compa.txt” file (see Section 2.4). Plots are available in the “plots/” folder (see Section 2.5).

The complete set of outputs will be created only for the last defined energy ($E_{K_{MAX}}$). If the channels were indicated manually in the second tab of the GUI, only the first will be stored (see Ch_1). If the “All possible channels” checkbox has been marked, then the info for all channels will be stored.

Author’s advice: it is necessary to define at least N_{events} , one energy and one channel or the calculations will not be performed. It is advisable to begin with the “all possible channels” option in “single energy mode” and for $N_{events} = 5 \cdot 10^5$. One can then try to switch to the “multi energy mode” and define more channels.

NOTE: BASIC CALCULATIONS CAN BE PERFORMED AFTER FILLING IN THE FIRST THREE MENUS OF THE GUI.

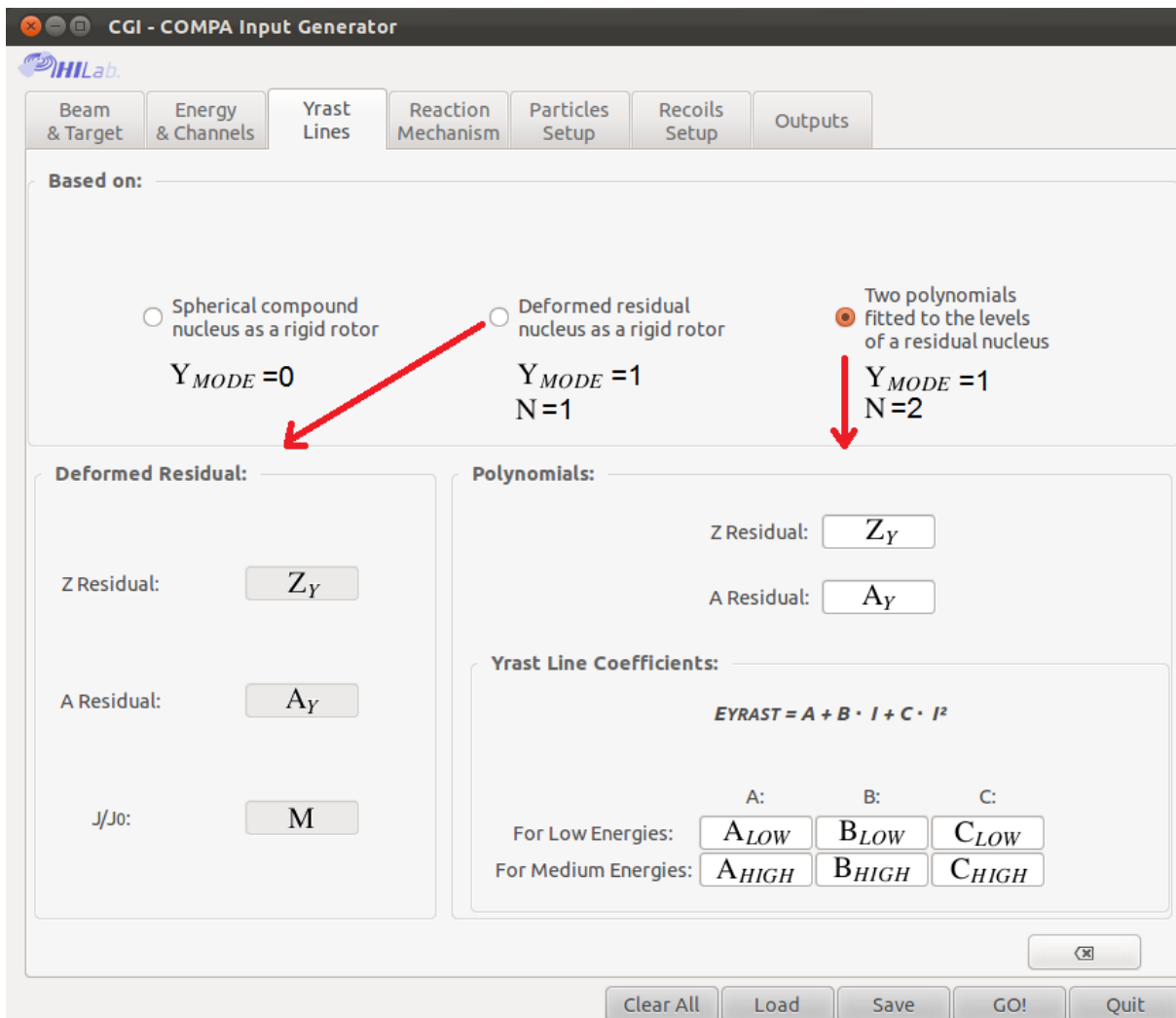


Figure 3: *

The third menu of the GUI. Corresponding input parameters from the “compa.inp” file are marked. In this menu the user defines the reference yrast line (see Appendix B). There are three possibilities available:

1. The easiest but the least exact one ($Y_{MODE} = 0$). It is assumed that the compound nucleus is spherical and treated as a rigid rotor with constant moment of inertia. This option does not require any input parameters.

2. A second possibility is to define the yrast line for a certain residual nucleus of Z_Y and A_Y atomic and mass number with moment of inertia M times bigger than the moment of a spherical nucleus of mass number A_Y . ($Y_{MODE} = 1, N = 1$)

3. It is possible to define two polynomials describing the yrast levels of a nucleus of Z_Y and A_Y atomic and mass number:

$$\begin{cases} E_{LOW}(I) = A_{LOW} + B_{LOW} \cdot I + C_{LOW} \cdot I^2, \\ E_{HIGH}(I) = A_{HIGH} + B_{HIGH} \cdot I + C_{HIGH} \cdot I^2. \end{cases}$$

For each spin the program will choose the minimum value of these two polynomials. This option sets the following parameter values: $Y_{MODE} = 1$ and $N = 2$.

Author’s advice: We suggest that calculations using option 1 are performed first. One has to remember that this is a very rough approximation. Afterwards it is possible to look through the level scheme and prepare a good fit of the yrast line (options 2. or 3.)

NOTE: BASIC CALCULATIONS CAN BE PERFORMED AFTER FILLING IN THE FIRST THREE MENUS OF THE GUI.

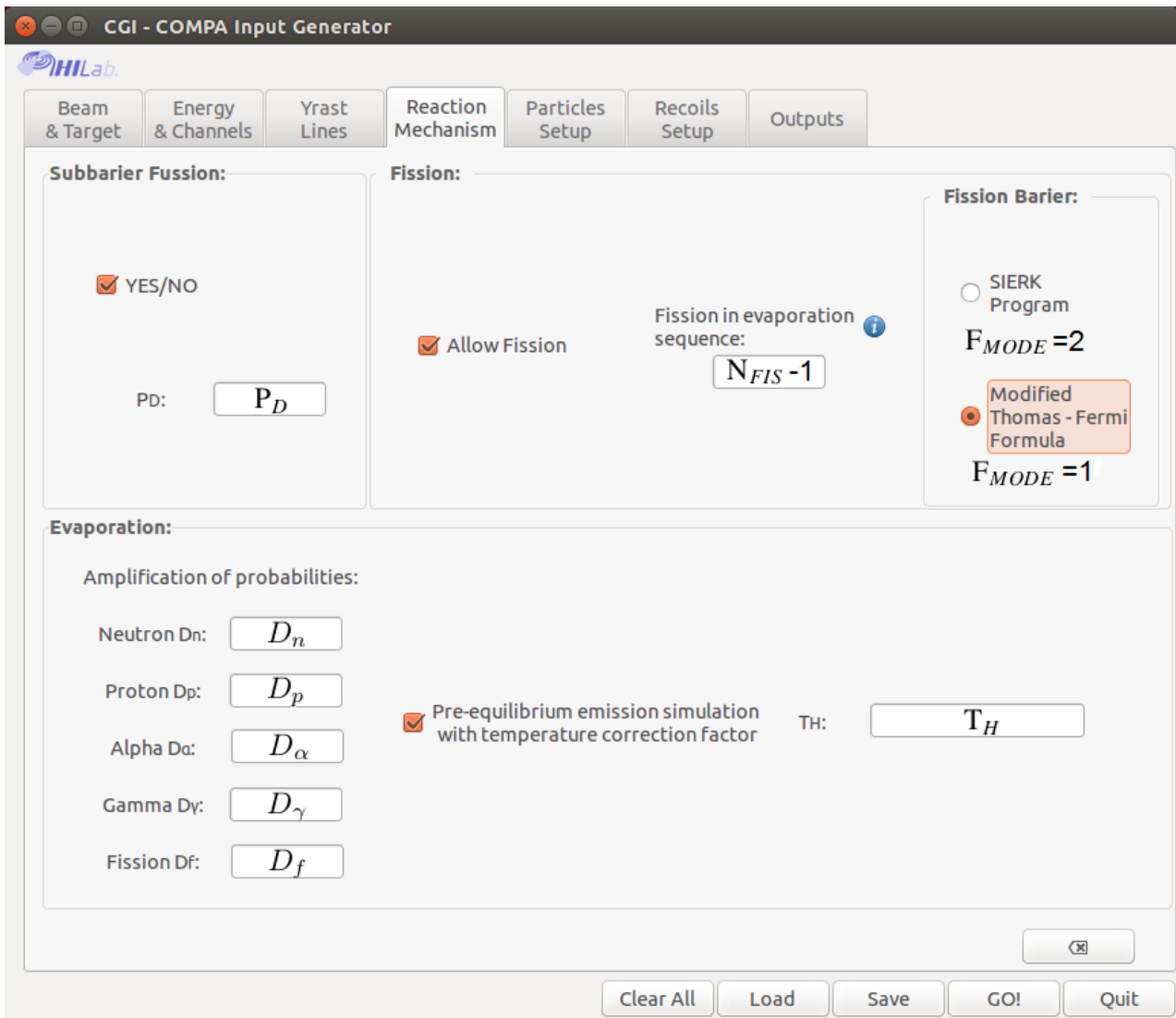


Figure 4: *

The fourth menu of the GUI. The corresponding input parameters from the “compa.inp” file are marked. In this menu the user defines the reaction mechanism.

The P_D correction factor for sub-barrier fusion calculations can be defined (see Appendix A.2).

It is possible to modify the probabilities of the decay of the compound nucleus with the parameters D_n , D_p , D_α , D_γ and D_f (see Section 3.2.5).

The model of preequilibrium particle emission can be switched on (see checkbox). The temperature correction factor T_H is described in Section 3.2.2.

The competition between evaporation and fission can be implemented (see checkbox). The user can ask whether fission is possible only for the compound nucleus ($N_{FIS} = 1$) or after a number of evaporations ($N_{FIS} = 2$ means that fission is possible also after the evaporation of the first particle). The fission barrier can be calculated with the SIERK program ($F_{MODE} = 2$) or with the Thomas-Fermi formulae [11] ($F_{MODE} = 1$).

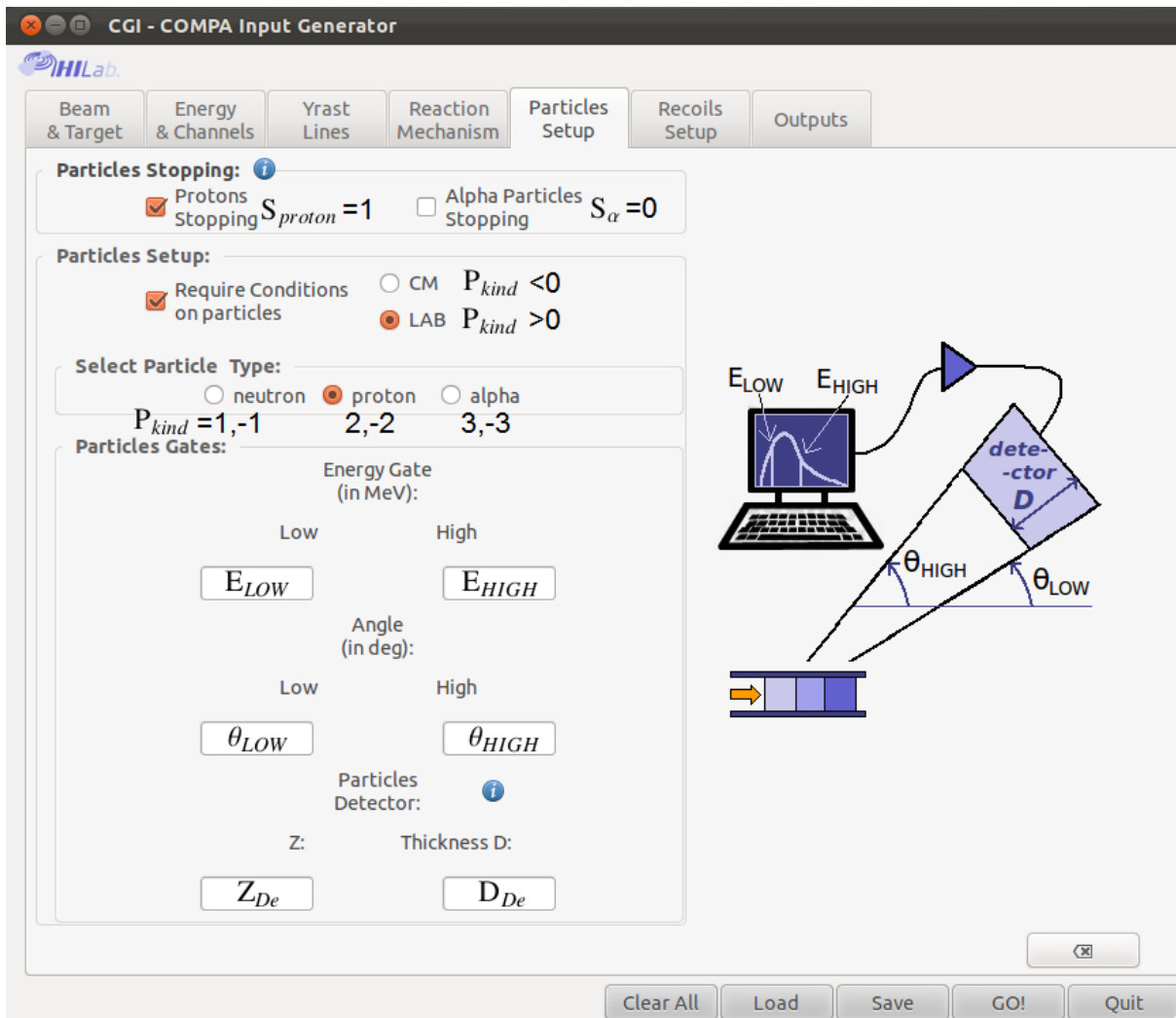


Figure 5: *

The fifth menu of the GUI. Corresponding input parameters from the “compa.inp” file are marked. In this menu the user defines the gates on the angles and energies of the emitted particles, and asks for models of stopping of protons and α particles in the passive elements of the setup.

The user can ask for protons stopping (S_{proton}) and α particles stopping (S_{α}).

It is possible to require a certain particle: neutron, proton or α particle ($|P_{kind}| = 1, 2, 3$, see Section 3.3.3).

The user can set additional gates on energies (E_{LOW} , E_{HIGH}) and gates (θ_{LOW} , θ_{HIGH}) in CM ($P_{kind} < 0$) or in LAB frame ($P_{kind} > 0$) for the requested particle.

It is possible to simulate a simple detector (Z_{De} , D_{De}) covering the angles between θ_{LOW} and θ_{HIGH} , and set the gates on the energy spectrum from E_{LOW} to E_{HIGH} (see Section 3.3.3).

The spectra are stored in the folder “outputs/particles/” (see Section Appendix G.5). Plots of particle spectra are available in “plots/evaporation.ps”. The detector spectra are available in “plots/detection.ps” (see Section 2.5).

The complete set of outputs will be created only for the last defined energy ($E_{K_{MAX}}$). If the channels were indicated manually in the second tab of the GUI, only the first will be stored (Ch_1). If the “All possible channels” checkbox has been marked (see the second menu of the GUI), then the info for all channels will be stored.

Author’s advice: A ΔE detector can cover only a limited range of angles. 30° is a reasonable limit.

NOTE: GATING AND DETECTION ARE POSSIBLE ONLY FOR ONE PARTICLE AT A TIME.

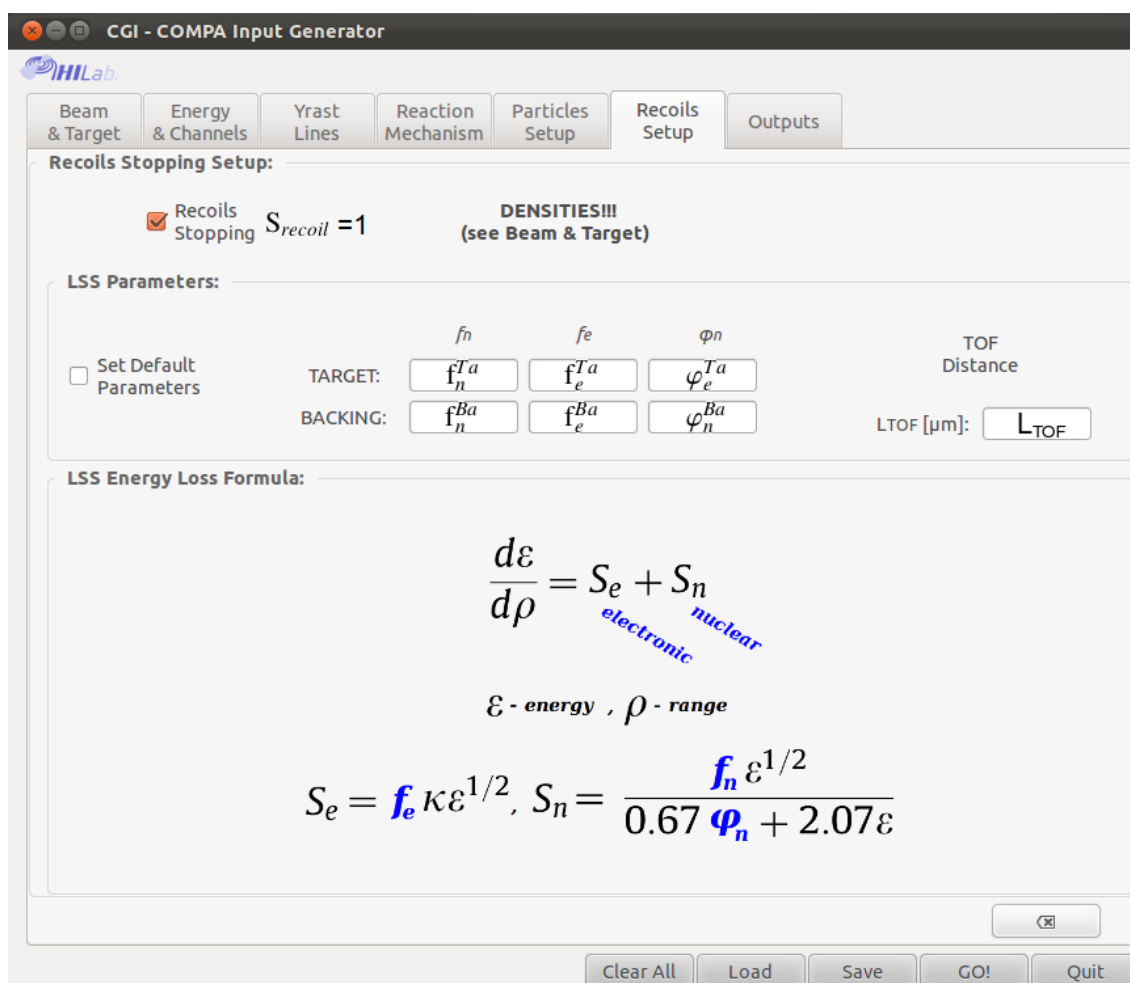


Figure 6: *

The sixth menu of the GUI. The corresponding input parameters from the “compa.inp” file are marked. This menu enables the user to control the stopping of the recoils in the target and backing (S_{recoil}). The user can define the LSS parameters (see Section 3.3.4) for the target (f_e^{Ta} , f_n^{Ta} , φ_e^{Ta}) and the backing (f_e^{Ba} , f_n^{Ba} , φ_n^{Ba}). It is possible to assume the default values of LSS parameters (see checkbox).

The distance L_{TOF} for time of flight calculations can be defined (see Section 3.3.4).

The densities of the target and backing are also required (see first menu of GUI).

The spectra are stored in folder “outputs/recoils/” (see Section Appendix G.3).

The plots of the recoil spectra are available in “plots/recoils.ps” (see Section 2.5).

The complete set of outputs will be created only for the last defined energy ($E_{K_{MAX}}$). If the channels were indicated manually in the second tab of the GUI, only the first will be stored (Ch_1). If the “All possible channels” checkbox has been marked (see the second menu of the GUI), then the info for all channels will be stored.

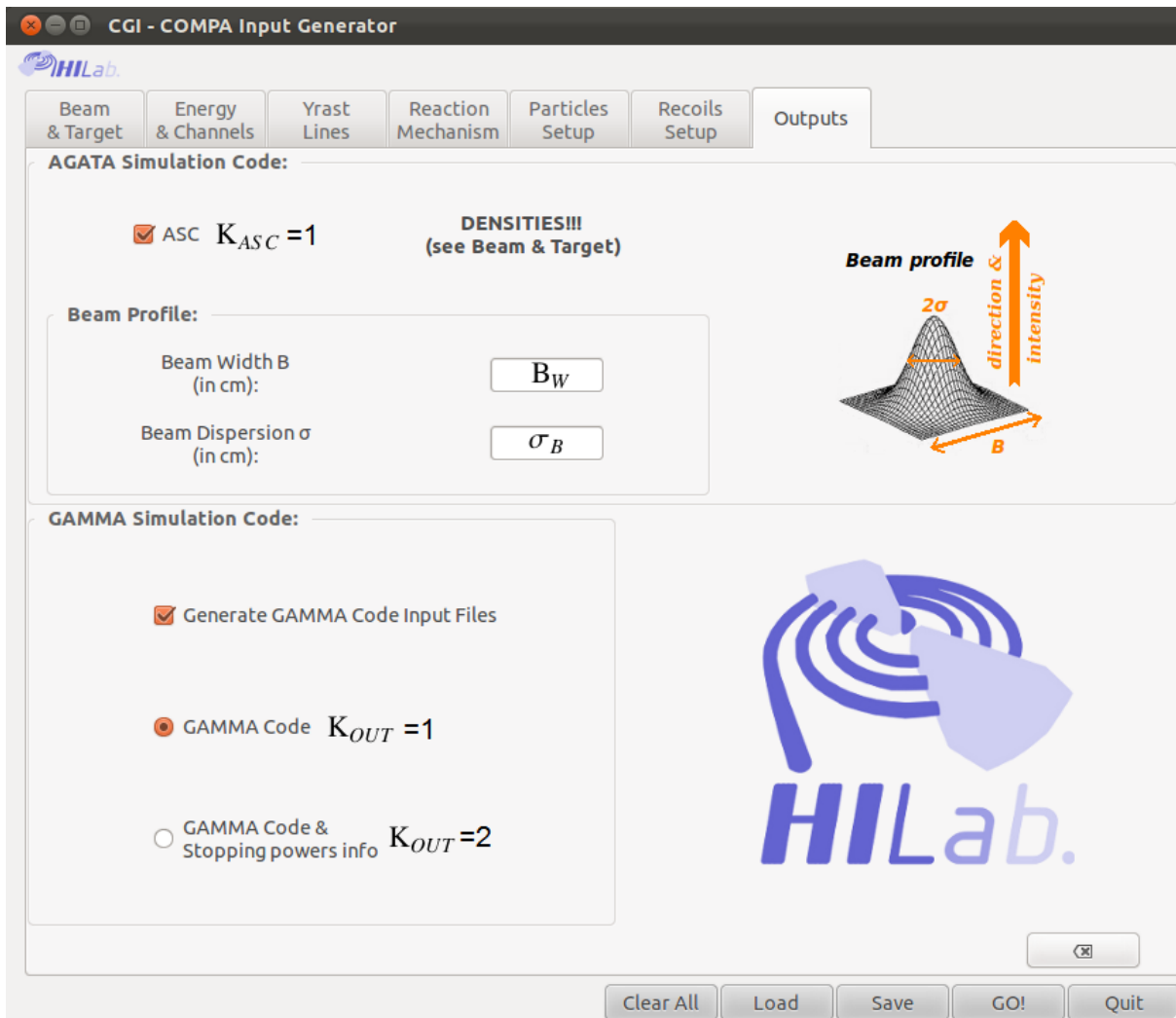


Figure 7: *

Seventh menu of the GUI. Corresponding input parameters from the “compa.inp” file are marked. This menu enables the user to ask for inputs for Agata Simulation Code (K_{OUT}) and for the GAMMA code (K_{ASC}).

For the ASC, the beam width B_W and beam dispersion σ_B must be additionally defined. The densities of the target and backing are also required (see the first menu of the GUI).

The ASC inputs are available in the “outputs/agata/” folder (see Section Appendix G.9).

GAMMA inputs are available in the “outputs/others/” folder (see Section Appendix G.10).

The complete set of outputs will be created only for the last defined energy ($E_{K_{MAX}}$). If the channels were indicated manually in the second tab of the GUI, only the first will be stored (Ch_1). If the “All possible channels” checkbox has been marked (see the second menu of the GUI), then the info for all channels will be stored.

2.3. Input files

COMPA requires the following input files (all in folder inputs/): “compa.inp”, “massdefects.inp”, “s12.inp”, “bf.inp” and “yrastinput.inp”. An exact description of their contents follows.

2.3.1. Main input - compa.inp

The main COMPA input file (“inputs/compa.inp”) has the following structure:

Z_P, A_P, Z_{Ta}, A_{Ta}
 $K_{MAX}, E_1, \dots, E_{K_{MAX}}$
 $K_{Ch}, Ch_1, \dots, Ch_n$
 D_{Ta}, N_{events}
 –More details. Change them if you want to be more exact–
 K_{OUT}
 R_{MODE}, N_{FIS}
 $S_{proton}, S_\alpha, S_{recoil}$
 $P_{kind}, E_{LOW}, E_{HIGH}, \theta_{LOW}, \theta_{HIGH}, Z_{De}, D_{De}$
 $Z_{Su}, D_{Su}, Z_{Ba}, A_{Ba}, D_{Ba}, Z_{Tu}, D_{Tu}$
 $R_0, D_{ICF}, e_f, \sigma_L, \sigma_R, \delta, F, h_\alpha$
 $C_{FAC}, L_{MAX}, N_R, P_D, R_{KA}, D_{KA}, T_H$
 $H_{CUT}, N_{CUT}, P_{CUT}, A_{CUT}$
 $D_n, D_p, D_\alpha, D_\gamma, D_f$
 I_P, I_T
 C_a, S_T, n, S_h, S_P
 $F_{MODE}, P_{FIS}, M_F, L_{SH}, B_{CUT}$
 Y_{MODE}, N, M
 Z_Y, A_Y
 $A_{LOW}, B_{LOW}, C_{LOW}$
 $A_{HIGH}, B_{HIGH}, C_{HIGH}$
 $K_{ASC}, B_W, \sigma_B, \rho_{Ta}, \rho_{Ba}$
 $f_e^{Ta}, f_n^{Ta}, \varphi_e^{Ta}$
 $f_e^{Ba}, f_n^{Ba}, \varphi_n^{Ba}$
 L_{TOF}

The parameters in the file are separated by spaces, not comas.

Most of the parameters have a specific physical meaning and they are precisely described in Section 3. The following are not described:

N_{events} - The number of Monte Carlo events for a given beam energy.

The second line of the input defines beam energies of interest. The parameters are: $K_{MAX}, E_1 \dots E_{K_{MAX}}$.
 K_{MAX} - the number of beam energies from E_1 to $E_{K_{MAX}}$, i.e. if we want to simulate three energies, 80, 90 and 100 MeV, the whole line should be as follows:

$K_{MAX} = 3, E_1 = 80, E_2 = 90, E_3 = 100.$

For only one energy, i.e. 100 MeV, the line will be:

$K_{MAX} = 1, E_1 = 100.$

Third line of the input defines the channels of interest. The parameters are: $K_{CH}, Ch_1, \dots, Ch_n$

K_{CH} is the number of channels.

Ch_1 to $Ch_{K_{CH}}$ are the channel codes. The code consists of three numbers: x, y and z :

x is the number of neutrons and $0 < x < 15$.

y is the number of protons and $0 < y < 9$.

z is the number of α particles and $0 < z < 4$.

COMPA allows evaporation of a maximum of 16 nucleons so the value of $x + y + 4z$ must not be greater than 16. I.e. 300 means the 3n channel, 1100 means the 11n channel, 1010 means the p10n channel, 231 means the $\alpha 3p2n$ channel. If we want to simulate three channels: 3n, p3n, $\alpha 2n$, the whole line should be as follows: $K_{CH} = 3, Ch_1 = 300, Ch_2 = 310, Ch_3 = 201.$

If we want to simulate one channel, i.e. 5n, the line should be as follows:

$K_{CH} = 1, Ch_1 = 500.$

If we want to simulate all channels, regardless of the number of emitted particles, the line should be as follows:

$K_{CH} = 1, Ch_1 = 0.$

Please note that the files with the most exact results can be prepared only for one channel at one beam energy, which was chosen to be the last given energy ($E_{K_{MAX}}$) and the first given channel (Ch_1). If the “All possible channels” checkbox has been marked, then the info for all channels will be stored. If only one energy and one channel are asked for, they will be considered as the last and first respectively.

The parameters K_{ASC}, B_W and σ_B are used for preparing the Agata Simulation Code input (outputs/agata/eventbyevent.mas). The Agata input will be prepared for $K_{ASC} = 1$. B_W is the beam diameter in cm. The intensity of the beam is assumed to have a planar gaussian distribution with a standard deviation σ_B [cm].

The K_{OUT} parameter is responsible for the preparation of GAMMA code input files (for $K_{OUT} = 1$, see Section Appendix G.10) or files containing stopping power coefficients taken from SRIM2006 (for $K_{OUT} = 2$, see Section Appendix G.8).

$R_{MODE}, R_0, D_{ICF}, e_f, \sigma_L, \sigma_R, \delta, F, h_\alpha$ - not active in this version.

The „examples.inp” file consists of examples of inputs used in the calculations presented in this work.

2.3.2. Yrast line information - yrastinput.inp

The yrast lines are defined in “compa.inp” file. One of the possibility is to read the yrast line from the “yrastinput.inp” file (see Appendix B), which contains the yrast line levels in the following format:

Energy(Spin=1)[MeV]

Energy(Spin=2)[MeV]

.

.
.
Energy(Spin=101)[MeV]

Please note that 100 energies must be defined, otherwise the program will stop.

2.3.3. Fission barrier - *bf.inp*

The method of fission barrier calculation is defined in “compa.inp” file. One of the possibility is to read the fission barrier from the “bf.inp” file (see Appendix E), which contains the fission barrier in the following format:

The file “bf.inp” contains the fission barrier. The fission barrier for the compound nucleus will be read from this file if asked in the “compa.inp” ($F_{MODE} = 0$). The barrier values are in the following format:

Spin[\hbar], Barrier(Spin)[MeV]
.
.
.

It is not necessary to prepare the barrier values for the whole spin range from 1 to 101 \hbar . Only the trailing edge can be input, from spin $I = I_0$ where $Barrier(I_0) < B_{CUT}$, to the spin where the fission barrier vanishes. For spin $I < I_0$, the barrier will be considered equal to B_{CUT} .

2.3.4. Mass excess table - *massdefects.inp*

File “massdefects.inp” contains a table of mass defects [10] in the following format:

A,Z,Delta(A,Z)
.
.
.

The file is available at the Atomic Mass Data Center (<http://www.nndc.bnl.gov/amdc/>)

COMPA assumes that the mass defect is equal to 0 when the mass is unknown. Therefore the “massdefects.inp” file is modified by putting 0.000001 MeV/c² for ¹²C.

2.3.5. Stopping powers for beam and light particles - *s12.inp*

File “s12.inp” contains stopping powers taken from the SRIM2006 code [4].

2.4. Aggregate output file - *compa.txt*

“compa.txt” is a text file with basic information on the simulation result. It consists of the description of the most important parameters and quantities necessary to evaluate the analysed reaction: the cross-sections, the entry states

distribution, the ranges of beam and reaction products etc. An exact description is included in the file.

COMPA generates numerous output files, which are stored in folder “outputs/”. The “compa.txt” file and the other files in folder “xsections/” contain information for all asked channels and beam energies. All remaining files contain detailed information for the first defined channel Ch_1 and for the last defined beam energy ($E_{K_{MAX}}$, see Section 2.3.1). The remaining output files are described in Appendix G.

2.5. Plots

COMPA prepares some drawings using GNUPLOT and PYTHON. In order to create an input file for GNUPLOT, the PYTHON script plots/compa.py is prepared. The input file for this script is outputs/others/input_for_python.inp (see Section Appendix G.10). To run it manually do the following:

1. Enter the plots/ folder by typing “cd plots”
 2. Generate the file plot.cmd by typing “python compa.py”.
 3. Draw postscript figures by typing “gnuplot plot.cmd”.
- The following drawings will be prepared:

1. compactplot.ps - a set of most the important figures.
2. evaporation.ps - figures related to light particle and γ emission.
3. nuclei.ps - figures related to the spin and excitation energy of the nuclei.
4. recoils.ps - figures related to the kinematics of the recoils.
5. xsection.ps - figures related to excitation functions.
6. detection.ps - figures related to particle detection.

2.6. Source files, list of modules and block scheme

In order to make the project manageable, the source is split into main program and 6 files : *read.cpp*, *momenta.cpp*, *evapor.cpp*, *fission.cpp*, *kinematics.cpp* and *utils.cpp*. A corresponding header files (*.h*) are prepared. The vast majority of code functions are documented with comment lines referring to formulae described in this manual. The files and functions are listed and briefly described below.

2.6.1. *read.cpp*

File consist of the following functions:

1. READ - reading from compa.inp.
2. MASS_EXCESS - reading from massdefects.inp
3. YRAST_LINE - reading from compa.inp, preparation of the yrast line.

2.6.2. *momenta.cpp*

File consist of the following functions:

1. TL_AND_SE
- calculations of the transmission coefficients and the cross sections as a function of input angular momentum.
2. TLSE - subfunction of TL_AND_SE.
- 3,4. CROSS_SECTION1, CROSS_SECTION2 - subfunctions of TLSE. Calculations of the transmission coefficients for fusion induced by ions of mass number greater than 5 (based on Appendix A).
5. CROSS_SECTION3 - subfunctions of TLSE. Calculations of the transmission coefficients for fusion induced by neutrons, protons, deuterons, tritons, α particles and ${}^3\text{He}$ (based on Appendix A.3).

2.6.3. *evapor.cpp*

File consist of the following functions:

1. LEVEL_DENSITIES - calculations of the level density as a function of excitation energy.
2. SHELL_CORRECTION - calculations of Δ_{sh} value for the level densities (based on Appendix F).
3. TEMPERATURE - calculations of the temperature as a function of the excitation energy (based on Appendix F.1).
4. PART_EVAPOR_BASE - preparation of data for neutron, proton and α particle evaporation (based on Section 3.2.1).
5. FORMX - preparation of data for the „hot spot” particle emission (based on Section 3.2.2).
6. E1_GDR_BASE - preparation of data for E1 gamma emission (based on Section Appendix D).
7. PAIRING_SHIFT - calculations of pairing shift P_C for the yrast line (based on Appendix B.2).
8. TOTAL_CROSS_SECTION - calculations of the integrated cross section and preparation of data for projectile energy calculations (based on Section 3.1).
9. PROJECTILE_ENERGY - calculations of the projectile energy and the reaction point (based on Section 3.1).
10. COMPOUND_SPIN - calculations of the spin of the compound nucleus (based on Section 3.1).
- 11,12,13. NEUTRON_PROB, PROTON_PROB and ALPHA_PROB - calculations of the probability of neutron, proton and α particle evaporation (based on Sections 3.2.1, 3.2.2).
14. EVAPOR - subfunction for NEUTRON_PROB, PROTON_PROB and ALPHA_PROB.
15. E1_PROB - calculations of the probability of E1 gamma emission (based on Section 3.2.3).
- 16,17,18. NEUTRON_OUT, PROTON_OUT and ALPHA_OUT - realization of neutron proton and α particle evaporation (based on Section 3.2.1).
19. EVAPOR_OUT - subfunction for NEUTRON_OUT, PROTON_OUT and ALPHA_OUT.
20. EVAPOR_OUT_HOTSPOT - subfunction for NEUTRON_OUT, PROTON_OUT and ALPHA_OUT when „hot spot” emission is realized (based on Section 3.2.2).

21. E1_OUT - realization of E1 gamma emission (based on Section 3.2.3).

2.6.4. *fission.cpp*

File consist of the following functions:

1. FISSION_BASE - preparing fission barrier
2. BARIERA - **TBD** (To Be Described)
3. FB - **TBD**
4. BARFIT - **TBD**
5. LPOLY - **TBD**
6. FISSION_MS - **TBD**
7. FISSION_PROB - calculating the probability of fission

2.6.5. *kinematics.cpp*

File consist of the following functions:

1. KINEMATICS - calculating the reaction products velocity vectors, taking into account stopping in the target, support, backing and tube.
2. COSINE - **TBD** (To Be Described)
3. PARTICLE_SLOW - **TBD**
4. BEAM - **TBD**
5. PARTICLE_STOP_BASE - reading from s12.inp, preparing data for proton and α stopping in the target, support, backing and tube
6. STOP - **TBD**
7. IFOER - **TBD**
8. GLAD2 - **TBD**
9. HISTOP - **TBD**
10. PSTOP - **TBD**
11. INIT_TARGET - reading from compa.inp, preparing data for recoils stopping in the target.
12. INIT_BACKING - reading from compa.inp, preparing data for recoils stopping in the backing
13. CONST - **TBD**
14. TVVT - **TBD**
15. RVVR - **TBD**
16. RECOIL_SLOW - **TBD**
17. IVCO2 - **TBD**
18. ICOFU - **TBD**
19. ICOFF - **TBD**

2.6.6. *utils.cpp*

File consist of the following functions:

1. randomizer - GSL mezzanine twister random generator type: mt19937 (header gsl_rng.h).
2. FIT2 - linear interpolation for two points.
3. FIT3 - GSL spline functions (headers gsl_errno.h and gsl_spline.h).
4. FERF - calculations of the error function (gauss integral).

2.6.7. *Block scheme*

The block diagram with general flow chart is presented in Fig. 8.

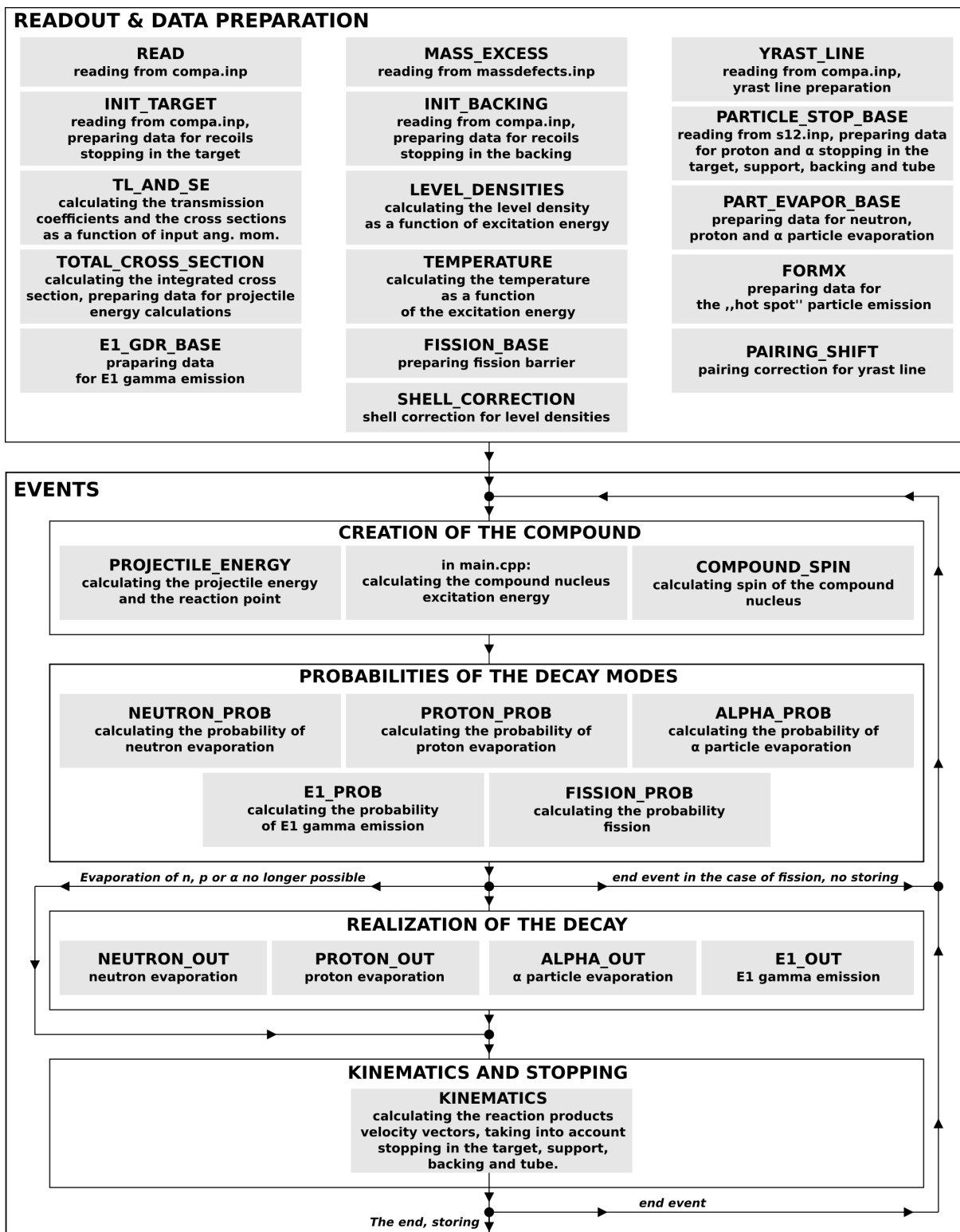


Figure 8: The code initially reads all the necessary data from input files and fulfils arrays consisting of useful physical quantities, which have to be quickly accessible while events are processed (ie. nuclear level densities, transmission coefficients etc.) The event begins with creation of compound nucleus somewhere in the target. At this point the probabilities of the following decay modes are calculated: emission of neutron, proton, α particle, E1 γ quantum or fission. In the case of fission event is stopped. In the case of emission, particle parameters are stored in a buffer, new nucleus is created and probabilities of decay modes are calculated again. When evaporation of neutron, proton, α particle is no longer possible, calculations of kinematics and stopping of the reaction products in target material occur. After declared number of events all the data is stored and program finishes computation.

3. Physics

3.1. Creation of the compound nucleus

The Statistical Theory determines the entrance angular momentum for fusion by appeal to the transmission coefficients. For a given projectile energy E , the cross-section is calculated using the standard expression:

$$\sigma_E(L) = \pi \lambda^2 T_E^{D, L_{1/2}}(L) \cdot (2L + 1), \quad (1)$$

where L is the relative angular momentum. The total cross-section is given by

$$\sigma_E = \sum_L \sigma_E(L). \quad (2)$$

In this work the transmission coefficients are calculated using the general expression:

$$T_E^{D, L_{1/2}}(L) = \left(1 + \exp\left(\frac{L(L+1) - L_{1/2}(L_{1/2}+1)}{D}\right) \right)^{-1}. \quad (3)$$

For heavier projectiles with a mass number greater than 5, parameters D and $L_{1/2}$ are calculated using the Blatt-Weisskopf approximation [23] and the empirical formula proposed by Kailas et al. [24]. For projectiles like neutrons, protons, deuterons, tritons, α and ${}^3\text{He}$, the values of D and $L_{1/2}$ are calculated in the framework of the optical model [25]. Appendix A contains a detailed description of the calculation of the transmission coefficients.

The cross-section dependence on the entrance angular momentum is calculated (Eq. 1) and used as a probability distribution in order to determine the entrance angular momentum of the projectile. Both the transmission coefficient and the probability distribution for the ${}^{12}\text{C}+{}^{24}\text{Mg}$ system are shown in Fig. 9.

In order to calculate the spin of the compound nucleus it is necessary to consider the spins of both the projectile and the target. The spin of the projectile I_P and the target I_T are input parameters for the code. They are added to the relative momentum according to the spin addition rules.

3.1.1. Summary - input parameters

The following parameters were introduced in this section:

I_P - the spin of the projectile (ground state).

I_T - the spin of the target (ground state).

3.2. Competition between particle evaporation, gamma emission and fission

Once the compound nucleus is created, further de-excitation may occur by means of gamma or light particle emission. The compound nucleus can also break apart. COMPA takes into account only the possibility of neutron, proton and α particle evaporation, E1 gamma emission

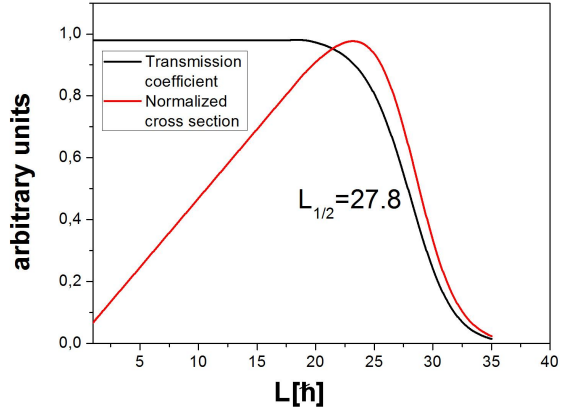


Figure 9: Transmission coefficient in the ${}^{12}\text{C}+{}^{24}\text{Mg}$ system at 150 MeV ${}^{12}\text{C}$ energy (black) and normalized cross-section calculated with Eq. 1 (red).

and fission. Probabilities for each of these processes are calculated. In the case of fission, the event finishes. In the case of particle evaporation or gamma emission, another set of probability distributions is calculated in order to determine the spin of the nucleus after the emission and the kinetic energy of the emitted particle. This procedure is repeated until the evaporation of light particles becomes impossible. The program allows evaporation of a maximum of 16 nucleons.

Before evaporation, gamma emission or fission occurs, the nucleus has spin I_i and excitation energy E_i^* . After gamma emission or evaporation of a particle of energy e and angular momentum l , the nucleus has spin I_f and excitation energy E_f^* . E_i and E_f are energies over the yrast line¹:

$$E_i = E_i^* - E_{YR}(I_i), E_f = E_f^* - E_{YR}(I_f). \quad (4)$$

3.2.1. Evaporation

Calculations are easier to follow with Fig. 10 where a schematic drawing of the decay is presented. The probability of such a decay is proportional to the energy integrated transmission function $F_l^{I_i, I_f}$ (see Eq. 8.9 in ref. [26]), given by the formula:

$$F_l^{I_i, I_f}(e) = \int_0^e T_l(\epsilon) \rho(E_f) d\epsilon, \quad (5)$$

where $T_l(\epsilon)$ is the transmission coefficient for particle evaporation². $\rho(E_f)$ is the level density³. E_f depends on ϵ :

$$E_f = E_M - \epsilon, \quad (6)$$

¹Preparation of the yrast line $E_{YR}(I)$ is described in Appendix B

²Calculation of the transmission coefficients for evaporated particles is described in Appendix C

³Calculation of level densities is described in Appendix F

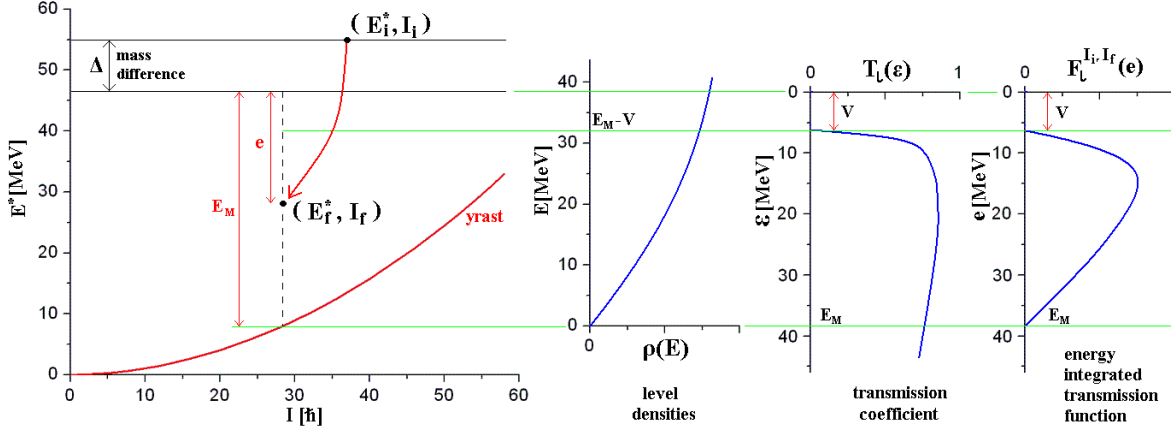


Figure 10: Schematic drawing of the decay of a highly excited nucleus by particle emission. A nucleus of spin I_i and energy E_i decays to another nucleus of spin I_f and energy E_f by emission of a light particle of energy e and angular momentum l . In order to calculate the energy integrated transmission function (right) one needs to know the level densities and transmission coefficients. The mass difference between initial and final nuclei is Δ .

so we have

$$F_l^{I_i, I_f}(e) = \int_0^e T_l(\epsilon) \rho(E_M - \epsilon) d\epsilon. \quad (7)$$

E_M is given by

$$E_M = E_i^* - \Delta - E_{YR}(I_f), \quad (8)$$

where Δ is the mass difference between the initial and final nucleus (see Fig. 10). Taking into account the level density at the initial state and Heisenberg's uncertainty principle, we obtain the probability of an emission $P_l^{I_i, I_f}$:

$$P_l^{I_i, I_f} = \frac{1}{\tau} \frac{1}{\rho(E_i)} F_l^{I_i, I_f}(E_M) \left[\frac{1}{s} \right]. \quad (9)$$

the $\frac{1}{\tau}$ factor is calculated as $\frac{1MeV}{1\hbar}$. The code takes into account the evaporation of particles carrying maximum angular momentum equal to $19\hbar$. Finally we obtain the total probability of particle emission, which is proportional to P_{part} :

$$P_{part} = \sum_{l=0}^{19} \sum_{I_f=I_i-l}^{I_i+l} P_l^{I_i, I_f}. \quad (10)$$

When it comes to evaporation of a given particle, the $P_L^{I_i, I_f}$ probabilities are used to determine the particle angular momentum l and the spin of the nucleus after emission. The $F_l^{I_i, I_f}(e)$ dependence is used as a probability distribution to determine the particle energy e in the CM system. It also allows us to find the excitation energy of the nucleus after the evaporation.

Three values proportional to the probability of a particle evaporation are calculated using Eq. 10: P_n for neutron, P_p for proton and P_α for α particle evaporation. Fig. 11a illustrates the energy spectra of the evaporating light particles in the CM system in the $^{64}\text{Ni} + ^{64}\text{Ni}$ reaction

at 260 MeV beam energy. The next stage is to calculate the emission angle of the evaporated particle. For the angular distribution, the following approximation is used (see Eq. 8.39 in ref. [26]):

$$\frac{\delta^2 \sigma_{\alpha\beta}}{\delta \epsilon_\beta \delta \Omega_\beta} \approx \frac{d\sigma_{\alpha\beta}}{d\epsilon_\beta} \frac{1}{4\pi} (1 + A_2 P_2(\cos \theta_\beta)), \quad (11)$$

where

$$A_2 = \frac{l \cdot (l+1) \cdot I_i \cdot (I_i+1)}{12 \cdot J^2 \cdot T^2(E_i)} \quad (12)$$

and l is the angular momentum of the particle, I_i is spin of the nucleus, J is nuclear moment of inertia and is deduced from the yrast line shape (see Appendix B) and T is the nuclear temperature (see Appendix F). In Fig. 11b the angular distributions of particles from the $^{64}\text{Ni} + ^{64}\text{Ni}$ reaction are shown. Distributions of the angular momentum carried away by the evaporated particles are shown in Fig. 11c.

The kinematics can be transformed to the laboratory frame. The distributions obtained are presented in Fig. 12.

Each evaporating particle changes the kinetic energy of the nucleus and the direction of its flight. The nuclei slow down in the passive elements of the setup. Information on the calculation of kinematics and the stopping procedures, as well as some simulated particle spectra, can be found in Section Appendix G.8.

3.2.2. "Hot spot" particle emission

The incomplete fusion mechanism is just one explanation of preequilibrium particle emission. In this work we propose a simple model of so-called "hot spot" [27] emission. It is based on the assumption that the first particle escapes from the coalescing system. In such a system,

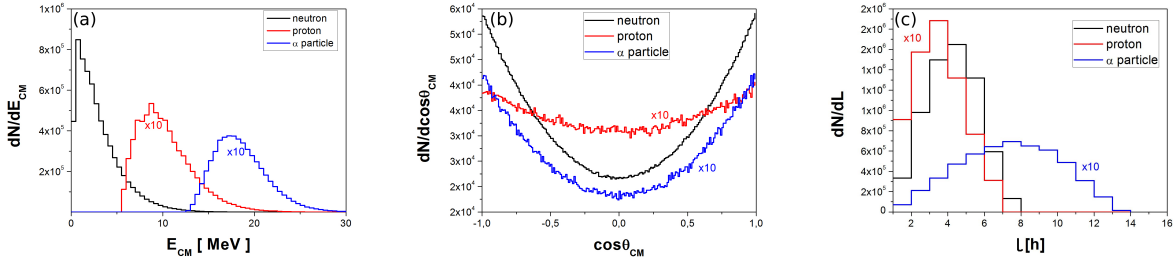


Figure 11: Evaporation of neutrons (black), protons (red) and α particles (blue) in the $^{64}\text{Ni}+^{64}\text{Ni}$ reaction at 260 MeV and $0.5\text{mg}/\text{cm}^2$ target thickness; a.) energy spectra in CM; b.) angular distribution, c.) angular momentum distribution. Particle stopping in the target material was not taken into account.

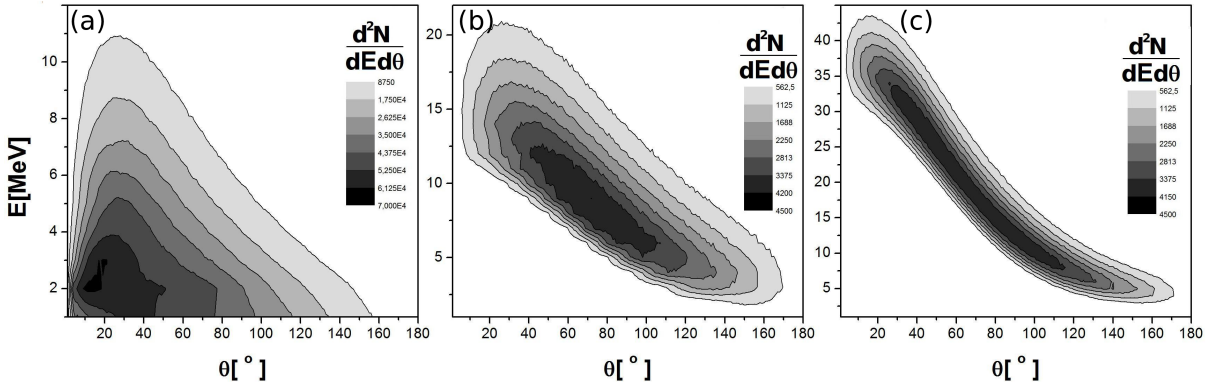


Figure 12: Energy vs angle in the Laboratory frame for evaporating (a) neutrons, (b) protons and (c) α particles produced in the $^{64}\text{Ni}+^{64}\text{Ni}$ reaction at 260 MeV and $0.5\text{mg}/\text{cm}^2$ target thickness. Particle stopping in the target material was not taken into account.

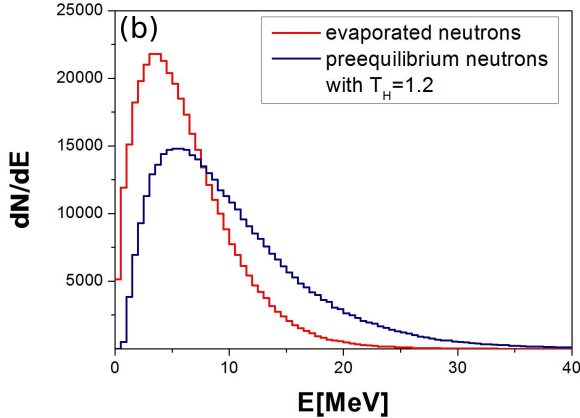


Figure 13: Comparison of the calculated spectra of the first neutrons emitted in the $^{20}\text{Ne}+^{122}\text{Sn}$ reaction at 150 MeV: preequilibrium with $T_H = 1.2$ (blue) and evaporated (red).

equilibrated areas of higher temperature appear locally. Therefore the shape of the spectra is similar to the evaporation case, but the energies are higher. It is thus necessary to introduce temperature correction factor T_H . Since the angular momentum L is determined with probabilities cal-

culated by means of Eq. 10, the following assumptions are made. The angular momentum l and nuclear temperature T are modified:

$$l \Rightarrow l \cdot \sqrt{T_H}, \quad T \Rightarrow T \cdot T_H. \quad (13)$$

The kinetic energy of the first emitted particle is calculated using the formula

$$e = \epsilon \cdot (E_M - V)T^2 + V, \quad (14)$$

where ϵ is calculated by a Maxwell-like probability distribution. Finally, the angular distribution is calculated with the new l and T values by Eq. 12. Fig. 13 illustrates a comparison between two neutron spectra: the evaporated ones and those emitted in a preequilibrium mechanism, with $T_H = 1.2$ used in calculations. The preequilibrium spectrum is much wider, with the higher mean energy value. T_H is a code input parameter; the correction will be realised for $T_H > 1$, otherwise the first particle will be simulated using the evaporation mechanism.

3.2.3. Gamma emission

The probability of the emission of a gamma quantum of energy e and XL multipolarity is proportional to the $F_{XL}^{I_i, I_f}$ function, provided by the equation (see Eq. 8.12 to

Eq. 8.14 in ref. [26]):

$$F_{XL}^{I_i, I_f}(e) = \int_0^e T_{XL}(\epsilon) \rho(E_f - \epsilon) d\epsilon. \quad (15)$$

$T_{XL}(\epsilon)$ is the transmission coefficient for gamma emission⁴. Taking into account the level density of the initial state we conclude that the probability of an emission is proportional to $P_{XL}^{I_i, I_f}$:

$$P_{XL}^{I_i, I_f} = 10^{12} \frac{1}{\rho(E_i)} F_{XL}^{I_i, I_f}(E_M) \left[\frac{1}{s} \right], \quad (16)$$

where

$$E_M = E_i^* - E_{YR}(I_f). \quad (17)$$

The $\frac{1}{\tau}$ normalisation factor, present in the case of particle evaporation, is replaced by a constant value of $10^{12} \left[\frac{1}{s} \right]$. Normalisation with a $\frac{1}{\tau}$ factor Eq. 16 leads to unrealistic values for the probabilities. The choice of a constant value of 10^{12} provides a good description of experimental data.

COMPASS allows only E1 transitions. Such an approach is reasonable since COMPASS finishes processing the event when the excitation energy reaches the quasi-continuum area, where evaporation is no longer possible and E2 and M1 resonances become competitive. De-excitation via E1, E2 and M2 γ quanta in the quasi-continuum area is handled by the next piece of the software suite - an application called GAMMA [5, 6, 2].

The total probability of an E1 gamma emission is provided by the equation:

$$P_\gamma = \sum_{I_f=I_i-1}^{I_i+1} P_{E1}^{I_i, I_f}. \quad (18)$$

COMPASS assumes that the probability of a decay into each of the three possible final states of $I_i - 1, I_i, I_i + 1$ spins is equally probable. Another simplification assumed is that E1 γ quantum emission always leads to an $I_f = I_i$ state. The total probability of an E1 emission is then:

$$P_{E1} = 3P_{E1}^{I_i, I_i}. \quad (19)$$

The function $F_L^{I_i, I_f}(E_\gamma)$ is calculated (Eq. 15) and used as the probability distribution for the determination of the emitted γ ray energy. The angular distribution of γ quanta is assumed to be isotropic.

Fig. 14 illustrates the calculated gamma spectra for the $^{20}\text{Ne} + ^{122}\text{Sn}$ reaction. This case is widely discussed in Appendix D.

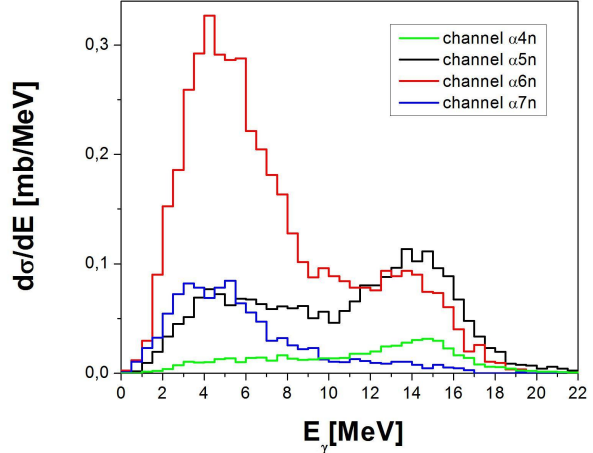


Figure 14: Simulated γ spectra for four different channels in the $^{20}\text{Ne} + ^{122}\text{Sn}$ reaction at 150 MeV. The smaller the number of evaporated particles, the stronger the E1 Giant Resonance (maximum at ≈ 14 MeV).

3.2.4. Fission

In order to calculate the fission probability, we introduce the energy above the fission barrier:

$$E_b(I_i) = E_i - B_f(I_i), \quad (20)$$

where B_f is the fission barrier.⁵ The probability of fission is provided by the equation (see Eq. 8.16 in ref. [26]):

$$P_f = \frac{1}{\tau} \frac{1}{\rho(E_i)} \sum_{J=0}^{L_f} \sum_{L=0}^J \left(\frac{2}{\pi K_0^2} \right)^{1/2} \cdot \exp\left(\frac{(L - I_i)^2}{2K_0^2} \right) \cdot \int_0^{E_b(I_i)} \rho(\epsilon) d\epsilon \left[\frac{1}{s} \right], \quad (21)$$

where the $\frac{1}{\tau}$ factor is calculated as $\frac{1MeV}{\hbar}$, $\rho(E_i)$ is the level density of the initial state and L_f is the nuclear spin at the moment the fission barrier disappears. K_0 is related to the nuclear temperature T and the moment of inertia J_{eff} :

$$K_0^2 = \frac{T(E_i) J_{eff}}{\hbar^2}, J_{eff} = \frac{J_\perp J_\parallel}{J_\perp - J_\parallel}. \quad (22)$$

J_\parallel and J_\perp are the parallel and perpendicular moments of inertia at the saddle point configuration, respectively. In COMPASS, J_{eff} is calculated in the following way:

$$J_{eff} = J \frac{P_{FIS}}{1 - P_{FIS}}, \quad (23)$$

where the static moment of inertia J is calculated based on the yrast line (see Appendix B) and P_{FIS} is a code

⁴Preparation of transmission coefficients for gamma emission is described in Appendix D

⁵Fission barrier calculations are described in Appendix E

parameter.

It must be noted that fission is also possible after subsequent particle evaporation. In Fig. 15, the energy vs spin diagram for nuclei that have fissioned is shown. Fission of the compound nucleus is, of course, the most probable scenario, but the nucleus can also decay after the first or second evaporation. The parameter N_{FIS} is introduced to control this part of the calculation. The user can ask whether fission is possible only for the compound nucleus ($N_{FIS} = 1$) or after a number $N_{FIS}-1$ of evaporations. N_{FIS} is a code parameter.

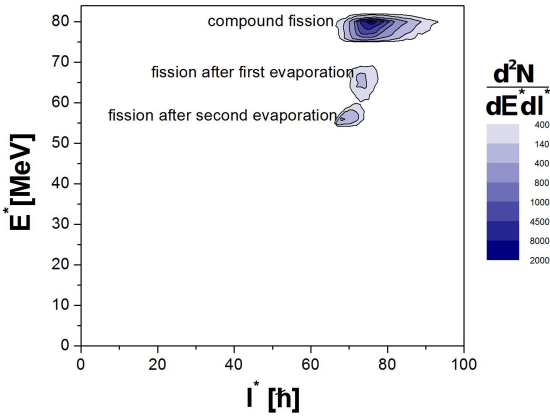


Figure 15: Energy vs spin diagram for nuclei that fission after fusion of ^{40}Ar and ^{109}Ag .

The fusion barrier can be calculated by the SIERK [28] program or with Thomas-Fermi formulae [11] or can be read from a separate input file.

3.2.5. Amplification of the probabilities

Five values proportional to the probabilities of the different decay modes of the compound nucleus are calculated: P_n , P_p and P_α for the evaporation of neutrons, protons and α particles (see Eq. 10), P_γ for the E1 γ emission (see Eq. 16) and P_f for the fission process (see Eq. 21). Since the statistical model quite often doesn't reproduce the cross sections for weakly populated and exotic channels, it is possible to modify these probabilities with D_n , D_p , D_α , D_γ and D_f coefficients, with the following rule: $P_i \rightarrow D_i \cdot P_i$, where the D_i coefficients are input parameters. Such an approach allows the experimental data to be reproduced in cases where precisely calculated probabilities P_i fail to describe the experimental values.

3.2.6. Entry state distribution

The event ends when the evaporation of neutrons, protons or α particles is no longer possible. All information is stored and a new event begins with the creation of a compound nucleus. After evaporation the spin and excitation

energy of the residual nucleus are known. The so-called *entry state* distributions for the $^{122}\text{Sn}(^{20}\text{Ne},\alpha\text{n})^{132}\text{Ce}$ reaction are shown in Fig. 16. The calculations were performed for a 5.4 mg/cm^2 thick ^{122}Sn target and a set of four different ^{20}Ne beam energies: 140 MeV (Fig. 16a), 150 MeV (Fig. 16b), 160 MeV (Fig. 16c) and 170 MeV (Fig. 16d).

Knowledge of the *entry state* distribution is very useful at the planning stage of the experiment. Given such a distribution, the user can adjust the beam energy to populate the residual nuclei of the expected spin and excitation energies values.

In the case of RDM and DSAM measurements, where the result strongly depends on the *side feeding* time, it is recommended to populate states close to the yrast line. The *side feeding* times are then relatively short. In the case presented the beam energy of 140 MeV (Fig. 16a) seems optimal for evaluating the lifetimes.

3.2.7. Summary - input parameters

The following parameters were introduced in this section:

N_{FIS} - Allowing fission or not. For $N_{FIS} = 0$ fission is not possible, for $N_{FIS} = 1$ fission is possible for the compound nucleus, for $N_{FIS} = 2$ fission is possible for a compound nucleus and after the evaporation of the first particle, etc. Default is $N_{FIS} = 1$.

F_{MODE} - method of fission barrier calculation. $F_{MODE} = 2$ - with SIERK code, $F_{MODE} = 1$ - from Thomas-Fermi formulae, $F_{MODE} = 0$ - from bf.inp input file. Default is $F_{MODE} = 2$.

P_{FIS} - coefficient describing the ratio of the parallel to perpendicular moment of inertia of the fissioning nucleus. Default is $P_{FIS} = 1$.

T_H - Temperature correction factor for preequilibrium emission. Default is $T_H = 1$ (no correction).

3.3. Experimental setup and products stopping in the material.

COMPA pays special attention to the processes of slowing down that occur in the solid targets and other passive elements of the experimental setup. A schematic drawing of the setup is given in Fig. 17. It is possible to include the

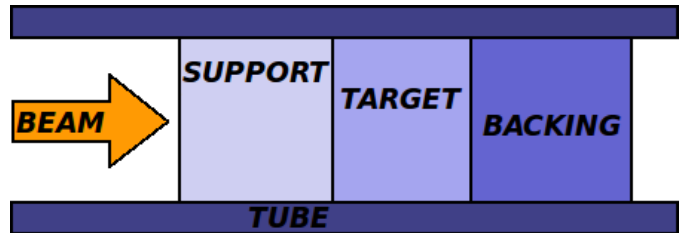


Figure 17: Configuration of experimental setup. Often used elements are shown.

four standard elements often present in nuclear reactions:

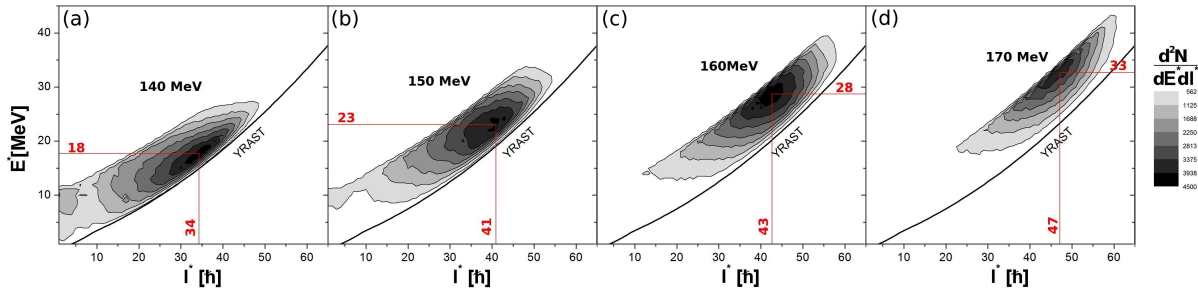


Figure 16: Calculated energy vs spin (*entry state*) diagrams for $^{122}\text{Sn}(^{20}\text{Ne}, \alpha 6n)^{132}\text{Ce}$ reaction at four different ^{20}Ne beam energies: 140 MeV (a), 150 MeV (a), 160 MeV (c) and 170 MeV (d). ^{122}Sn target thickness was 5.4 mg/cm^2 .

target, support, backing and a covering tube.

While thick targets are usually self-supporting, thin ones need to be placed on supporting layers made of a different material. If the supporting layer is facing away from the incident beam, it is called a “backing”, if it is facing towards of, we call it a “support”. A backing is often used in the Doppler Shift Attenuation Method (DSAM) and Recoil Distance Method (RDM).

When it comes to the particle detection, Si detectors are often used. Since they are vulnerable to heavy ions of relatively large kinetic energy, the target has to be mounted in an absorber tube. Its role is to stop the scattered beam on the one hand and let the protons and α particles pass through on the other.

The calculations can take into account the stopping of the beam, the charged particles, and the recoils.

3.3.1. Beam stopping

The beam can be slowed down in the support before entering the target and in the target itself. COMPA, however, only computes the reaction in the target material. In the first step the possible energy range is found. When the target is thick enough the projectile can slow down below the Coulomb barrier or pass through the target. Given a range of possible energies, the cross-section dependence on energy is used as a probability density, which allows the projectile kinetic energy to be determined. Once the energy is determined, it is possible to find the reaction point. All the necessary data (the ranges, energy losses, etc.) are taken from the SRIM code [4]. Straggling of the beam is not taken into account - the beam does not change its direction, either when moving inside the support or inside the target. This approach is reasonable in the typical energy ranges characteristic for heavy-ion induced reactions.

Thanks to the implementation of the beam stopping procedure, COMPA gives reasonable estimates of the cross-section for relatively thick targets. Fig. 18a illustrates the influence of the thickness of the target on cross section for the $^{122}\text{Sn}(^{20}\text{Ne}, \alpha 6n)^{132}\text{Ce}$ channel. When the thickness of the target increases, the maximum of the excitation function moves towards higher beam energies. The probability of the event population depends on the cross-section and the target thickness. The probability of the $\alpha 6n$ channel

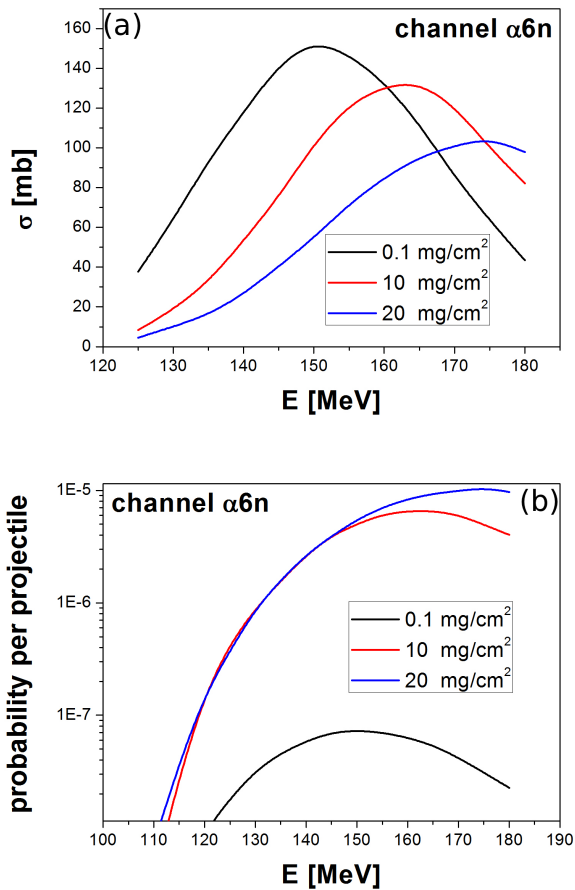


Figure 18: a) Calculated excitation functions (a) and probabilities (b) for the $^{122}\text{Sn}(^{20}\text{Ne}, \alpha 6n)^{132}\text{Ce}$ reaction for three different target thicknesses: 0.1 mg/cm^2 (black), 10 mg/cm^2 (black) and 20 mg/cm^2 (black).

population as a function of energy is shown in Fig. 18b, The influence of the target thickness is easily noticeable. Such calculations are especially important at the experiment planning stage. The energy should be adjusted in order to obtain the maximum cross section. One can estimate the expected counting rate in the experiment on

the basis of the detection efficiency. This makes COMPA a useful tool for a quick and easy evaluation of different experimental setups.

3.3.2. Proton and α particle stopping.

The situation is similar to the case of the beam. The charged particles are assumed to move straight ahead through the matter. Stopping in the target, the support, the backing and the covering tube can be realized. The necessary ranges and the energy losses are taken from the SRIM code [4]. The α particle laboratory angle vs kinetic energy diagrams for the $^{64}\text{Ni}+^{64}\text{Ni}$ reaction at 260 MeV are shown in Fig. 19, where the picture from Fig. 12c is shown again, along with diagrams of α particles after passing through subsequent elements of the setup are presented: the target (Fig. 19b), the ^{27}Al backing (Fig. 19c) and the ^{27}Al tube (Fig. 19d). The thicknesses were as follows: for the target 10 mg/cm², for the backing 20 mg/cm² and for the tube 15 mg/cm². The corresponding energy

E_{HIGH} , θ_{LOW} and θ_{HIGH} are input parameters. Compa allows some simple simulations of particle detection. This approach makes any fitting procedure much quicker when comparing to GEANT4 simulations. It also allows quick evaluation of the detection setup without time consuming GEANT4 geometry descriptions. Only the detection of protons (for $P_{kind} = 2$) and α particles (for $P_{kind} = 3$), obviously in the LAB system, is included. As in the previous cases, the particles are assumed to move straight ahead through the detector material. The user can define the atomic number of the material of which the detector is built (only of one element) as well as its thickness. θ_{LOW} and θ_{HIGH} define the angle covered by the detector. It is also possible to set a gate on the energy measured by the detector. A schematic drawing of the detection setup is shown in Fig. 21. An example of α particle spectra in

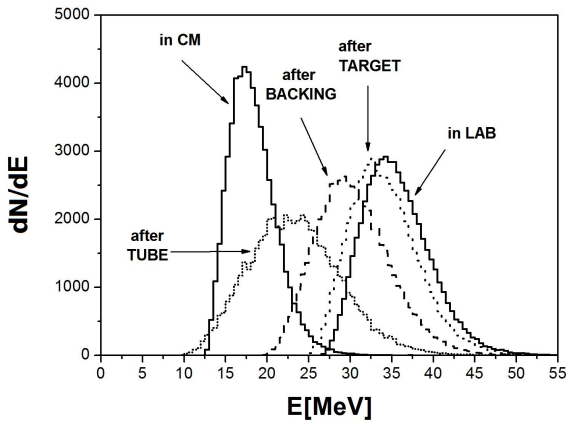


Figure 20: Evolution of the α particles while passing through the elements of the experimental setup. Energy spectra are shown for: a.) particles as they were emitted from the compound; b.) after passing through the ^{64}Ni target of 10 mg/cm² thickness; c.) after passing through the ^{27}Al backing of 20 mg/cm² thickness; c.) after passing through the ^{27}Al tube of 15 mg/cm² thickness.

spectra in the 15°-25° angular range are shown in Fig. 20, which illustrates the evolution of the α particle spectra at various stages of passing through the experimental setup.

3.3.3. Neutron, proton and α particle gating and detection.

Compa allows gates on energies (from E_{LOW} to E_{HIGH}) and angles (from θ_{LOW} to θ_{HIGH}) of the emitted particles in both LAB and CM systems to be set. Only one kind of particle can be gated at a time and the parameter P_{kind} controls it. For $|P_{kind}| = 1$ the gate will be set on neutrons, for $|P_{kind}| = 2$ on protons and for $|P_{kind}| = 3$ on α particles. For $P_{kind} < 0$ the gates will be set in the CM system while for $P_{kind} > 0$ in the LAB system. P_{kind} , E_{LOW} ,

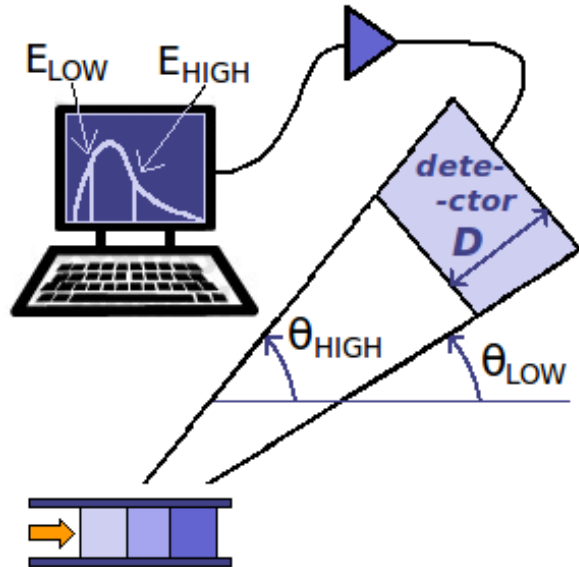


Figure 21: Schematic illustration of the charged particle detection setup. The detector of thickness D covers the angles from θ_{LOW} to θ_{HIGH} . The energy gate can be set to values ranging from E_{LOW} to E_{HIGH} .

detectors of various thicknesses, covering angles from 15°-25° is shown in Fig. 22. The α particle spectrum after the tube, which was previously shown in Fig. 20, is shown here again along with the spectra measured in Si detectors of thicknesses varying from 15 to 60 mg/cm². The characteristic edges for ΔE detectors are visible for thicknesses of 30, 45 and 60 mg/cm². The edges correspond to the maximum possible energy loss in the Si layer: 15 MeV for 30 mg/cm², 19 MeV for 40 mg/cm² and 22 MeV for 60 mg/cm² thickness.

3.3.4. Recoils

COMPA allows the recoils to be slowed down in both the target and backing material. The energy loss is calculated in the framework of Lindhard, Scharff and Schiøtt (LSS)

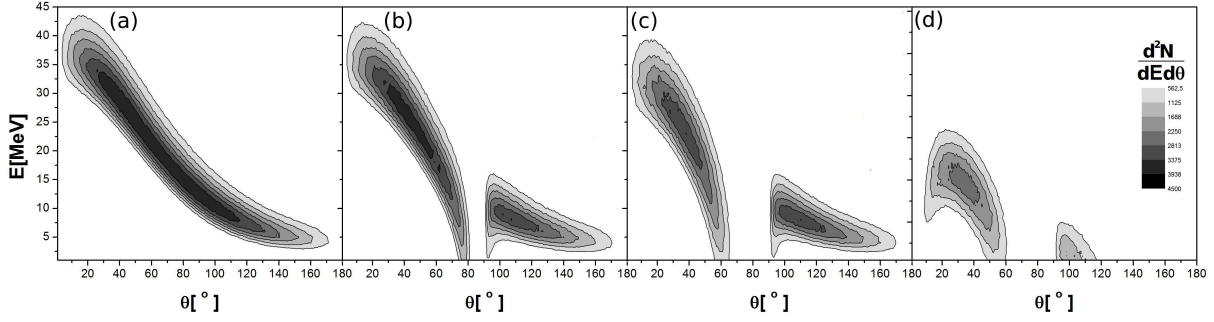


Figure 19: The evolution of α particles passing through the elements of the experimental setup. Laboratory angle vs kinetic energy diagrams are shown for: a.) particles as they were emitted from the compound; b.) after passing through the ^{64}Ni target of 10 mg/cm^2 thickness; c.) after passing through the ^{27}Al backing of 20 mg/cm^2 thickness; d.) after passing through the ^{27}Al tube of 15 mg/cm^2 thickness.

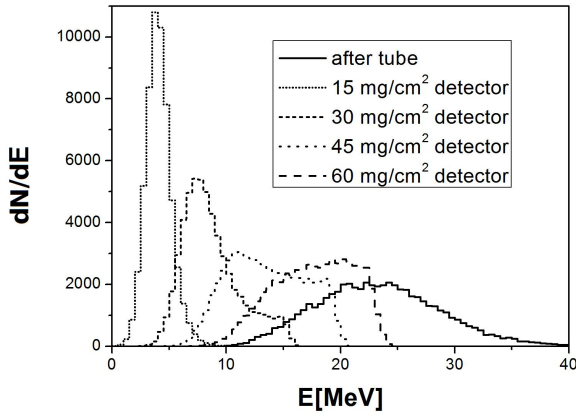


Figure 22: α particle spectra in Si detectors of different thicknesses, compared to the original α particles slowed down in target, backing and tube (solid). Presented spectra correspond to the following detector thicknesses. 15 mg/cm^2 (short dotted), 30 mg/cm^2 (short dashed), 45 mg/cm^2 (dotted) and 60 mg/cm^2 (dashed).

theory [3]. For relatively small velocities ($v < 2Zv_B$, $v_B = c/137$ being the Bohr velocity), the energy loss can be described as follows [2]:

$$\frac{d\epsilon}{d\rho} = S_e + S_n = f_e \kappa \epsilon^{1/2} + \frac{f_n \epsilon^{1/2}}{0.67\varphi_n + 2.07\epsilon}, \quad (24)$$

where ϵ and ρ are the scaled (dimensionless) energy and range equivalents, S_e and S_n are the electronic and nuclear stopping powers. κ is the Lindhard electronic stopping-power coefficient, assumed to be $\kappa = 0.15$. f_e and f_n are the correction factors describing the deviation of LSS predictions from experimental values. The φ_n parameter is an additional correction factor of the nuclear stopping power, allowing for a better fit of S_n over a wide range of energies. f_e, f_n and φ_n are code parameters. The velocities of the recoils populated in a typical fusion-evaporation reaction usually fulfill the condition $v < 2Zv_B$. The laboratory angle vs kinetic energy diagram for ^{132}Ce recoils populated in the $^{122}\text{Sn}(^{20}\text{Ne}, \alpha n)^{132}\text{Ce}$ reaction at 150 MeV beam

energy, is shown in Fig. 23. The ^{122}Sn target thickness was 0.5 mg/cm^2 , distributions after passing 0.5 mg/cm^2 and 1 mg/cm^2 of ^{208}Pb backing are also shown. The corresponding velocity distributions of the recoils are shown in Fig. 24.

Having a velocity distribution, one can calculate the time

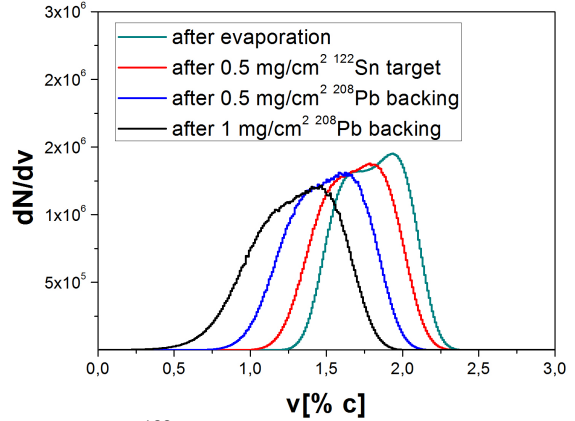


Figure 24: ^{132}Ce recoil velocity distributions: after evaporation (dark cyan), after a ^{122}Sn target of 0.5 mg/cm^2 thickness (red), after ^{208}Pb backing of 0.5 mg/cm^2 (blue) and 1 mg/cm^2 thickness (black). The recoils were produced in the $^{20}\text{Ne}+^{122}\text{Sn}$ reaction at 150 MeV.

of flight distribution at a given distance L_{TOF} , which is an input parameter. Such distributions are shown in Fig. 25. COMPA also enables recoil transition time through the target and backing to be calculated. Such distributions are shown in Fig. 26.

The distributions presented in Figures 23 - 26 are very useful at the planning stage of the experiments, where the kinematics of recoils matters. The angle vs kinetic energy diagram (see Fig. 23) allows optimal configuration of the recoil detectors, such as Kraków's Recoil Filter Detector (RFD) [29] to be adjusted. The angle covered by the RFD detectors is adjustable and such distribution facilitates the proper choice. The distribution of recoil velocity

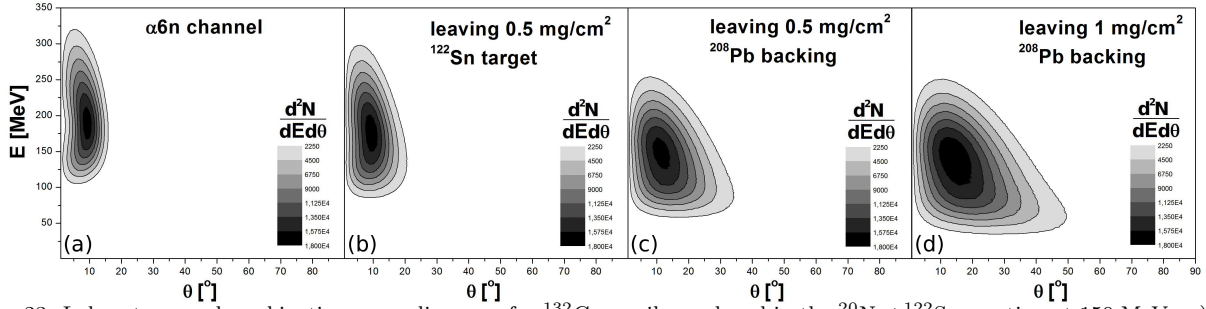


Figure 23: Laboratory angle vs kinetic energy diagrams for ^{132}Ce recoils produced in the $^{20}\text{Ne}+^{122}\text{Sn}$ reaction at 150 MeV: a.) as they were created somewhere in the target; b.) leaving a 0.5 mg/cm^2 thick ^{122}Sn target; c.) after passing through a ^{208}Pb backing of 0.5 mg/cm^2 thickness; d.) after passing through a ^{208}Pb backing of 1 mg/cm^2 thickness.

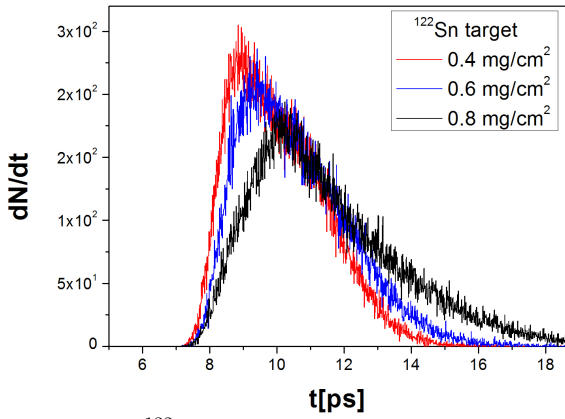


Figure 25: ^{132}Ce recoil time of flight distributions at a distance of $L_{TOF} = 50\text{ }\mu\text{m}$ after ^{122}Sn targets of 0.4 mg/cm^2 (red), 0.6 mg/cm^2 (blue) and 0.8 mg/cm^2 thickness (black). The recoils were produced in the $^{20}\text{Ne}+^{122}\text{Sn}$ reaction at 150 MeV.

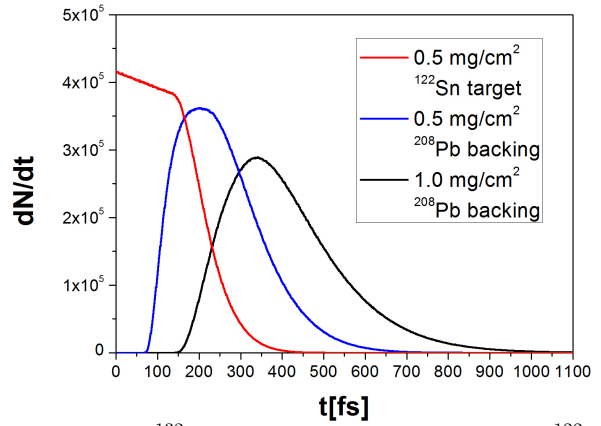


Figure 26: ^{132}Ce recoil transition time through a ^{122}Sn target of 0.5 mg/cm^2 thickness (red), a ^{208}Pb backing of 0.5 mg/cm^2 (blue) and 1.0 mg/cm^2 thickness (black). The recoils were produced in $^{20}\text{Ne}+^{122}\text{Sn}$ reaction at 150 MeV.

(see Fig. 24) and of time of flight (see Fig. 25) are useful in the case of RDM measurements. The recoil velocities should be high enough to ensure the separation of the „in flight” and „stopped” components in the γ spectrum, while the time of flight should be comparable with the estimated lifetimes which are going to be measured. In the case of DSAM, the distribution of the transition time through the target is important (see Fig. 26). The mean transition time should be comparable with the lifetimes of the levels of interest. Adding cross section integrated over the target thickness (see Section 3.3.1) and the *entry state* distribution (see Section 3.2.6), COMPA gives the complete set of data required at the planning stage of the experiment.

3.3.5. Summary - input parameters

The following parameters were introduced in this section:

- Z_P, A_P - atomic and mass numbers of the projectile.
- Z_{Ta}, A_{Ta} - atomic and mass numbers of the target.
- D_{Ta} - target thickness [mg/cm^2].

ρ_{Ta} - target density [g/cm^3].

Z_{Ba}, A_{Ba} - atomic and mass numbers of backing.

D_{Ba} - backing thickness [mg/cm^2].

ρ_{Ba} - backing density [g/cm^3].

Z_{Su} - support atomic number.

D_{Su} - support thickness [mg/cm^2].

Z_{Tu} - tube atomic number.

D_{Tu} - tube thickness [mg/cm^2].

S_{proton} - protons stopping in support, target, backing and tube. $S_{proton} = 0$ - no, $S_{proton} = 1$ -yes.

S_α - α particles stopping in support, target, backing and tube. $S_\alpha = 0$ - no, $S_\alpha = 1$ -yes.

S_{recoil} - recoils stopping in target and backing. $S_{recoil} = 0$ - no, $S_{recoil} = 1$ -yes.

$\phi_{Ta}^n, f_{Ta}^n, f_{Ta}^e$ - LSS theory parameters for target. The default values are $\phi_{Ta}^n = 1, f_{Ta}^n = 0.9$ and $f_{Ta}^e = 1$.

$\phi_{Ba}^n, f_{Ba}^n, f_{Ba}^e$ - LSS theory parameters for backing. The default values are $\phi_{Ba}^n = 1, f_{Ba}^n = 0.9$ and $f_{Ba}^e = 1$.

L_{TOF} - distance for time of flight calculation [μm]. The

default value is $L_{TOF}=50\mu\text{m}$.

P_{kind} - particle required:

$P_{kind} = -1,1$ - neutron.

$P_{kind} = -2,2$ - proton.

$P_{kind} = -3,3$ - α particle.

If $P_{kind} < 0$ - in CM system, if $P_{kind} > 0$ - in LAB system.

$\theta_{LOW}, \theta_{HIGH}$ - gate on angles (only when $P_{kind} \neq 0$).

E_{LOW}, E_{HIGH} - gate on energies (only when $P_{kind} \neq 0$).

Z_{De} - the atomic number of the material of which the detector is built (only of one element).

D_{De} - particle detector thickness [mg/cm^2].

4. Comparison with experiment.

In this section we present a comparison with a set of experimental data.

4.1. Complete fusion and fission

In order to illustrate the accuracy of complete fusion and fission simulations with COMPA, we chose three cases:

1. Fusion of $^{16}\text{O}+^{148,150,152,154}\text{Sm}$ at sub barrier energies.
2. Fusion of $^{16,18}\text{O}+^{92}\text{Mo}$ at sub barrier energies.
3. Fission in the $^{40}\text{Ar}+^{109}\text{Ag}$ system.

In the first two cases the absolute cross-sections for fusion were measured as well as yields of fusion-evaporation residues. In the third case, the absolute cross sections for fusion and fission were measured.

4.1.1. Fusion in the $^{16}\text{O}+^{148,150,152,154}\text{Sm}$ reaction

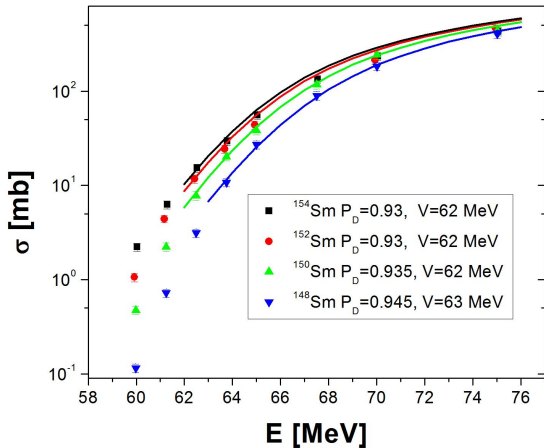


Figure 27: Comparison of experimental cross sections (points) with COMPA calculations (lines) for ^{16}O beam hitting: a.) ^{148}Sm (black); b.) ^{150}Sm (red); c.) ^{152}Sm (green); d.) ^{154}Sm (blue).

In this section we present a comparison of the absolute and fusion-evaporation cross-sections in the $^{16}\text{O}+^{148,150,152,154}\text{Sm}$ reactions at the energies between 60 and 75 MeV [30].

This case was chosen to illustrate the cross-section calculations for production of fusion-evaporation residues created by neutron emission. The created compound nuclei of Yb lie close to the stability line, therefore neutron evaporation dominates. The sub-barrier region was chosen in order to present the COMPA performance in this range of energies, but also to avoid pre-equilibrium emission and fission influence. The entire cross-section for fusion consist thus of fusion evaporation channels.

In Fig. 27 we present absolute cross-sections as a function of beam energy.

Since the beam energies are in the sub-barrier region, it was necessary to employ a P_D correction factor for the calculations (see Appendix A.2). Best fits were obtained with $P_D \approx 0.93$. COMPA is unable to reproduce values for energies lower than 62 MeV; however, for higher energies the data are well reproduced. Cross sections for individual channels were also measured. The relative amounts of the various evaporation residues expressed as the percentage of absolute cross section are shown in Fig. 28. The value of n denotes the number of mass units evaporated from the compound. Since the emission of charged particles is small, the n parameter approximates the number of neutrons emitted. COMPA reproduces the experimental values well.

4.1.2. Fusion in the $^{16,18}\text{O}+^{92}\text{Mo}$ reaction

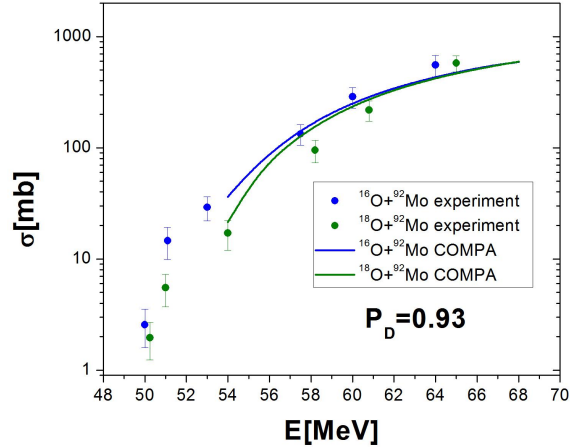


Figure 29: Experimental (points) and COMPA (lines) absolute cross sections for complete fusion of $^{16}\text{O}+^{92}\text{Mo}$ (blue) and $^{18}\text{O}+^{92}\text{Mo}$ (olive).

As in the previous case, the $^{16,18}\text{O}+^{92}\text{Mo}$ reaction [31] was chosen to present calculations in the sub barrier region, where fusion evaporation constitutes the whole fusion cross section.

In this case, the ^{92}Mo target has the smallest number of neutrons among stable Mo isotopes. The evaporation of charged particles is thus relatively strong. The measurements were performed for $^{16,18}\text{O}$ beam energies between 50 and 65 MeV. In order to reproduce the absolute cross section, the P_D correction factor (see Appendix A.2) was used. As shown in Fig. 29, best fits were obtained with $P_D = 0.93$. Similar to the $^{16}\text{O}+^{148,150,152,154}\text{Sm}$ systems, COMPA does not reproduce the entire sub barrier region. However, for energies above 54 MeV, the data are well reproduced. In Fig. 30 one can see cross-sections for various evaporation residues. The agreement is fair, taking into account that the statistical model usually does not reproduce yields of charged particles.

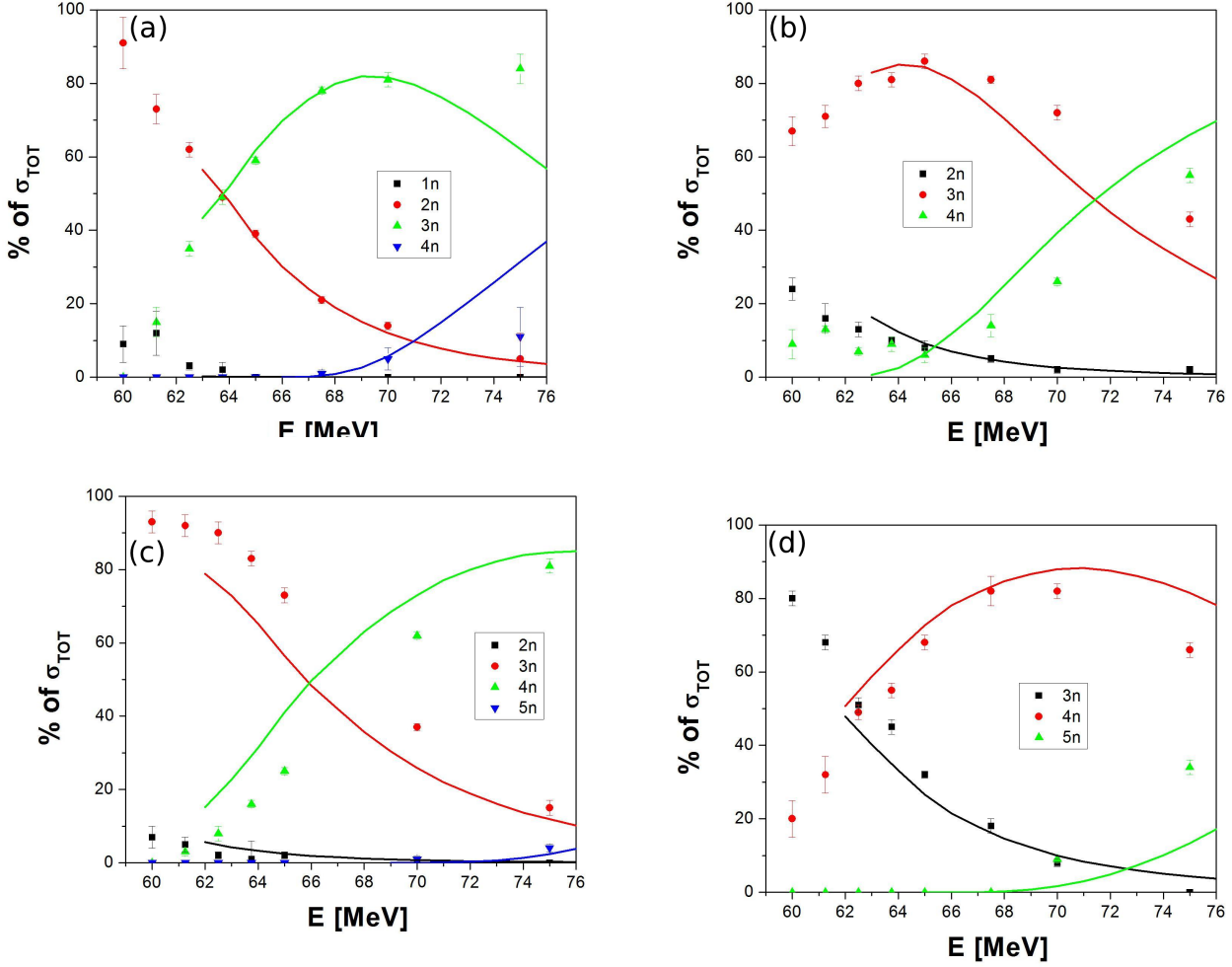


Figure 28: The distributions of the evaporation residues as a function of bombarding energy for ^{16}O beam and four different targets: a.) ^{148}Sm ; b.) ^{150}Sm ; c.) ^{152}Sm ; d.) ^{154}Sm ; experimental points are compared to COMPA simulations (lines); n denotes the number of atomic mass units removed from the compound nucleus.

4.1.3. Fission in the $^{40}\text{Ar}+^{109}\text{Ag}$ system

Here we present COMPA calculations of fission cross-sections. Fusion and fission cross sections were measured in the $^{40}\text{Ar}+^{109}\text{Ag}$ reaction [32] at ^{40}Ar beam energies between 170 and 290 MeV. Fig. 31 illustrates calculated fission barriers (a) and the experimental cross-sections compared to the COMPA calculations (b). The fusion cross-section was calculated with a default set of parameters. Fission cross-sections were calculated with $M_F = 2$, which is the default value. Fission barriers were calculated with the SIERK code or the Modified Thomas Fermi formula (see Appendix E). The default value of $k = 2$ reproduces the experiment well. In the case of the SIERK fission barrier it was necessary to use $L_{SH} = 5$ in order to reproduce the experimental values.

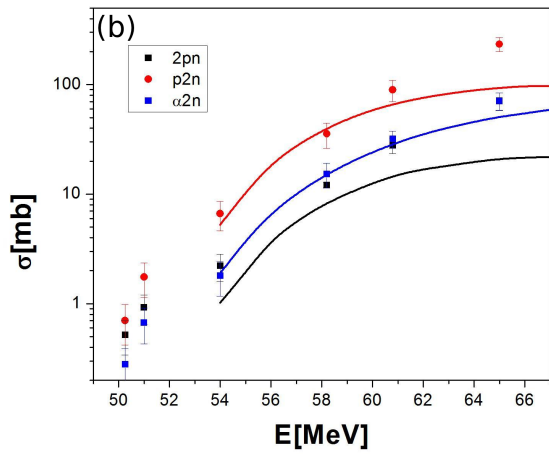
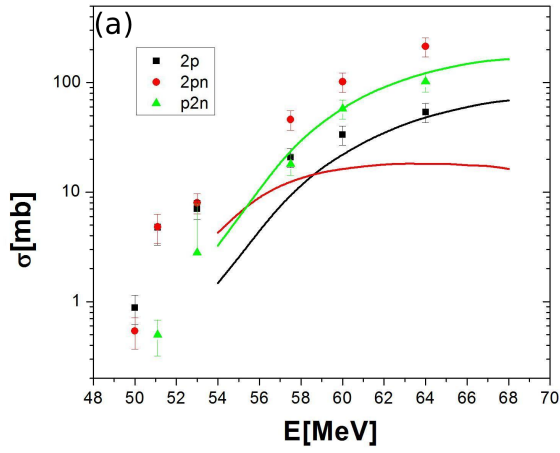


Figure 30: Experimental (points) and COMPA (lines) absolute cross sections for complete fusion of $^{16}\text{O}+^{92}\text{Mo}$ (blue) and $^{16}\text{O}+^{92}\text{Mo}$ (olive).

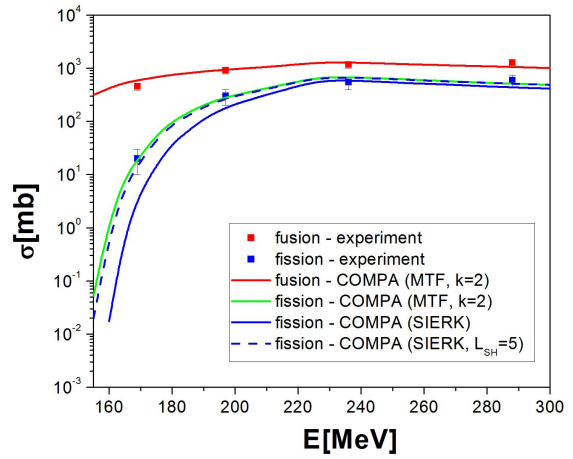
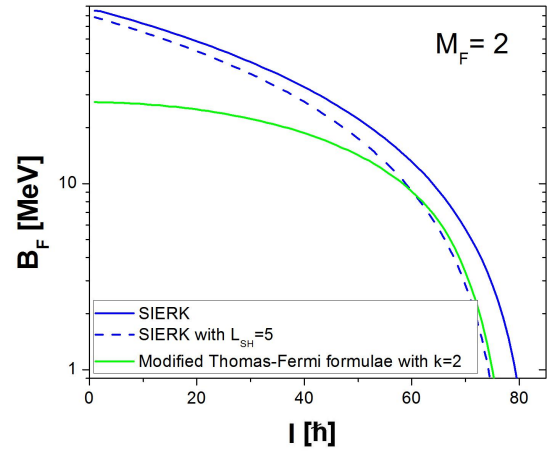


Figure 31: a.) Fission barriers for ^{149}Tb calculated with the MTF formulae with $k = 2$ (green) and with the SIERK program (blue) for $M_F = 2$ and two values of L_{SH} : 0 (solid) and 5 (dashed); b.) Comparison of complete fusion and Fission cross sections (points) in the $^{40}\text{Ar}+^{109}\text{Ag}$ reaction, compared with COMPA calculations (lines).

5. Acknowledgments

Appendix A. The transmission coefficients for fusion

Appendix A.1. Heavy projectiles ($A > 5$).

We consider that for a given projectile energy E , the formula:

$$T_E^{D,L_{1/2}}(L) = \left(1 + \exp\left(\frac{L(L+1) - L_{1/2}(L_{1/2}+1)}{D}\right)\right)^{-1} \quad (\text{A.1})$$

is optimal for the calculations of the transmission coefficients. L is the relative angular momentum, the D and $L_{1/2}$ values must be determined, and in order to do so, the Blatt-Weisskopf approximation [23] is used, with the transmission coefficient defined as:

$$T_E^{bw}(L) = \frac{4 \cdot S_L \cdot \rho}{\Delta_L^2 + (S_L + \rho)^2}, \quad (\text{A.2})$$

where

$$\begin{aligned} \Delta_L &= \rho a, \\ S_L &= \sqrt{b} \cdot e^{-R \cdot (\gamma \cdot \log(b) + g \cdot \arctan \frac{2a}{a-g} - 2a)}, \\ a &= 5 \cdot A_{KG}, \\ A_{KG} &= \left(\frac{2-g}{9 \cdot R}\right)^{2/3}, \quad b = \frac{(a+\gamma)^2 + 1}{(a-\gamma)^2 + 1}, \\ g &= \sqrt{\frac{V}{E}}, \quad \gamma = \sqrt{1+a-g}, \\ R &= \frac{R_l}{g^2}. \end{aligned}$$

$T_L^{bw}(L)$ is calculated for two different values of the angular momentum: L_1 and L_2 , which are chosen to be

$$L_1 = \sqrt{R_l \cdot \left(1 - \sqrt{\frac{V}{E}}\right)}, \quad L_2 = \gamma \cdot R_l, \quad (\text{A.3})$$

where V is the Coulomb barrier between the projectile and the target, and R_l is the grazing radius given by the formula:

$$R_l = 0.2624 \cdot \sqrt{R_1 \frac{Z_1 \cdot Z_2 \cdot A_1 \cdot A_2}{A_1 + A_2}}. \quad (\text{A.4})$$

The standard expressions for the Coulomb barrier V and distance R_1 between the centres of two nuclei are:

$$V = 1.44 \cdot \frac{Z_1 \cdot Z_2}{R_1}, \quad R_1 = R_0 \cdot (A_1^{1/3} + A_2^{1/3}). \quad (\text{A.5})$$

R_0 is the nucleon radius (see Eq. C6 in [26]):

$$R_0 = \frac{1.12 \cdot (A_1^{1/3} + A_2^{1/3})}{A_1^{1/3} + A_2^{1/3}} + \frac{0.94 \cdot (A_1^{-1/3} + A_2^{-1/3}) + 3}{A_1^{1/3} + A_2^{1/3}}. \quad (\text{A.6})$$

It can be thus derived that for $L = L_1$ and $L = L_2$ in Eq. A.3, the Blatt-Weisskopf coefficients (Eq. A.2) are

$$\begin{cases} T_L^{bw}(L_1) = 4 \cdot \frac{\frac{0.7615}{\sqrt{A_{KG}}}}{0.2311 + (1 + \frac{0.7615}{\sqrt{A_{KG}}})^2} \\ T_L^{bw}(L_2) = 4 \cdot \frac{S_L}{a \cdot (1 + (S_L + a^{-1})^2)}. \end{cases} \quad (\text{A.7})$$

Finally, the two equations can be written by combining Eq. A.7 with Eq. A.1:

$$\begin{cases} T_L^{bw}(L_1) = T_E^{D,L_{1/2}}(L_1) = \left(1 + \exp\left(\frac{L_1 \cdot (L_1+1) - L_{1/2} \cdot (L_{1/2}+1)}{D}\right)\right)^{-1}, \\ T_L^{bw}(L_2) = T_E^{D,L_{1/2}}(L_2) = \left(1 + \exp\left(\frac{L_2 \cdot (L_2+1) - L_{1/2} \cdot (L_{1/2}+1)}{D}\right)\right)^{-1}. \end{cases} \quad (\text{A.8})$$

After solving these equations with respect to D and $L_{1/2}$ we obtain:

$$\begin{aligned} D &= \frac{A_{L1} - A_{L2}}{A_{K1} - A_{K2}}, \\ L_{1/2} \cdot (L_{1/2} + 1) &= \frac{A_{L2} \cdot A_{K2} - A_{L1} \cdot A_{K2}}{A_{K1} - A_{K2}}, \end{aligned} \quad (\text{A.9})$$

where

$$\begin{aligned} A_{K1} &= \log\left(\frac{1}{T_L^{bw}(L_1)} - 1\right), \\ A_{K2} &= \log\left(\frac{1}{T_L^{bw}(L_2)} - 1\right), \end{aligned} \quad (\text{A.10})$$

and

$$A_{L1} = L_1 \cdot (L_1 + 1), \quad A_{L2} = L_2 \cdot (L_2 + 1). \quad (\text{A.11})$$

Once the values of D and $L_{1/2}$ are set, the transmission coefficients for complete and incomplete fusion can be calculated (Eq. A.1).

When calculating total cross section with this method, the values obtained are often higher than the experimental results. They also tend to exceed the cross sections calculated with the empirical formula of Kailas et. al [24], where the fusion cross section is given by the equation:

$$\sigma_E^K = 10\pi R_{KA} \cdot (R_{KA} - D_{KA}), \quad (\text{A.12})$$

and the parameters R_{KA} and D_{KA} are calculated automatically (they can also be input parameters⁶). An example is shown in Fig. A.32, where measured and calculated cross sections for ^{12}C hitting a ^{24}Mg target differ strongly. The Kailas values reproduce the experimental values accurately, but the cross-section calculated with the coefficients from Eq. A.1 exceeds the experimental points for relatively high energies.

A so-called empirical correction is proposed to handle this problem.

⁶More options concerning the Kailas cross section are described at the end of this section

$$D = D^{i-1} \sqrt{\frac{L_{1/2} \cdot (L_{1/2} + 1)}{L_{1/2}^{i-1} \cdot (L_{1/2}^{i-1} + 1)}}. \quad (\text{A.15})$$

If D is smaller than D^{i-1} then $D^i = D$. If $L_{1/2}$ is smaller than $L_{1/2}^{i-1}$ then $L_{1/2}^i = L_{1/2}$. If σ_T is still smaller than σ_K , a new f_{AC}^{i+1} is calculated:

$$f_{AC}^{i+1} = f_{AC}^i \sqrt{\frac{L_{1/2} \cdot (L_{1/2} + 1)}{L_{1/2}^{i-1} \cdot (L_{1/2}^{i-1} + 1)}}, \quad (\text{A.16})$$

and calculations are performed again from Eq. A.13. If not, the transmission coefficients are calculated with the f_{AC}^i correction factor. Calculations for the $^{12}\text{C}+^{24}\text{Mg}$ reaction are shown in Fig. A.32. $f_{AC} = 0.928$ was obtained and the experimental values are well reproduced. The user can decide whether to perform this correction or not (parameter C_{FAC}).

An analysis of the multiplicity of emitted γ -rays can lead to a determination of the maximum spin of the created compound nucleus. When it differs from the value predicted by the COMPA calculations with f_{AC} factor, another correction may be performed. Let L_{MAX} be the maximum spin value observed in the experiment. The f_{AC} correction is made in the same way as presented before (Eq. A.13-A.16), but with the final condition that the transmission coefficient $T_E^{D, L_{1/2}}(L_{MAX})$ in Eq. A.1 has to be equal to 0. An example is shown in Fig. A.33, where calculations were performed for $L_{MAX} = 20$. The final f_{AC} value was equal to 0.43. L_{MAX} is an input parameter.

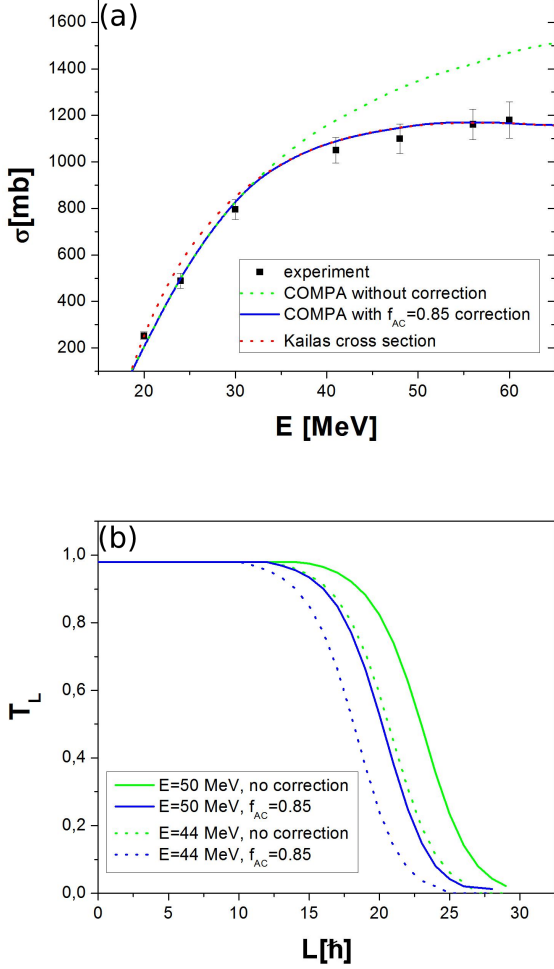


Figure A.32: a.) The experimental cross section for fusion for the $^{12}\text{C}+^{24}\text{Mg}$ reaction [33] and three theoretical curves: COMPA with an $f_{AC} = 0.928$ correction (red), COMPA without correction (green) and Kailas [24] values (blue); b.) The transmission coefficients calculated by COMPA with the f_{AC} correction (dotted lines) and without correction (solid lines) for two projectile energies: 50 MeV (green) and 44 MeV (blue).

A cross section (σ_K) calculated with the Kailas empirical expression (Eq. A.12) is compared to one based on the transmission coefficients (σ_T). If $\sigma_K < \sigma_T$, D and $L_{1/2}$ values are calculated once again with some modifications. The f_{AC}^i correction parameter is introduced into Eq. A.4, defining the grazing radius:

$$R_i^i = 0.2624 \cdot \sqrt{R_1 \cdot \frac{Z_1 \cdot Z_2 \cdot A_1 \cdot A_2}{A_1 + A_2}} f_{AC}^i. \quad (\text{A.13})$$

In the first step ($i = 1$), D and $L_{1/2}$ are again calculated with $f_{AC}^1 = 0.99$:

$$L_{1/2} \cdot (L_{1/2} + 1) = \frac{\sigma_K}{\sigma_T} L_{1/2}^{i-1} \cdot (L_{1/2}^{i-1} + 1), \quad (\text{A.14})$$

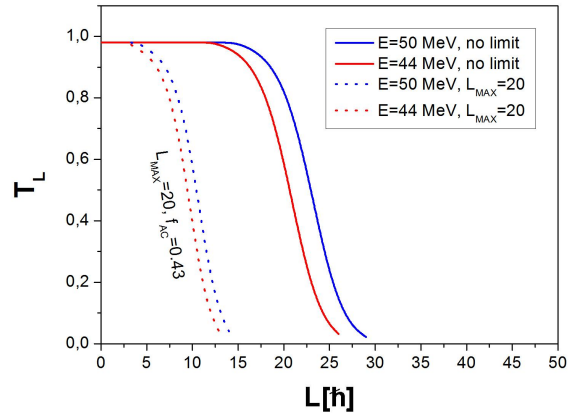


Figure A.33: The transmission coefficients for the $^{12}\text{C}+^{24}\text{Mg}$ reaction at two energies: 65 MeV (blue) and 55 MeV (red), with an $L_{MAX} = 20$ correction (dotted lines) and without correction (solid lines). Calculations finished with $f_{AC} = 0.49$.

ter.

Kailas cross section based on experimental points.

If the Kailas cross section does not reproduce the experimental values, R_{KA} and D_{KA} can be calculated based on

two experimental points. Let us call them $\sigma(E_1) = a$ and $\sigma(E_2) = b$. The user can calculate R_{KA} and D_{KA} in the following way:

$$R_{KA} = 0.1784 \cdot \frac{a}{b},$$

$$D_{KA} = 0.1784 \cdot E_1 \cdot E_2 \frac{\sigma(E_1) - \sigma(E_2)}{a \cdot b}, \quad (\text{A.17})$$

where

$$a = \sqrt{\sigma(E_1) \cdot E_1 - \sigma(E_2) \cdot E_2}, b = \sqrt{E_1 - E_2}. \quad (\text{A.18})$$

R_{KA} and D_{KA} can be input parameters.

Appendix A.2. Close to the Coulomb barrier

COMPACT is also able to calculate the subbarrier fusion. The Coulomb barrier calculated with [24] limits the possibility of fusion. The P_D correction factor is proposed in order to make fusion possible for energies smaller than this barrier. The barrier value (Eq. A.5) and the D parameter (Eq. A.9) are modified in the following way:

$$V' = P_D \cdot V, D' = D \cdot P_D^2. \quad (\text{A.19})$$

The transmission coefficients are calculated with Eq. A.1. With such a modification we can choose where to limit the possibility of fusion. Fig. A.34 presents total cross section and transmission coefficient calculations for the $^{16}\text{O}+^{152}\text{Sm}$ reaction compared to experimental values. With $P_D = 0$ (black lines) the correction is not applied and the limit for fusion is equal to the Kailas Coulomb barrier (70 MeV). Assuming $P_D = 1$, the limit for fusion is calculated with Eq. A.5, giving 66 MeV (red lines). When $P_D = 0.93$, the limit is equal to 62 MeV (green lines), and the cross-section is well reproduced beyond this limit. Such an approach does not allow values for lower energies to be reproduced.

Appendix A.3. Light projectiles

For neutrons, protons, deuterons, tritons, α and ^3He projectiles, D and $L_{1/2}$ values are calculated in the framework of the optical model [25]. Fig. A.35 illustrates the coefficients for deuterons and α particles hitting a ^{118}Sn target. The f_{AC} correction is not available for light projectiles.

Appendix A.4. Transmission coefficient for fusion cut-off

For energies close to the Coulomb barrier, the transmission coefficients are small and the calculations must be very precise. This is the reason why the H_{CUT} parameter was introduced, which enables one to define a stopping point for the calculation of the transmission coefficients. For values below H_{CUT} , the transmission coefficient for fusion will be considered to be zero. Figure A.36 illustrates how H_{CUT} works. For energies beyond the Coulomb barrier, calculations may be performed with relatively high H_{CUT} values ($\approx 10^{-2}$). Closer to the barrier, where coefficient values are small, H_{CUT} should also be small ($\approx 10^{-4}$).

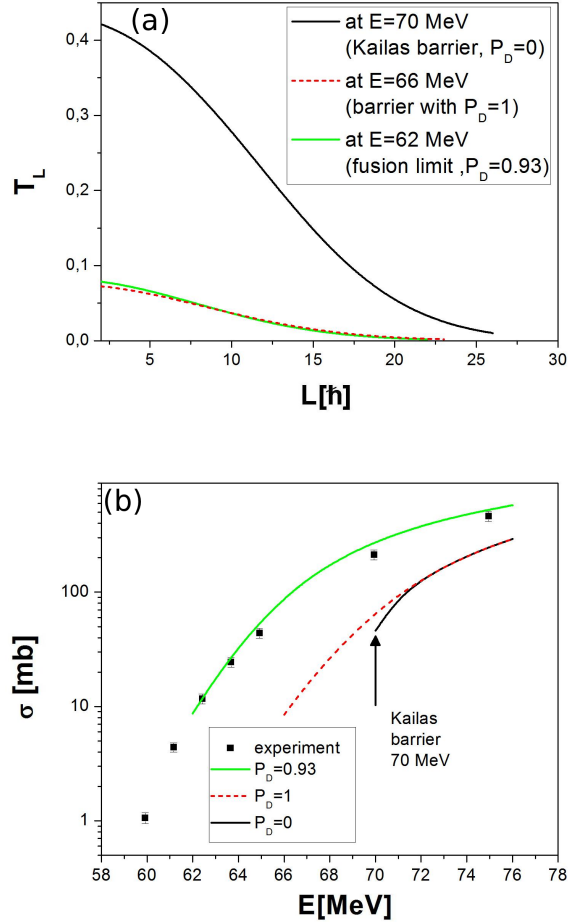


Figure A.34: a.) The transmission coefficients for energies near the Coulomb barrier in the $^{16}\text{O}+^{152}\text{Sm}$ reaction: when $P_D = 0$ and the barrier is calculated with Kailas [24] (black), when $P_D = 1$ and the barrier is calculated with Eq. A.5 (red) and with a $P_D = 0.93$ correction (green); b.) comparison with experiment for $P_D = 0$ (black), $P_D = 1$ (red) and $P_D = 0.93$ (green).

Appendix A.5. Summary - input parameters

The following parameters were introduced in this section:

C_{FAC} - controls empirical correction to the transmission coefficients. The correction will be made for $C_{FAC} = 1$, which is the default value. The correction is omitted for $C_{FAC} = 0$.

L_{MAX} - active if $C_{FAC} = 1$ - spin limit for the transmission coefficients for fusion. The default value is $L_{MAX}=100$, which is the maximum spin allowed in COMPACT.

P_D - subbarrier correction. The default value is $P_D = 0$, but for beam energies close to the Coulomb barrier it is suggested to use $P_D \approx 0.93$. This value reproduced the experiment well in two cases, described in Sections 4.1.1 and 4.1.2. The C_{FAC} correction will not be performed if

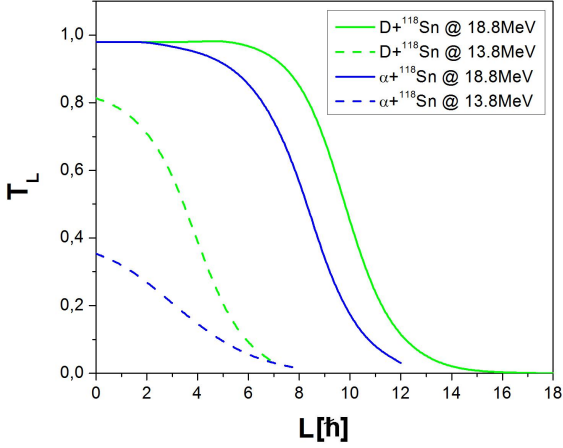


Figure A.35: Transmission coefficients for two systems: $D+^{118}\text{Sn}$ (green) and α particle $+^{118}\text{Sn}$ (blue), for two different LAB energies: 18.8 MeV (solid lines) and 13.8 MeV (dashed lines).

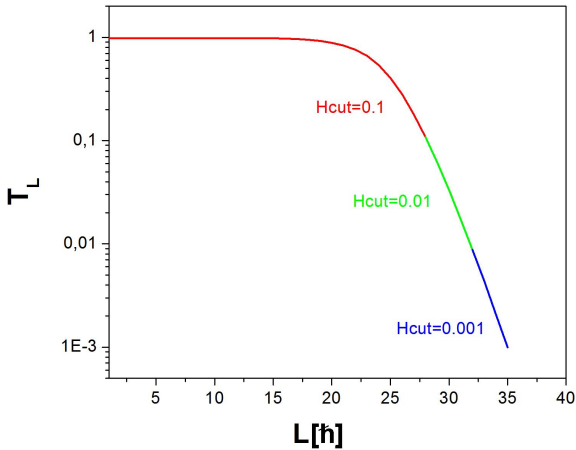


Figure A.36: Different values of H_{CUT} in the $^{12}\text{C}+^{24}\text{Mg}$ system. T_L is considered to be equal to 0 if $T_L < H_{CUT}$.

$P_D > 0$.

R_{KA} , D_{KA} - external parameters for Kailas cross section calculation. They are active when both values are greater than 0.

H_{CUT} - transmission coefficient cut-off parameter. The default value is $H_{CUT} = 10^{-2}$. It assumes ($C_{FAC} = 1$) beyond the Coulomb barrier, and $H_{CUT} = 10^{-4}$ at sub barrier energies ($P_D > 0$).

Appendix B. Yrast lines

In order to calculate the nucleus excitation energy, the yrast line must be known. The exact definition of an yrast

levels is: the lowest possible energy for a given spin. The yrast line can also be interpreted as the energy of a rotating cold nucleus (with no excitation energy) at spin I . The shape of the yrast line must be defined by the user. This application allows the user to define one yrast line assigned to a given residual nucleus. All remaining yrast lines are calculated automatically, based on the reference one. We can define the reference yrast line in three different ways. The first possibility, the easiest and the least exact one, is to assume the compound nucleus to be spherical and to treat it as a rigid rotor with a constant moment of inertia. The energy of a rotating nucleus having static moment of inertia J is given by the equation:

$$E_{YR}(I) = \frac{1}{2J} I \cdot (I + 1). \quad (\text{B.1})$$

In COMPA, J is calculated in the following way. Let J_0 be the static moment of inertia of a spherical nucleus of mass number A . Taking a standard expression for the nuclear radius, $R = r_0^{1/3}$, and a mass equal to A_{mu} , we can use the formula for the moment of inertia of the solid ball:

$$\begin{aligned} J_0 &= \frac{2}{5} \cdot m \cdot R^2 = \\ &= A_{mu} \cdot r_0^2 \cdot A^{5/3} \approx 0.0152 \cdot A^{5/3} \left[\frac{\hbar^2}{\text{MeV}} \right]. \end{aligned} \quad (\text{B.2})$$

The reference yrast line will be calculated with Eq. B.1. This option is realised with parameter $Y_{MODE} = 0$. A second possibility is to define the yrast line for a certain residual nucleus Z_Y, A_Y with a moment of inertia M times bigger than the moment of a spherical nucleus of mass number A_Y . $J = M \cdot J_0$ is substituted into Eq. B.1 and the yrast line is calculated. Z_Y , A_Y and M are code parameters. This option is realised when $Y_{MODE} = 1$ and $N = 1$. In Fig. B.37, the levels in ^{162}Ho are shown along with calculated curves for different M values. We can see that for $M = 1$ the levels are inaccurate while for $M = 1.4$ (dashed green curve) the yrast lines are pretty similar. Obviously, not all nuclei are equal. The levels in ^{132}Ce can not be described with the rigid rotor model (see Fig. B.37b). The third option is supposed to handle such cases. It is possible to define two polynomials describing the yrast levels:

$$\begin{cases} E_{LOW}(I) = A_{LOW} + B_{LOW}I + C_{LOW}I^2, \\ E_{HIGH}(I) = A_{HIGH} + B_{HIGH}I + C_{HIGH}I^2. \end{cases} \quad (\text{B.3})$$

For each spin the program will choose the minimum value of these two polynomials.

$$E_{YR}(I) = \text{minimum} (E_{LOW}(I), E_{HIGH}(I)). \quad (\text{B.4})$$

This option is realised when the values of $Y_{MODE} = 1$ and $N = 2$. A_{LOW} , A_{HIGH} , B_{LOW} , B_{HIGH} , C_{LOW} and C_{HIGH} are the input parameters. In Fig. B.38 the two curves are shown along with the yrast levels of ^{132}Ce . In the case of ^{162}Ho , the polynomial fit also seems to be a better choice than the rigid rotor model (see B.37).

If none of the three approaches is adequate, then the yrast

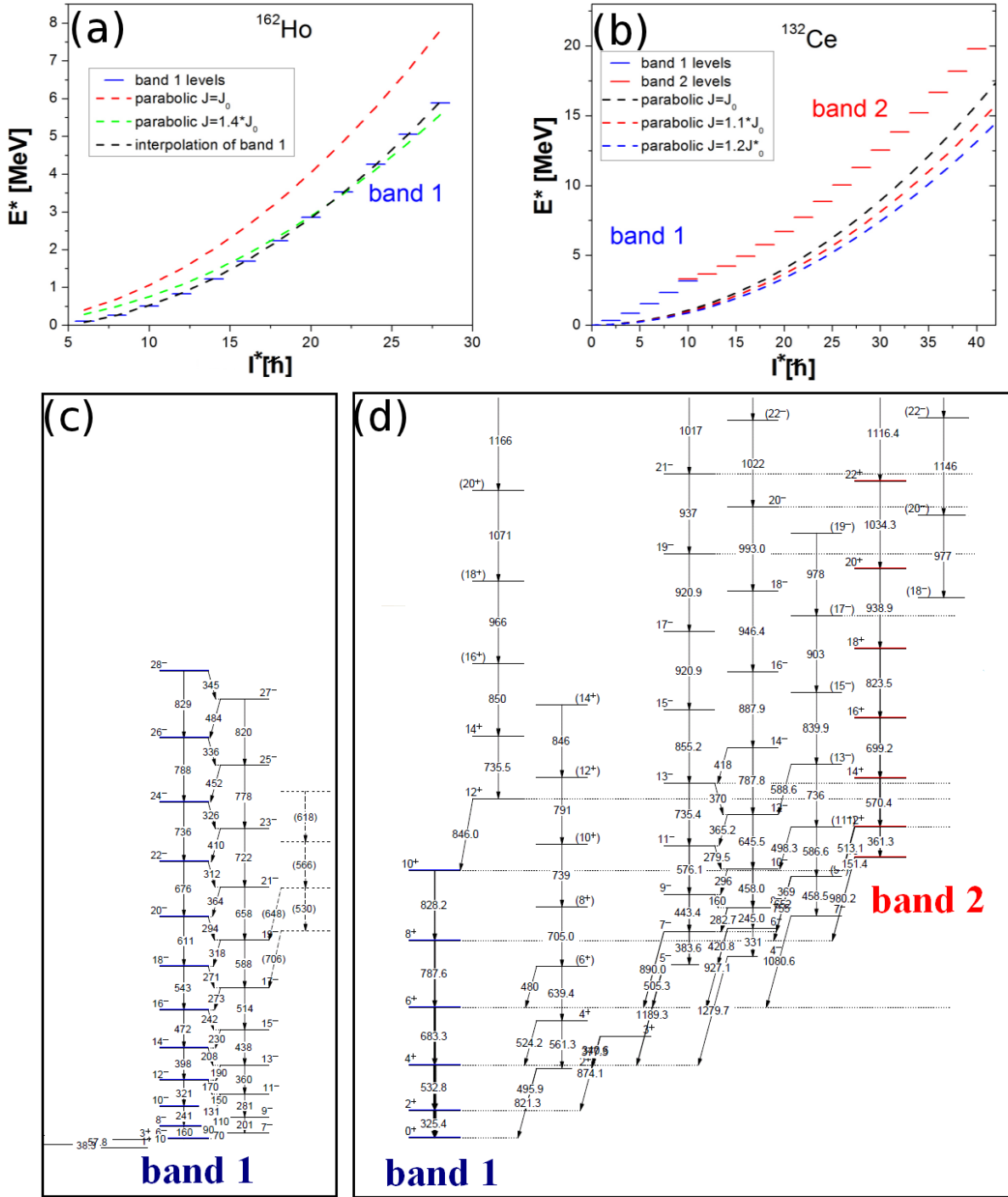


Figure B.37: Experimental and calculated Yrast levels in two nuclei. a.) the levels in ^{162}Ho (blue) are well reproduced by a rigid rotor model with $J = J_0$ (dashed green) and with an interpolated polynomial (dashed black). b.) the levels in ^{132}Ce can not be described in the same way - none of three curves (dashed black, red and blue) calculated with three different moments of inertia reproduce the yrast line. Level schemes of ^{162}Ho (c) and ^{132}Ce (d) are also shown. Bands of interest are marked.

line can be provided to COMPA in a separate file. This option is realised with $Y_{MODE} = 1$ and $N = 0$.

COMPA allows for evaporation of maximum 16 nucleons. The yrast lines of all 256 possible residual nuclei need to be calculated. As it is shown in Fig. B.39a, the yrast

lines for the nuclei in the same mass region are usually similar in shape. The energy gap between odd-odd, even-odd, odd-even and even-even nuclei levels can be explained by the pairing interaction. The energies of the yrast levels in different pairing configurations can be described by the

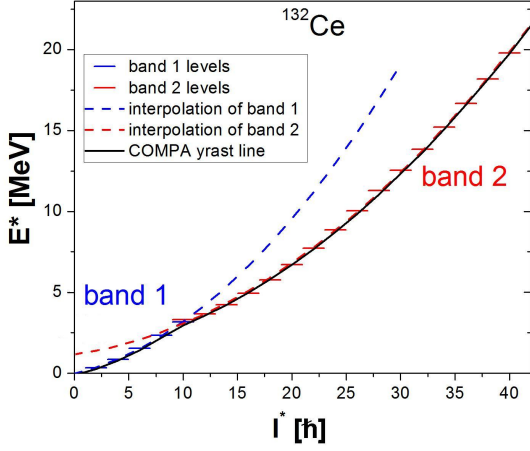


Figure B.38: The levels in ^{132}Ce and fitted polynomials. Each band can be described by a separate polynomial (dashed blue and red). The yrast line used by COMPA will be the minimum of these two (black).

following formula [34]:

$$E_{YR}^{\text{even-even}} = E_{YR}^{\text{odd-even}} + \Delta_p = E_{YR}^{\text{odd-odd}} + 2\Delta_p. \quad (\text{B.5})$$

In COMPA, the standard value $\Delta_p = 12/\sqrt{A}$ MeV is used. The S_P input parameter was introduced in order to control the Δ_p value:

$$\Delta_p = S_P \cdot \frac{12}{\sqrt{A}}. \quad (\text{B.6})$$

The $2\Delta_p$ energy gap, calculated with $S_P = 1$, is marked in Fig. B.39a. For spins smaller than $25\hbar$ the difference between neighbouring yrast lines is close to Δ_p . The situation gets more complicated for higher spins. In the second example (see Fig. B.39b) the two even-even nuclei, ^{132}Ce (black) and ^{136}Nd (green) have very similar yrast lines. But in the case of even-odd and odd-even nuclei the situation is different. The ^{135}Pm (even-odd) and ^{135}Nd (odd-even) lines differ from each other. Regardless of the pairing configuration of the nucleus, the yrast lines for the rest of the nuclei can be calculated with Eq. B.1. Consequently, all the even-even nuclei will have the same yrast line, all the even-odd and odd-even nuclei will have the yrast line shifted by Δ_p and all the odd-odd nuclei will have the yrast line shifted by $2\Delta_p$ gaps. Fig. B.39a shows the calculated yrast lines, the polynomial fit to the ^{132}Ce levels, which is the reference yrast line in this case, and the calculated yrast lines for ^{135}Nd (blue) and ^{134}Pr (red). For relatively low spins ($I < 25\hbar$) the levels are well reproduced. In the second example (see Fig. B.39b), it is evident that our approach is useless. The ideal solution for this problem is to input every needed yrast line independently. The preparation of polynomials describing 320 yrast lines seems to be nonsense from the point of view of the user.

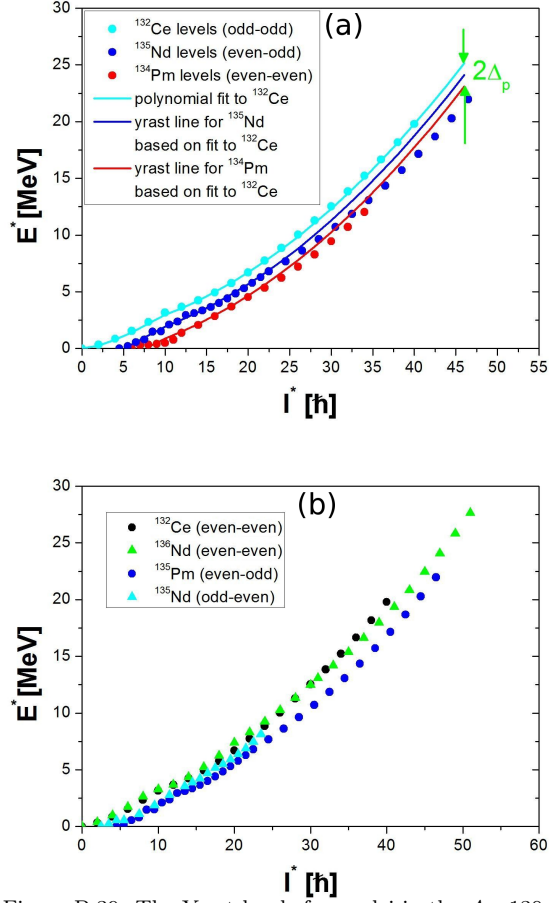


Figure B.39: The Yrast levels for nuclei in the $A \approx 130$ mass region. a.) The nuclear levels (bars), and the yrast lines (solid lines) prepared in COMPA for: ^{132}Ce (cyan), ^{135}Nd (blue) and ^{134}Pm (red) nuclei. The energy gap between the yrast lines is Δ_p (green). The calculated yrast lines reproduce the yrast levels well for low spins ($I < 25\hbar$); b.) The levels in the even-even nuclei ^{132}Ce (black) and ^{136}Nd (green) and odd-even ^{135}Nd (blue) and even-odd ^{135}Pm . While the even-even nuclei have almost identical yrast lines, even-odd and odd-even nuclei differ strongly from each other.

Another problem is that the experimental levels are usually known up to a spin of $40\hbar$ while in heavy ion induced reactions, spins around $60\hbar$ are easily reached. In this case COMPA does not provide any solution.

The role of the shape of the yrast line in calculations becomes obvious with Fig B.40, where simulated excitation functions for the $^{20}\text{Ne} + ^{122}\text{Sn}$ reaction are represented. Cross sections for $8n$, $p7n$ and $\alpha 6n$ channels were calculated with yrast lines based both on the rigid rotor model and the experimental data. The difference between these two approaches is evident.

Appendix B.1. Moments of inertia

The moment of inertia of a nucleus is a quantity required in numerous stages of the statistical theory. The static moment of inertia is used in the fission probability

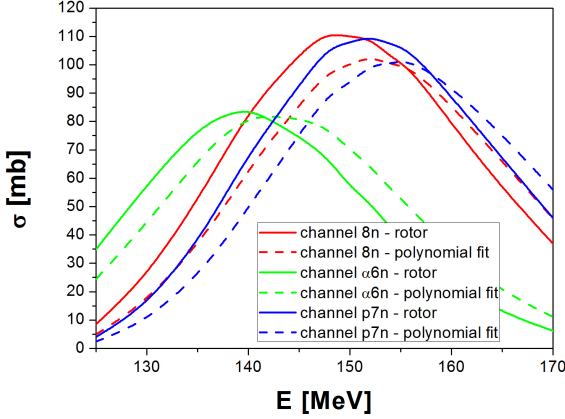


Figure B.40: Excitation functions for 8n (red), p7n (blue) and $\alpha 6n$ (green) channels, produced in the $^{20}\text{Ne}+^{122}\text{Sn}$ reaction. Each channel was calculated twice: with the yrast line based on a polynomial fit to the ^{132}Ce levels (dashed lines) and with $J = J_0$ in a rigid rotor model (solid lines).

calculations (Eq. 23), the determination of the evaporated particles angular distribution (Eq. 12), and for level density purposes (Eq. F.4).

In COMPA, three different moments of inertia are calculated based on $E_{YR}(I)$ dependence: static J , kinematic J_K and dynamic J_D . With the rigid rotor model the static moment can be calculated from Eq. B.1:

$$J(I) = \frac{I(I+1)}{2E_{YR}(I)}. \quad (\text{B.7})$$

The kinematic moment of inertia is defined as

$$E'_{YR}(I) = \frac{2I+1}{J_K(I)} \Rightarrow J_K(I) = \frac{2I+1}{2E'_{YR}(I)}. \quad (\text{B.8})$$

$E'_{YR}(I)$ is the first spin derivative, numerically calculated as

$$E'_{YR}(I) = \frac{E_{YR}(I+1) - E_{YR}(I-1)}{2}. \quad (\text{B.9})$$

The dynamic moment of inertia is defined as

$$E''_{YR} = \frac{1}{J_D(I)} \Rightarrow J_D(I) = \frac{1}{E''_{YR}}, \quad (\text{B.10})$$

where $E''_{YR}(I)$ is the second spin derivative, numerically calculated as

$$E''_{YR}(I) = \frac{1}{2} \left(\frac{E_{YR}(I+1) + E_{YR}(I-1)}{2} - E_{YR}(I) \right). \quad (\text{B.11})$$

These three moments of inertia should be equal when using the yrast line $E_{YR}(I)$ based on the rigid rotor model. When using polynomial fits, all three can be different. The static, kinematic and dynamic moments of inertia, calculated with yrast lines based on a polynomial fit to the ^{132}Ce levels, are shown in Fig. B.41.

The characteristic change in the J_D moment of inertia at a spin of $11\hbar$, which signals *back bending*, can be seen.

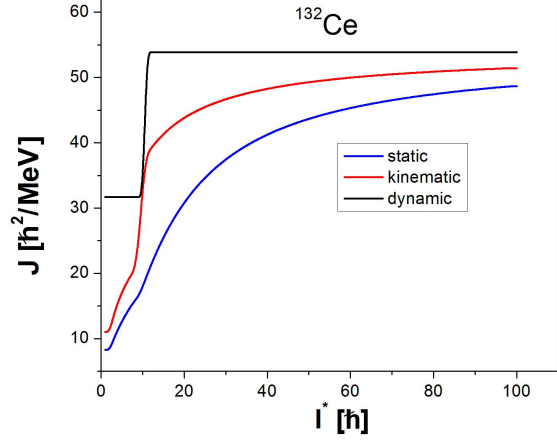


Figure B.41: Three moments of inertia of a rotating ^{132}Ce nucleus: static (blue), kinematic (red) and dynamic (black). The moments were calculated from the yrast line calculated from a polynomial fit to the ^{132}Ce levels (Fig. B.38).

Appendix B.2. Pairing shift

The pairing interaction becomes weaker as the excitation energy increases [34, 35]. To handle this problem, COMPA slightly modifies Eq. B.5, which describes the yrast lines for different pairing configurations, by adding the P_C factor:

$$E_{YR}^{even-even} = E_{YR}^{odd-even} + \Delta_p \cdot P_C = E_{YR}^{odd-odd} + 2\Delta_p \cdot P_C, \quad (\text{B.12})$$

where

$$P_C = \frac{1 - e^{-\xi}}{\xi}, \quad (\text{B.13})$$

$$\xi = S_P \cdot \frac{0.47}{A^{1/3}} E, \quad (\text{B.14})$$

where E is the excitation energy and A is the mass number. $S_P > 0$ is the code input parameter. The Evolution of P_C with excitation energy, for $S_P = 1$ is illustrated in Fig. B.42. This way for low energies we have three different yrast lines while for higher excitation energies these three yrast lines merge into the even-even one. The larger the S_P value is, the quicker the decrease of the P_C correction factor becomes. In order to switch off this pairing shift, $S_P = -1$ has to be used.

Appendix B.3. Summary - input parameters

The following parameters were introduced in this section:

Y_{MODE} - defines the method of calculating the reference yrast line :

$Y_{MODE} = 0$ - with the compound nucleus assumed to be a rigid rotor of spherical shape.

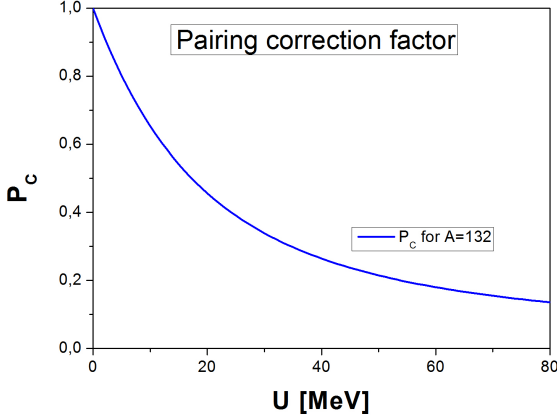


Figure B.42: The pairing correction factor P_C as a function of excitation energy in the $A = 132$ nucleus.

$Y_{MODE} = 1$ - for a certain nucleus of Z_Y , A_Y atomic and mass numbers.

N - defines the method of calculation when $Y_{MODE} = 1$:
 $N = 0$ - from input file inputs/yrastinput.inp (see Section 2.3.2).

$N = 1$ - the method based on the rigid rotor with the given moment of inertia being M times bigger than the moment of inertia of a spherical nucleus.

$N = 2$ - the method based on the polynomial coefficients which are:

A_{LOW} , B_{LOW} , C_{LOW} - the first polynomial coefficients.

A_{HIGH} , B_{HIGH} , C_{HIGH} - the second polynomial coefficients.

S_P - the pairing shift control. The default is $S_P = 1$. In such a case, the pairing shift is included.

Appendix C. Transmission coefficients for evaporated particles.

As in the case of fusion (see Appendix A), the transmission coefficients for neutron, proton and α particle evaporation are parametrized in terms of a simple empirical expressions [25], generated from a global optical potential. In order to determine the probability of an evaporation (Eq. 9), the transmission coefficients are calculated as a function of particle energy $T_l(E)$. COMPA allows the evaporation of particles of angular momentum from $l = 0$ to $l = 19$ at energies ranging from 0 to 100 MeV. Fig. C.43 shows the transmission coefficients and simulated evaporation spectra in the CM system for the $^{64}\text{Ni} + ^{64}\text{Ni}$ reaction at 260 MeV. The spectra have a Maxwell-like shape. The minimal energies of protons and α particles correspond well to the transmission coefficients leading edges.

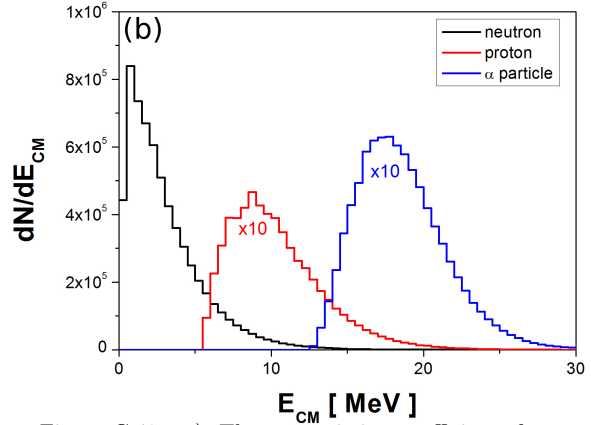
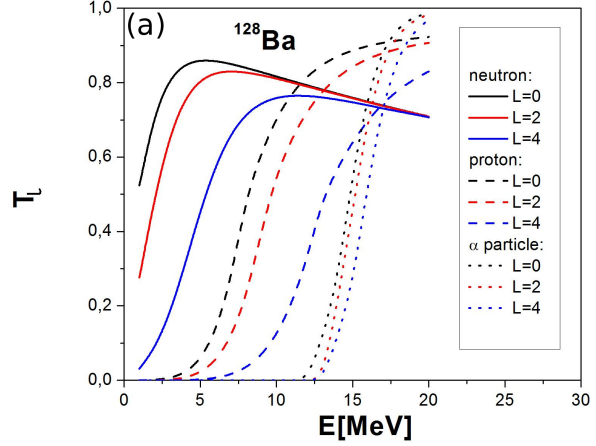


Figure C.43: a.) The transmission coefficients for neutron, proton and α particle evaporation from a ^{128}Ba nucleus; b.) simulated evaporation spectra in the CM system for the $^{64}\text{Ni} + ^{64}\text{Ni}$ reaction at 260 MeV.

Appendix C.1. Reduction of α particle yield.

One can find it quite disturbing that the total amount of emitted α particles is bigger than protons. Even in the case of a neutron deficient compound nucleus like ^{128}Ba (see Fig. C.43b), the evaporation of protons should be stronger than the evaporation of α particles. In order to suppress the α particle evaporation, we decided to modify the transmission coefficients in the following way. The coefficients for the α particle are normalized:

$$T_l^{\alpha, norm}(E) \rightarrow \frac{1}{N_\alpha} \cdot T_l^\alpha(E), \quad (\text{C.1})$$

$T_l^{\alpha, norm}(E)$ is the normalized transmission coefficient and the N_α normalization factor is calculated as:

$$N_\alpha = \frac{\sum_l \sum_E T_l^{protons}(E)}{\sum_l \sum_E T_l^\alpha(E)}, \quad (\text{C.2})$$

where $T_l^\alpha(E)$ and $T_l^{proton}(E)$ are coefficients for α particle and proton evaporation. Finally, the sum of the coefficients for proton emission, $\sum_l \sum_E T_l^{protons}(E)$, will be equal to the sum of the coefficients for α particles, $\sum_l \sum_E T_l^{\alpha,norm}(E)$. In Fig. C.44a normalized and unnormalized coefficients for α particles are compared. Corresponding evaporation spectra are also illustrated in Fig. C.44b. After normalization with $N_\alpha = 1.74$, the total

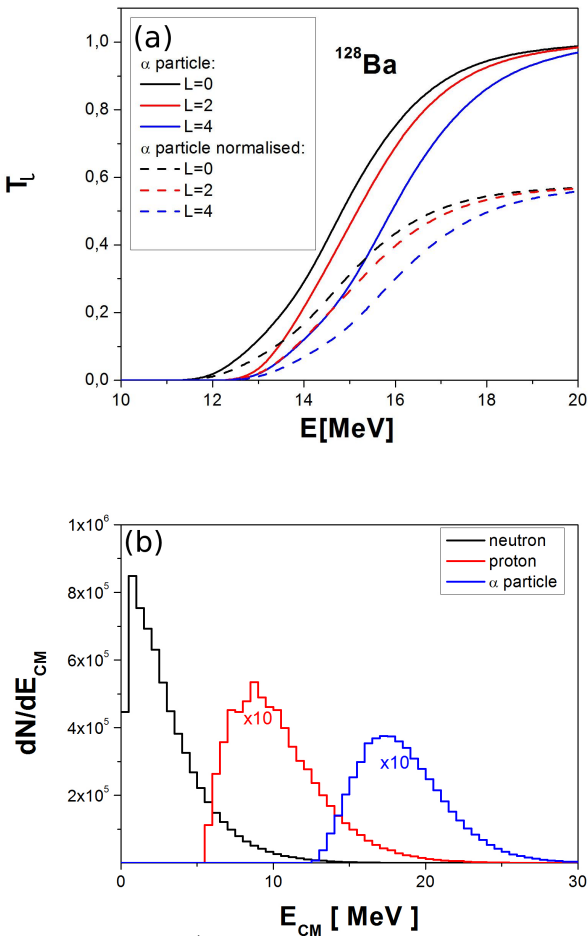


Figure C.44: a.) Transmission coefficients for neutron, proton and α particle emission from a ^{128}Ba nucleus with (dashed) and without (solid) the $N_\alpha = 1.74$ normalization factor; b.) simulated spectra for the $^{64}\text{Ni}+^{64}\text{Ni}$ reaction in the CM system, calculated with normalized coefficients.

number of α particles decreases significantly. This option is controlled by the N_R parameter. Normalization will be performed when the value of N_R is 2. If the number of α particles is still unsatisfactory, the user can define the N_α value. For $N_R \in \langle 0,1 \rangle$, calculations will be performed with $N_\alpha = N_R$.

Appendix C.2. Evaporated particle coefficients cut-off.

As in the case of fusion calculations (see parameter H_{CUT} in Appendix A.4), limits on the evaporated particle coefficients can also be set. The N_{CUT} , P_{CUT} and A_{CUT} parameters are responsible for cutting of the neutron, proton and α particle coefficients $T_l(E)$. As in the case of H_{CUT} , for $T_l^{neutron}(E) < N_{CUT}$, $T_l^{neutron}(E)$ vanishes. Such a correction is indispensable in order to control this crucial area of the statistical model. When it comes to evaporation from an odd-even nucleus of a relatively low excitation energy (≈ 5 MeV above the yrast line), the evaporation of neutrons leads to an even-even nucleus while proton escape results in an odd-odd nucleus. Ie. As shown

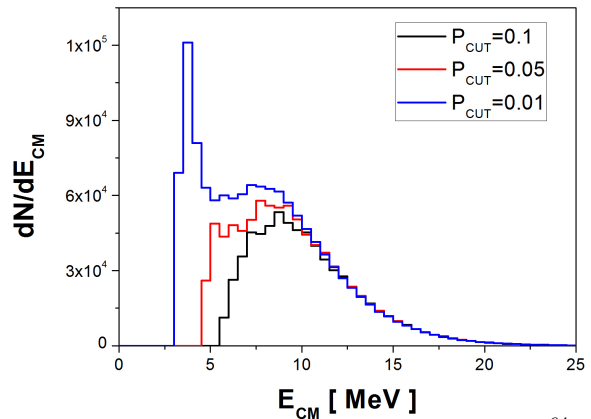


Figure C.45: Calculated CM proton spectra for the $^{64}\text{Ni}+^{64}\text{Ni}$ reaction for three different values of P_{CUT} : 0.1 (black), 0.05 (red) and 0.01 (blue).

in Appendix B (see Eq. B.5), there is a $2\Delta_p$ energy gap between the even-even and odd-odd nuclei yrast lines. Combining it with the low energy tail of the transmission coefficient for proton evaporation (see Fig. C.43), we get a much higher probability of a proton evaporation than of a neutron evaporation. It can be that neutron emission is not yet possible, while there is already a chance of emitting a proton, even in the case of proton-deficient nuclei. The conclusion is that a low energy tail in the transmission coefficient is unrealistic. This problem can be solved by appeal to the P_{CUT} parameter. Examples of proton spectra calculated with different values of P_{CUT} are shown in Fig. C.45. For $P_{CUT} = 0.01$, a strong peak shows up for low energies. These peaks tend to disappear as P_{CUT} is increased.

The bigger the P_{CUT} value, the higher the minimum possible energy of a proton. This results in the higher excitation energy needed for proton evaporation. Simultaneously, for higher excitation energies, neutron evaporation becomes competitive. Ultimately, for $P_{CUT} = 0.1$ proton spectra become Maxwell-like shaped. N_{CUT} , P_{CUT} and A_{CUT} are code parameters. It is recommended to use the following values: $N_{CUT} = 0.01$, $P_{CUT} = 0.1$ and $A_{CUT} = 0.1$.

Appendix C.3. Summary - input parameters

The following parameters were introduced in this section:

N_R - normalisation of transmission coefficients for α particle evaporation: For $N_R = 0$ - evaporation is impossible.

For $N_R \in \langle 0, 1 \rangle$ - $N_\alpha N_R$.

For $N_R = 2$ - normalisation to protons.

N_{CUT} , P_{CUT} , A_{CUT} - the cut-off parameters for the transmission coefficients. Defaults are $N_{CUT} = 0.01$, $P_{CUT} = 0.1$ and $A_{CUT} = 0.1$.

Appendix D. E1 GDR strength functions.

It was mentioned (see Section 3.2.3) that the code allows for E1 γ -ray emission only.

Transmission coefficients T_{XL} (Eq. 15) are taken from the RIPL Handbook [36]⁷:

$$T_{XL}(E_\gamma) = 2\pi \cdot E_\gamma^{(2L+1)} \cdot f_{XL}(E_\gamma), \quad (\text{D.1})$$

where E_γ is the gamma quantum energy and f_{XL} is the gamma-ray strength function. COMPA uses a function derived from the standard Lorentzian (SLO):

$$f_{XL}^{SLO}(E_\gamma) = \frac{26 \cdot 10^{-8}}{2L+1} \sigma_0 \cdot \Gamma_0 \cdot E_\gamma^{3-2L} \frac{\Gamma_0}{(E_\gamma^2 - E_0^2)^2 + E_\gamma^2 \cdot \Gamma_0^2}, \quad (\text{D.2})$$

where the Lorentzian parameters σ_0 , Γ_0 , E_0 are A -dependent⁸.

Transmission coefficients for different masses A are illustrated in Fig. D.46a. As the mass increases, a resonance maximum starts to appear at lower energies. Simulated γ -ray spectra for the $^{20}\text{Ne} + ^{122}\text{Sn}$ reaction at 150 MeV are shown in Fig. D.46b. The smaller the number of evaporated particles, the larger the influence of the E1 resonance. The E1 giant resonance peak at 14 MeV (see Fig. D.46c) corresponds well to the maximum for $A = 142$ (see Fig. D.46a).

Appendix E. Fission barrier calculations.

The fission barrier dependence on spin $B_f(I)$ is required for determining the probability of fission (Eq. 20,21). In COMPA, the fission barrier can be calculated with Modified Thomas-Fermi (MTF) formulae [11] or with the SIERK [28] program. The F_{MODE} parameter is responsible for this choice. For $F_{MODE} = 1$ the barrier will be calculated with the MTF formulae while $F_{MODE} = 2$ will switch on the SIERK function.

In the case of the Thomas-Fermi formulae, the k value (see Eq. A25 in ref. [11]), interpreted as

$$k = \frac{J_{high}}{J_{low}} \quad (\text{E.1})$$

is yet another input parameter. J_{high} and J_{low} are static moments of inertia for high and low spins, respectively. The k value can be calculated from the moments of inertia based on the yrast line. In the Fig. B.41, the evolution of the static moment of inertia is shown. Assuming $J_{low} \approx 32$ and $J_{high} \approx 54$, a $k \approx 1.7$ value is obtained. It will be shown further in this section that calculating the k parameter automatically, based on the yrast line shape, may be risky. It is thus a better choice to make it an input parameter. The default value should be around 2 as suggested by the authors of ref. [11].

For a given spin I , the fission barrier $B_f(I)$ is defined as the difference between the saddle-point energy $E_S(I)$ and the energy of rotation, assumed to be the yrast line energy $E_{YR}(I)$. When the saddle-point energy becomes equal to the rotational one, the fission barrier vanishes.

$$B_f(I) = E_S(I) - E_{YR}(I). \quad (\text{E.2})$$

Both the SIERK and the MTF method allow us to obtain the three dependencies mentioned above - let's name them B_f^{THEORY} , E_S^{THEORY} and E_{YR}^{THEORY} . Unfortunately, the calculated yrast line is usually different from that provided at the input (see Appendix B), called E_{YR}^{INPUT} here. There is no simple solution to this problem, so the user has to choose among four different approaches. The input parameter M_F is responsible for this choice.

First, the simplest and the least exact idea is to ignore the input yrast line and use a theoretical one in the calculations. This is risky since we have no control over the shape of the yrast line. Both the MTF and the SIERK methods use a rigid rotor model in yrast line calculations (see formulae (13) and (14) in ref. [11]), but the COMPA user can not change the value of the moment of inertia. It was shown before in Appendix B that the yrast line shape based on experimental values guarantees exact calculations. This option is realised with $M_F = 1$.

The second option is to use a calculated fission barrier and an input yrast line, modifying the saddle-point energy only:

$$E_S^{MODIFIED}(I) = B_f^{THEORY}(I) + E_{YR}^{INPUT}(I). \quad (\text{E.3})$$

This situation is illustrated in Fig. E.47 - the calculated saddle-point energy differs strongly from the theoretical one. Such a modification can lead to a situation where the saddle-point energy line makes no physical sense. E.g. if the input yrast line rises slowly as the spin increases, the saddle-point energy can start to decrease. Although the saddle point is not used anywhere in the calculations, the user should be very careful here, keeping an eye on the saddle point. Finally, $B_f^{THEORY}(I)$ and $E_{YR}^{INPUT}(I)$ will be used by the code. This option is realised with $M_F = 2$. The same procedure will be realised for $F_{MODE} = 0$, however $B_f^{THEORY}(I)$ will be read from a separate input file (inputs/bf.inp)

The third idea is to use the theoretical saddle-point energy

⁷see Chapter 6.2 in ref. [36].

⁸See *single GR hump targets* (page 102 in ref. [36]).

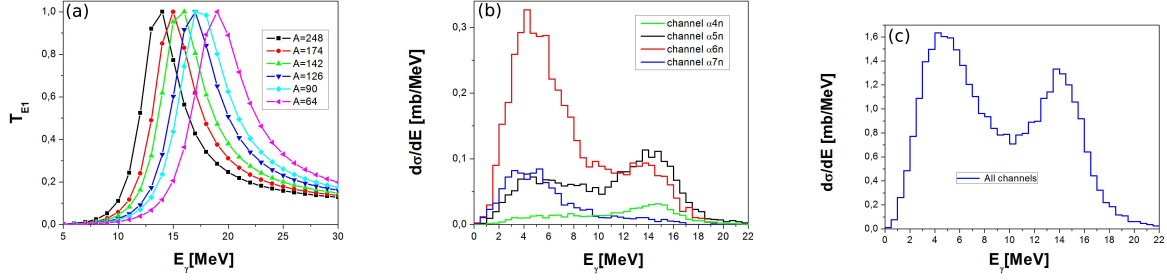


Figure D.46: a.) Transmission coefficients for E1 γ -ray emission for mass numbers varying from 64 to 248; b.) simulated γ -ray spectra for the $^{20}\text{Ne}+^{122}\text{Sn}$ reaction, for four channels: $\alpha 4n$ (green), $\alpha 5n$ (black), $\alpha 6n$ (red) and $\alpha 7n$ (blue); c.) simulated γ -ray spectrum from all channels in the same reaction.

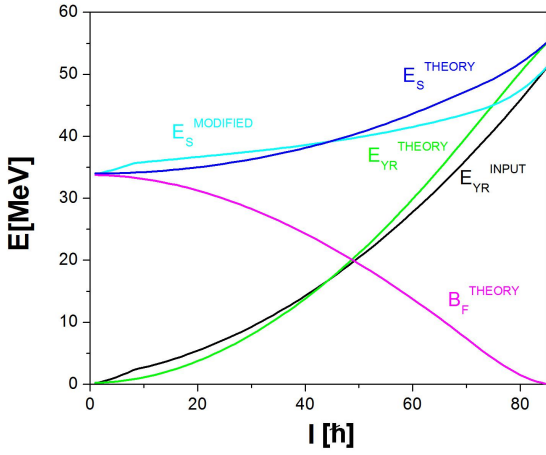


Figure E.47: ^{149}Tb fission barrier for $M_F = 2$. Three theoretical curves calculated with the SIERK program: the yrast line (green), the saddle point (blue) and the fission barrier (magenta), combined with the yrast line from the input (black) and the modified saddle point energy (cyan):
 $E_S^{\text{MODIFIED}}(I) = B_f^{\text{THEORY}}(I) + E_{YR}^{\text{INPUT}}(I)$.

and yrast line from the input, but to modify the fission barrier:

$$B_f^{\text{MODIFIED}}(I) = E_S^{\text{THEORY}}(I) - E_{YR}^{\text{INPUT}}(I). \quad (\text{E.4})$$

This situation is illustrated in Fig. E.48. The fission barrier can be essentially modified. The problem with SIERK and the modified Thomas-Fermi formulae is that the calculations end when $E_S^{\text{THEORY}}(I) = E_{YR}^{\text{THEORY}}(I)$. When the input yrast line lies below the theoretical one, the calculation of the fission barrier make no sense, so the saddle-point is not calculated. The user must again be very careful here and keep a physical sense of the calculated barrier. Finally, the $B_f^{\text{MODIFIED}}(I)$ and $E_{YR}^{\text{INPUT}}(I)$ will be used by the code. This option is realised with $M_F = 3$.

The last option is to use the input yrast line for the low spin region and the theoretical yrast line for the high

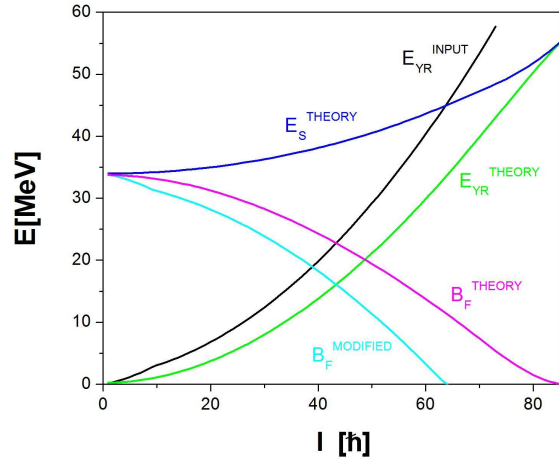


Figure E.48: ^{149}Tb fission barrier preparation for $M_F = 3$. Three theoretical curves calculated with the SIERK program: the yrast line (green), the saddle point (blue) and the fission barrier (magenta), combined with the yrast line from the input (black) and the modified fission barrier (cyan):
 $B_f^{\text{MODIFIED}}(I) = E_S^{\text{THEORY}}(I) - E_{YR}^{\text{INPUT}}(I)$.

spin region. This approach seems to be reasonable as we input yrast lines based on experimental levels, which are known up to relatively low spins (see Appendix B). The compound nucleus populated in heavy-ion induced reactions can reach a much higher spin. Using the yrast line based on the low spin region for higher-level spins can lead to inaccurate results. In this case, the preparation of the yrast line will be made in the following way. For the low spin region we use the input one, while for higher spin, the yrast line is modified so that it smoothly approaches the theoretical curve (see Fig. E.49). When the yrast line is changed, the fission barrier must also be shifted:

$$B_f^{\text{MODIFIED}}(I) = E_S^{\text{THEORY}}(I) - E_{YR}^{\text{MODIFIED}}(I). \quad (\text{E.5})$$

Finally $B_f^{\text{MODIFIED}}(I)$ and $E_{YR}^{\text{MODIFIED}}(I)$ will be used by the code. Performing such a modification is a delicate

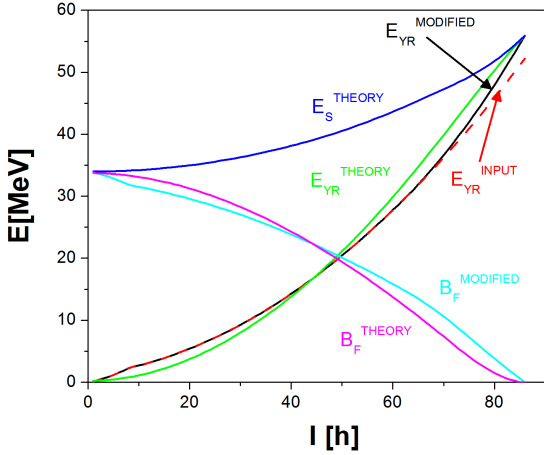


Figure E.49: ^{149}Tb fission barrier for $M_F = 0$. Three theoretical curves calculated with the SIERK program: the yrast line (green), saddle point (blue) and fission barrier (magenta) combined with the yrast line from the input (dashed red), the modified yrast line (black). The modified yrast line is equal to the input one and reaches the theoretical one. The modified fission barrier is then: $B_f^{\text{MODIFIED}}(I) = E_S^{\text{THEORY}}(I) - E_{YR}^{\text{MODIFIED}}(I)$.

matter, as a smooth transition from an input yrast line to a modified one does not necessarily give reasonable results. When the input yrast line lies beyond the theoretical one, a smooth transition may result in an yrast line that decreases as the spin increases. This makes no sense from the point of view of physics. Once again the user has to be very careful here. This approach, however, seems to be the most exact. This option is realised with $M_F = 0$.

The authors recommend the $M_F = 2$ option as a default as long as the modified saddle-point energy seems to be reasonable. Then, if possible, carefully switch to $M_F = 0$, when one strives for better accuracy.

A prepared fission barrier can be further modified. The L_{SH} parameter allows us to shift the barrier in the following way:

$$B_f(I) \rightarrow B_f(I + L_{SH}). \quad (\text{E.6})$$

It was shown in Section 4.1.3 that sometimes such a modification may be necessary.

Every piece of a Monte-Carlo code should be as fast as possible. When the barrier is high, the probability of fission is small compared to evaporation or γ -ray emission. Omitting the calculation of the fission probability will save some time. In order to increase the code speed, the B_{CUT} parameter was introduced. When the fission barrier is higher than B_{CUT} , the probability of fission will not be calculated and is assumed to be 0. The authors suggest the value $B_{CUT} = 12$ MeV.

Appendix E.1. Summary - input parameters

The following parameters were introduced in this section:

M_F - The fission barrier vs saddle point and yrast line. Default is $M_F = 2$.

L_{SH} - For moving the fission barrier left or right. Default is $L_{SH} = 0$.

B_{CUT} - The barrier value [MeV], when fission becomes possible. Default is $B_{CUT} = 12$.

Appendix F. Level densities

Level density and nuclear temperature as functions of the excitation energy are often used in this work (see Sections 3.2.1, 3.2.3, 3.2.4). The expression for the level density $\rho(U, I)$ in a nucleus of excitation energy U and spin I was obtained by Bethe [37] on the basis of the Fermi gas model:

$$\rho(U, I) = \rho(U) \cdot \frac{2I + 1}{2\sqrt{2\pi}\sigma^3} e^{-\frac{(I+1/2)^2}{2\sigma^2}}, \quad (\text{F.1})$$

where $\rho(U)$ is the level density as a function of excitation energy U . For low excitation energies the most suitable formula is [38]:

$$\rho_{\text{LOW}}(U) = \frac{\sqrt{\pi}}{48a^{1/4}} \frac{1}{U^{5/4}} e^{2\sqrt{aU}}, \quad (\text{F.2})$$

while for high energies [39] the level density is proportional to:

$$\rho_{\text{HIGH}}(U) = \text{const} \frac{1}{U^2} e^{2\sqrt{aU}}, \quad (\text{F.3})$$

where a is the level density parameter, σ is the spin cutoff parameter connected with the static moment of inertia J (see Eq. B.7) as $\sigma^2 = aJT$. T is the effective nuclear temperature. To merge Eq. F.2 and Eq. F.3, the following formula is introduced:

$$\rho_{\text{COMPA}}(U) = \frac{\sqrt{\pi}}{48a^{1/4}} \frac{1}{U^{\frac{5+d(U)}{4}}} e^{2\sqrt{aU}}, \quad (\text{F.4})$$

where $d(U)$ is given by the equation:

$$d(U) = 3 \cdot (1 - e^{-\gamma U}), \quad (\text{F.5})$$

and smoothly grows from 0 to 3 with increasing excitation energy U . γ is the shell-damping factor in Eq. F.8. The transition from the low energy ρ_{LOW} formula to the high energy ρ_{HIGH} formula is illustrated in Fig. F.50. The COMPA level density (Eq. F.4) smoothly evolves from ρ_{LOW} to ρ_{HIGH} for energies beyond 5 MeV.

The level density parameter a is calculated in the following way:

$$a = a_{\text{LDM}} \cdot F_{\text{SHELL}}. \quad (\text{F.6})$$

a_{LDM} is taken from the liquid drop model [40] and given by the formula:

$$a_{\text{LDM}} = A \cdot C_a \cdot (a_v + a_s B_s A^{-1/3} + a_c B_k A^{-2/3}), \quad (\text{F.7})$$

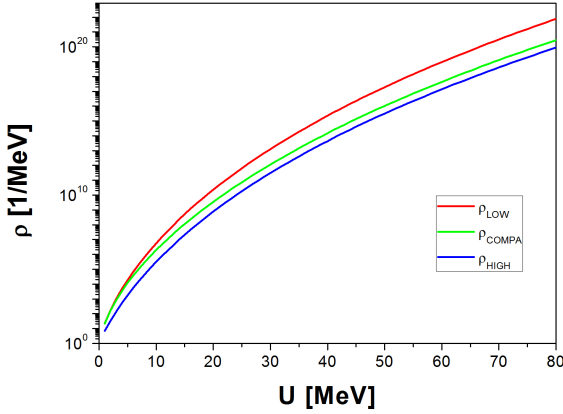


Figure F.50: Level densities for $A = 142$ isobars. Low and high energy ρ_{LOW} and ρ_{HIGH} (red and blue) along with COMPA level density ρ_{COMPA} (green).

where a_v , a_s , a_c are the volume, surface and curvature components. B_s and B_k describe the departures from a spherical shape for high excitation energies. The F_{SHELL} factor takes into account the contribution of shell effects, and is given by a phenomenological term, first developed by Ignatyuk et al. [41]:

$$F_{SHELL} = 1 + \frac{S_h \cdot \Delta_{sh}(A)}{U} (1 - e^{-\gamma U/A^{1/3}}),$$

$$\gamma = \frac{0.47}{A^{1/3}}, \quad (\text{F.8})$$

where Δ_{sh} is taken from fitting the data available in ref. [42]. γ is a shell-damping factor. C_a and S_h are input parameters allowing the user to control the correction strength.

Appendix F.1. Temperature correction

The level density parameter a depends on the effective temperature. Fig. F.51 presents the calculations of S. Shlomo and J. B. Natowitz [43] (points) compared to COMPA calculations (lines). It is shown how the level density parameter changes as the temperature increases. The function $F(T, A)$, shown in Fig. F.51, was obtained by fitting Shlomo's and Natowitz's calculations. $F(T, A)$ is given by the equation:

$$F(T, A) = 1 + S_T \cdot B(A) \cdot \exp(-\exp(-0.75T))^{C(A)}, \quad (\text{F.9})$$

where

$$B(A) = 0.096 \cdot A^{0.386}, \quad C(A) = 31 \cdot A^{-0.3}. \quad (\text{F.10})$$

The S_T parameter is introduced in order to control the temperature shift. $S_T = 1$ was used in the calculations presented here and it is suggested to use this value as the default.

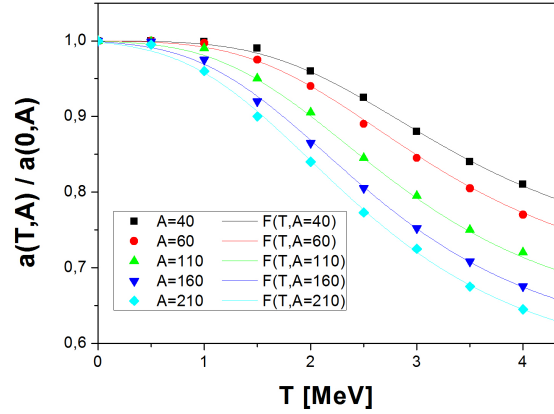


Figure F.51: The level density parameter correction factor $a(T, A)/a(T = 0, A)$ as a function of the temperature and the mass number A . The points are taken from Fig.1 in ref. [43]. Also shown are the corresponding $F(T, A)$ functions (Eq. F.9) obtained with COMPA (lines). Five different mass numbers ($A = 40, 60, 110, 160, 210$) were chosen for presentation.

On the other hand, the temperature can be approximately connected with U and a in the following way: $U = aT^2$. The following iteration procedure is introduced in the level density parameter calculations:

$$a_{n+1} = \frac{a_n}{F(T = \sqrt{U/a_n}, A)}. \quad (\text{F.11})$$

At the beginning, $a_0 = a_{LDM} \cdot F_{SHELL}$ is used. The level density is calculated after n iterations. n is the code parameter representing the number of iterations. An example of the temperature correction is shown in Fig. F.52.

One can see that $n = 5$ iterations is enough. Further iterations do not affect on the level density.

Finally, the temperature is calculated with the exact definition:

$$T(U) = \frac{\rho(U)}{\frac{\delta \rho(U)}{\delta U}}. \quad (\text{F.12})$$

The calculated temperatures are presented in Fig. F.52b.

Appendix F.2. Summary - input parameters

The following parameters were introduced in this section:

C_a - the liquid drop model correction to the level density parameter. Default is $C_a = 0.8$.

S_h - the shell correction to the level density parameter. Default is $S_h = 1$.

n - the number of iterations in the temperature correction to the level density parameter. Default is $n = 5$.

S_T - an additional control in the temperature correction to the level density parameter. Default is $S_T = 1$.

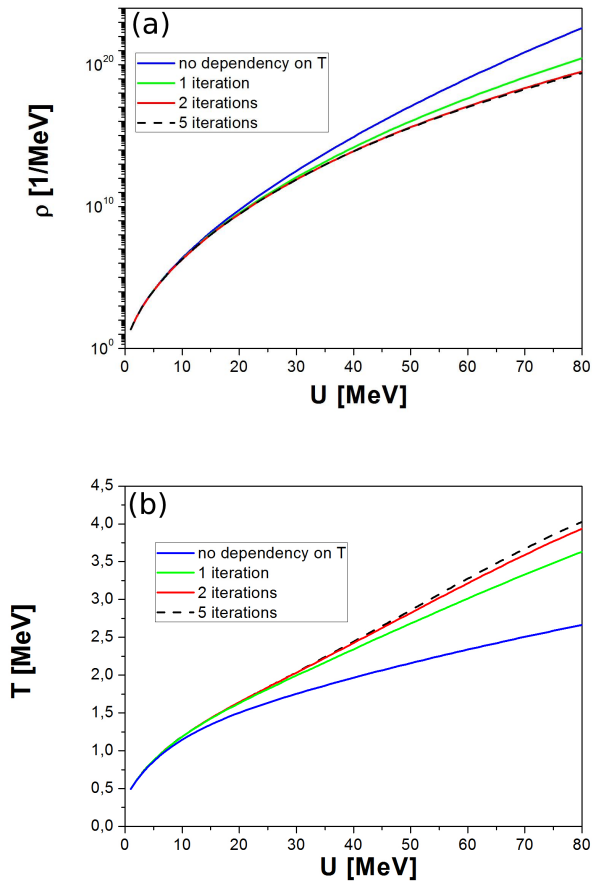


Figure F.52: Level density (a) and temperature (b) calculated with different numbers of n iterations in the temperature correction (Eq. F.11): without correction (blue), after one (green), two (red) and five (dashed black) iterations.

Appendix G. Remaining output files

Generated output files are stored in folder “outputs/”. The files in folder “xsections/” contain information for all asked for channels and beam energies. All remaining files contain detailed information for the first defined channel Ch_1 and for the last defined beam energy (E_{KMAX} , see Section 2.3.1).

Appendix G.1. tlese.txt

tlese.txt is a text file with basic information on transmission coefficients and cross sections for fusion and light particle evaporation. An exact description is included in the file.

Appendix G.2. xsections

The folder “xsections/” contains the excitation functions for the analysed reaction. It contains the following files:

- “channels.dat” - the cross-sections for a maximum of 10 strongest channels.
- “total.dat” - the competition between CF (or ICF if asked for) and fission.
- “yield.dat” - the events per 10^{12} projectiles.
- “cross_sections.dat” - the cross-section.
- “percent_crs.dat” - the percentage of total cross section.
- “relative_crs.dat” - channel yield with respect to the first defined channel (Ch_1).

Note: the files “yield.dat”, “cross_sections.dat”, “percent_crs.dat” and “relative_crs.dat” will be created only if at least two channels of interest $K_{CH} \geq 1$ are defined (see Section 2.3.1).

Appendix G.3. recoils

Folder “recoils/” contains information on the kinematics of the recoils. It contains the following files:

- “residuals_angles.1.dat” - recoil angular distribution. Columns:
Theta [deg].
 $dN/d(\theta) - \frac{dN}{d\theta} [\frac{10}{deg}]$, only for channel Ch_1 . error - statistical error.
- “residuals_angles.2.dat” - the angular distribution of the recoils, normalised to 1. Columns:
Theta - angle [deg].
 $dN/d(\theta) - \frac{dN}{d\theta} [\frac{10}{deg}]$, only for the channel Ch_1 .

- “residuals.dat” - the kinetic energy of the recoils vs the θ distribution, only for the channel Ch_1 . Description x,y,z:
 θ [deg].
energy [0.1 MeV].
 $\frac{d^2N}{dE d\theta} [10 \cdot \frac{1}{MeV} \cdot deg]$.
- “velocities.dat” - some velocity distributions. Columns:
v/c - velocity with respect to c.
recoil_dN/dv - recoils $\frac{dN}{dv} [\frac{1}{v/c}]$ (only for channel Ch_1).
r_error - statistical error.
compound_dN/dv - compound nucleus $\frac{dN}{dv} [\frac{1}{v/c}]$.
c_error - statistical error.
beam_dN/dv - beam $\frac{dN}{dv} [\frac{1}{v/c}]$.
b_error - statistical error.
- “tof.dat” - the distribution of the time of flight at a distance of L_{TOF} (see Section 3.3.4). Only for the channel Ch_1 and only if the stopping in the backing or target was switched on (see parameter S_{recoil}). Columns:
tof- time of flight [ns].
 $dN/dt - \frac{dN}{dt} [\frac{1}{ns}]$.
- “transition.dat” - the distribution of the transition time of the recoils through the target and backing. Only for the channel Ch_1 and only if stopping in the backing or target was switched on (see parameter S_{recoil}). Columns:
time - time [fs].
 $dN/dt - \frac{dN}{dt} [\frac{1}{fs}]$.

Appendix G.4. nuclei

Folder “nuclei/” contains some information on the spin and excitation energy of the nuclei. It contains the following files:

- “nuclei_energies.dat” - the excitation energy distributions. Columns:
E - energy [MeV].
compound - the compound nucleus $\frac{d\sigma}{dE} [\frac{mb}{MeV}]$.
entry - after evaporation $\frac{d\sigma}{dE} [\frac{mb}{MeV}]$. Only for the channel Ch_1 .
fission - just before fission $\frac{d\sigma}{dE} [\frac{mb}{MeV}]$.
- “nuclei_spins.dat” - spin distributions. Columns:
spin - $I[\hbar]$.
projectile - projectile input angular momentum $\frac{d\sigma}{dI} [\frac{mb}{\hbar}]$.
compound - compound nucleus $\frac{d\sigma}{dI} [\frac{mb}{\hbar}]$.
entry - after evaporation $\frac{d\sigma}{dI} [\frac{mb}{\hbar}]$. Only for the channel Ch_1 .
fission - just before fission $\frac{d\sigma}{dI} [\frac{mb}{\hbar}]$.
fission_barrier - fission barrier as a function of spin [MeV].

yrast_line - yrast levels [MeV] (based on the fit).

- “diagr.dat” - entry states distribution, only for the channel Ch_1 .
Description x,y,z:
Spin I [\hbar].
Energy [MeV].
 $\frac{d^2 N}{dE d\hbar} [\frac{1}{MeV \cdot \hbar}]$.
- “compounddiagr.dat” - the compound nucleus spin vs excitation energy distribution. The format is identical to diagr.dat.
- “fissiondiagr.dat” - the compounds that fissioned spin vs excitation energy distribution. The format is identical to diagr.dat.
- “barrier.dat” - the fission barrier and related dependencies. Columns:
spin - $I[\hbar]$.
barrier - the fission barrier used in the calculations [MeV].
yrast - the yrast line levels used in the calculations [MeV].
saddle - the saddle point energy used in the calculations [MeV].
barrier_function - the fission barrier from SIERK, MTF or bf.inp file [MeV] (see Appendix E).
yrast_function - the yrast line levels from SIERK or MTF (see Appendix E).
saddle_function - the saddle point energy from SIERK or MTF (see Appendix E).
static_mom - the static moment of inertia [$\frac{\hbar^2}{MeV}$] (see Appendix B).
kinematic_mom - the kinematic moment of inertia [$\frac{\hbar^2}{MeV}$] (see Appendix B).
dynamic_mom - the dynamic moment of inertia [$\frac{\hbar^2}{MeV}$] (see Appendix B).

Appendix G.5. particles

The folder “particles/” contains some information on the evaporated particles. It contains the following files:

- “ntetabeta.dat” - the θ vs kinetic energy diagram in the LAB frame.
Description x,y,z:
 θ [deg].
Kinetic energy [MeV].
 $\frac{d^2 N}{dE d\theta} [\frac{1}{MeV \cdot deg}]$.
- “ptetabeta.dat” - the same as “ntetabeta.dat”, except it is for protons.
- “atetabeta.dat” - the same as “ntetabeta.dat”, except it is for α particles.
- “ntetafi.dat” - θ vs ϕ diagram in the LAB frame.
Description x,y,z:
 θ [deg].
 ϕ [deg].
 $\frac{d^2 N}{d\phi d\theta} [\frac{1}{deg^2}]$.
- “ptetafi.dat” - the same as “ntetafi.dat”, except it is for protons.
- “atetafi.dat” - the same as “ntetafi.dat”, except it is for α particles.
- “particles_energy_in_cm.dat” - the evaporated particle energies in the CM frame. Columns:
E - the energy [MeV]
neutron - the neutron $\frac{dN}{dE} [\frac{2}{MeV}]$.
n_error - the statistical error.
proton - the proton $\frac{dN}{dE} [\frac{2}{MeV}]$.
p_error - the statistical error.
alpha - α particle $\frac{dN}{dE} [\frac{2}{MeV}]$.
a_error - the statistical error.
- “particles_energy_in_lab.dat” - the same as “particles_energy_in_cm.dat”, except it is in the LAB frame.
- “particles_ang_mom.dat” - the angular momenta of the evaporated particles. Columns:
L - angular momentum [\hbar].
neutron - $\frac{dN}{dL} [\frac{1}{\hbar}]$.
n_error - statistical error.
proton - $\frac{dN}{dL} [\frac{1}{\hbar}]$.
p_error - statistical error.
alpha - α particle $\frac{dN}{dL} [\frac{1}{\hbar}]$.
a_error - statistical error.
- “particles_theta_in_lab_1.dat” - $\frac{dN}{d\theta}$, the angular distributions of the evaporated particle in the CM frame. Columns:
Theta - θ [deg].
neutron - $\frac{dN}{d\theta} [\frac{1}{deg}]$.
n_error - the statistical error.
proton - $\frac{dN}{d\theta} [\frac{1}{deg}]$.
p_error - the statistical error.
alpha - α particles $\frac{dN}{d\theta} [\frac{1}{deg}]$.
a_error - the statistical error.
- “particles_theta_in_lab_2.dat” - $\frac{dN}{d\cos(\theta)}$, the angular distributions of the evaporated particles in the CM frame. Columns:
cos(Theta) - $\cos\theta$.
neutron - $\frac{dN}{d\cos(\theta)}$.
n_error - the statistical error.
proton - $\frac{dN}{d\cos(\theta)}$.
p_error - the statistical error.
alpha - the α particles $\frac{dN}{d\cos(\theta)}$.
a_error - statistical error.

- “particles_theta_in_lab_3.dat” - $\frac{dN}{d\Omega}$, the angular distributions of the evaporated particles in the CM frame. Columns:
Theta - θ [deg].
neutron - $\frac{dN}{d\Omega} [\frac{1}{srad}]$.
n_error - statistical error.
proton - $\frac{dN}{d\Omega} [\frac{1}{srad}]$.
p_error - statistical error.
alpha - α particle $\frac{dN}{d\Omega} [\frac{1}{srad}]$.
a_error - statistical error.
- “particles_theta_in_lab_1.dat” - the same as “particles_theta_in_cm_1.dat”, but in the LAB frame.
- “particles_theta_in_lab_2.dat” - the same as “particles_theta_in_cm_2.dat”, but in the LAB frame.
- “particles_theta_in_lab_3.dat” - the same as “particles_theta_in_cm_3.dat”, but in the LAB frame.
- “neutrons_coeffs_en.dat” - the transmission coefficients for neutron evaporation.
Description x,y,z:
L - the angular momentum [\hbar].
E - the projectile energy [MeV].
T(L,E) - the transmission coefficient.
- “protons_coeffs_en.dat” - the same as neutrons_coeffs_en.dat, but for the protons.
- “alphas_coeffs_en.dat” - the same as neutrons_coeffs_en.dat, but for the α particles.

Appendix G.6. gammas

The folder “gammas/” contains some information on the E1 γ quanta emission. It contains the following files:

- “lorentzE1.dat” - The Lorentz E1 giant resonance function for the nuclear mass numbers $A, \dots, A - 16$, where A is the mass number of the compound nucleus.
Description x,y,z:
 A - the mass number.
 E - γ energy [MeV].
 $F(A, E)$ - the function value.
- “gamma.dat” - the E1 γ spectrum. Columns:
 E - energy [MeV].
 $\frac{dN}{dE} - \frac{dN}{dE} [\frac{1}{MeV}]$.
error - the statistical error.
- “gammamult.dat” - E1 γ multiplicity spectrum. Columns:
multiplicity - obvious.
N - counts.
error - statistical error.

Appendix G.7. level density

The folder “levdens/” contains some information on the level density calculations. It contains the following files:

- “leveldens.dat” - the level densities for nuclei of mass numbers $A, \dots, A - 16$, where A is the mass number of the compound nucleus.
Description x,y,z:
 A - mass number.
 E - energy [MeV].
 $R(E,A)$ - level density [$\frac{1}{MeV}$].
- “temperature.dat” - temperatures for nuclei of mass numbers $A, \dots, A - 16$, where A is the mass number of the compound nucleus.
Description x,y,z:
 A - mass number.
 E - energy [MeV].
 $R(E, A)$ - temperature [MeV].

Appendix G.8. stopping

Folder “stopping/” contains some information on stopping power values. It contains the following files, which will be created for $K_{OUT}=2$ (see Section 2.3.1):

- “esr.dat” - the ranges and energy losses for projectiles in the target. Columns:
 E - energy [MeV].
 SE - stopping power $\frac{dE}{dR} [\frac{MeV}{cm^2}]$.
 R - range [$\frac{mg}{cm^2}$].
- “esrs.dat” - same as esr.dat, but for the projectiles in the support.
- “esrb.dat” - same as esr.dat, but for the projectiles in the backing.
- “esrd.dat” - same as esr.dat, but for the protons or α particles in the detector.
- “pesr0.dat” - same as esr.dat, but for the protons in the target.
- “pesr1.dat” - same as esr.dat, but for the protons in the backing.
- “pesrs.dat” - same as esr.dat, but for the protons in the support.
- “pesr2.dat” - same as esr.dat, but for the protons in the tube.
- “aesr0.dat” - same as esr.dat, but for the α particles in the target.
- “aesr1.dat” - same as esr.dat, but for the α particles in the backing.
- “aesrs.dat” - same as esr.dat, but for the α particles in the support.
- “aesr2.dat” - same as esr.dat but for α particles in the tube.

- “ede.dat” - the energy loss of protons or α particles in the detector. Columns:
 E - energy [MeV].
 dE - energy loss [MeV].
- “re.dat” - the projectile energy behind the target as a function of the thickness of the target. Columns:
 R - layer thickness [$\frac{mg}{cm^2}$].
 E - energy behind [MeV].
- “res.dat” - same as re.dat, but for the projectiles in the support.
- “reb.dat” - same as re.dat, but for the projectiles in the backing.
- “red.dat” - same as re.dat, but for the protons or α particles in the detector.
- “pre0.dat” - same as re.dat, but for the protons in the target.
- “pre1.dat” - same as re.dat, but for the protons in the backing.
- “pres.dat” - same as re.dat, but for the protons in the support.
- “pre2.dat” - same as re.dat, but for the protons in the tube.
- “are0.dat” - same as re.dat, but for the α particles in the target.
- “are1.dat” - same as re.dat, but for the α particles in the backing.
- “ares.dat” - same as re.dat, but for the α particles in the support.
- “are2.dat” - same as re.dat, but for the α particles in the tube.
- “massdefects.txt” - the masses that were used in the calculations. The program allows the evaporation of nuclei in the range: $< A; A - 16 >$ and $< Z; Z - 10 >$ where Z and A are respectively the atomic and mass numbers of the compound nucleus.
- “input_for_python.inp” - some parameters for the python script plots/compa.py to prepare command-file plots/plot.cmd for gnuplot (see Section 2.5).
- “yrastforplot.dat” - the yrast line for gnuplot (file plots/plot.cmd).
- “kin.mas”, “kin.inf” and “leg.mas” - the inputs for the GAMMA code (for $K_{OUT} = 1$, see Section 2.3.1).

Appendix G.9. Agata Simulation Code

The folder “agata/” contains the inputs for the Agata Simulation Code (prepared when $K_{ASC} = 1$, see Section 2.3.1). It contains the following files:

- “eventbyevent.dat” - the list of events in ASC format.
- “beamprofile.dat” - the beam intensity distribution as a function of distance from the beam axis (z). Columns:
 x - distance [cm].
intensity - relative intensity, normalised to 1.

Appendix G.10. others

Folder “others/” contains the following output files:

- “warnings.txt” - wrong events that should be noticed, i.e. the mass of the nucleus is unknown.

References

- [1] W. Hauser and H. Feshbach, *Phys. Rev.* **87**, 366 (1952)
- [2] E.O. Lieder, A.A. Pasternak, R.M. Lieder, R.A. Bark, E.A. Lawrie, J.J. Lawrie, S.M. Mullins, S. Murray, S.S. Ntshangase, P. Papka, N. Kheswa, W.J. Przybyłowicz, P.T. Sechogela, K.O. Zell, *Nucl. Inst. and Meth. A* **607**, 591 (2009)
- [3] J. Lindhard, M. Scharff, H.E. Schiøtt, *Mat. Fys. Medd. Dan. Vid. Selsk.* **33** (14) (1963) 10
- [4] J. F. Ziegler, M. D. Ziegler, J. P. Biersack, *Nucl. Instr. and Meth. B*, 268, 1818 (2010). The code is available from: <http://www.srim.org/>
- [5] R.M. Lieder, A. A. Pasternak, E. O. Podsvirova, A. D. Efimov, V. M. Mikhajlov, R. Wyss, Ts. Venkova, W. Gast, H.M. Jäger, L. Mihailescu, D. Bazzacco, S. Lunardi, R. Menegazzo, C. Rossi Alvarez, G. de Angelis, D.R. Napoli, T. Rzaca-Urban, W. Urban, A. Dewald, *Eur. Phys. J. A* **21**, 37 (2004)
- [6] E. Grodner, A. A. Pasternak, Ch. Droste, T. Morek, J. Srebrny, J. Kownacki, W. Plóciennik, A. A. Wasilewski, M. Kowalczyk, M. Kisieliński, R. Kaczarowski, E. Ruchowska, A. Kordyasz, M. Wolińska, *Eur. Phys. J. A* **27**, 325 (2006)
- [7] E. O. Lieder, A. A. Pasternak, R. M. Lieder, A. D. Efimov, V. M. Mikhajlov, B. G. Carlsson, I. Ragnarsson, W. Gast, Ts. Venkova, T. Morek, S. Chmel, G. de Angelis, D. R. Napoli, A. Gadea, D. Bazzacco, R. Menegazzo, S. Lunardi, W. Urban, Ch. Droste, T. Rzaca-Urban, G. Duchene, A. Dewald, *Eur. Phys. J. A* **35**, 135 (2008)
- [8] I.Kh. Lemberg, A.A Pasternak, *Modern Methods of Nuclear Spectroscopy Nauka, Leningrad, 1985*
- [9] J. Srebrny, Ch. Droste, T. Morek, K. Starosta, A. A. Wasilewski, A. A. Pasternak, E. O. Podsvirova, Yu. N. Lobach, G. H. Hagemann, S. Juutinen, M. Piiparinen, S. Törmänen, A. Virtanen, *Nucl. Phys. A* **683**, 21 (2001)
- [10] G. Audi, A. H. Wapstra, C. Thibault, J. Blachot, O. Bersillon, *Nucl. Phys. A* **729**, (2003)
- [11] D. Ward, R. M. Diamond, W. J. Swiatecki, R. M. Clark, M. Cromaz, M. A. Deleplanque, P. Fallon, A
- [12] K. Daneshvar, D.G. Kovar, S.J. Krieger, K. T. R. Davies, *Phys. Rev. C* **25**, 1342 (1982)
- [13] Reference Input Parameter Library book, chapter 5 by A. V. Ignatyuk
- [14] A. V. Ignatyuk, G. N. Smirenkin, A. S. Tishin, *Sov. J. Nucl. Phys.* **21**, 255 (1975)
- [15] Reference Input Parameter Library book, chapter 6 page 97 by J.Kopecky
- [16] H. Bethe, *Rev. Mod. Phys.* **9**,69 (1937)
- [17] T. Døssing and E. Vigezzi, *Nucl. Phys. A* **587**, 13 (1995)
- [18] F. Cristancho, K. P. Lieb, *Nucl. Phys. A* **486**, 353 (1988)
- [19] S. F. Mughabghab, C. Dunford, *Phys. Rev. Lett.* **81**, 4083 (1998)
- [20] A. V. Ignatyuk, G. N. Smirenkin, A. S. Tishin, *Yad. Fiz.* **21**, 485 (1974)
- [21] W. D. Myers and W. J. Swiatecki, *Ark. Phys.* **36**, 593 (1967)
- [22] S. Shlomo and J. B. Natowitz, *Phys. Rev. C* **44**, 2878 (1991). Goergen, G. J. Lane, I. Y. Lee, A. O. Macchiavelli, W. Myers, F. S. Stephens, C. E. Svensson, K. Vetter, *Phys. Rev. C* **66**, 024317 (2002)
- [23] V.V. Babikov *JETP* **38**, 264 (1960)
- [24] S. Kailas and S.K. Gupta, *Z. Phys. A* **302**, 355 (1981)
- [25] K. H. N. Murthy, S. K. Gupta, A. Chatterjee, *Z. Phys. A* **305**, 73 (1982)
- [26] R. Bass "Nuclear reaction with heavy ions" Springer-Verlag, 1980
- [27] R. Weiner, M. Westrom *Nucl. Phys. A* **286**, 282 (1977)
- [28] A. J. Sierk LANL T-9 February, 1984
- [29] W. Meczyński, P. Bednarczyk, J. Grebosz, J. Heese, M. Janicki, K. H. Maier, J. C. Merdinger, K. Spohr, M. Ziebliński, J. Styczeń *Nucl. Phys. A* **580**, 1310 (2007)
- [30] R.G. Stokstad, Y. Eisen, S. Kaplanis, D. Pelte, U. Smilansky, I. Tserruya, *Phys. Rev. C* **21**, 2427 (1980)
- [31] M. Benjelloun, W. Galster, J. Vervier, *Nucl. Phys. A* **560**, 715 (1993)
- [32] A. Gavron *Phys. Rev. C* **21**, 230 (1979)
- [33] K. Daneshvar, D.G. Kovar, S.J. Krieger, K. T. R. Davies, *Phys. Rev. C* **25**, 1342 (1982)
- [34] Reference Input Parameter Library book, chapter 5 by A. V. Ignatyuk
- [35] A. V. Ignatyuk, G. N. Smirenkin, A. S. Tishin, *Sov. J. Nucl. Phys.* **21**, 255 (1975)
- [36] Reference Input Parameter Library book, chapter 6 page 97 by J.Kopecky
- [37] H. Bethe, *Rev. Mod. Phys.* **9**,69 (1937)
- [38] T. Døssing and E. Vigezzi, *Nucl. Phys. A* **587**, 13 (1995)
- [39] F. Cristancho, K. P. Lieb, *Nucl. Phys. A* **486**, 353 (1988)
- [40] S. F. Mughabghab, C. Dunford, *Phys. Rev. Lett.* **81**, 4083 (1998)
- [41] A. V. Ignatyuk, G. N. Smirenkin, A. S. Tishin, *Yad. Fiz.* **21**, 485 (1974)
- [42] W. D. Myers and W. J. Swiatecki, *Ark. Phys.* **36**, 593 (1967)
- [43] S. Shlomo and J. B Natowitz, *Phys. Rev. C* **44**, 2878 (1991)